

UNIVERSITÁ DEGLI STUDI DI NAPOLI
“FEDERICO II”

FACOLTÁ DI FARMACIA
Dipartimento di Farmacologia Sperimentale

TESI DI DOTTORATO DI RICERCA IN
SCIENZA DEL FARMACO
XXIV CICLO

ALTERATIONS OF IRON METABOLISM DURING
HEART ISCHEMIA/REPERRFUSION INJURY
CYTOPROTECTIVE EFFECTS OF SIMVASTATIN

Tutor
Chiar.mo Prof.
Alfredo Colonna

Coordinatore
Chiar.mo Prof.
Maria Valeria D’Auria

Dottorando
Dott. Antonio Di Pascale
2008-2011

ACKNOWLEDGMENTS

I would like to thank my research supervisor Prof. Alfredo Colonna for his great support and encouragement at every stage of my PhD training. His invaluable advices and constant surveillance were essential to complete my research project and scientific formation.

Immense gratitude also goes to Prof. Rita Santamaria and to Prof. Carlo Irace for their precious suggestions and constant assistance.

I would like to thank Dr. Carmen Maffettone for her advices and for her significant contribute to my training.

Special thanks are due to Prof. Antonio Calignano, chief of the Department of Experimental Pharmacology, and to Prof. Maria Valeria D'Auria, director of my PhD.

I wish to express my gratitude to Marcella Maddaluno, Mariateresa Cipriano, Antonio Parisi, Maria Vittoria Di Lauro, Elisa Panza, and Anna Cantalupo to made unforgettable these three years and for their friendship.

Moreover, I would like to thank Dr. Mayka Sanchez, chief of the Cancer and Iron Group, and their collaborators Erica Moràn Martinez, Jessica de Aranda, Sara Luscieti, and Ricky Joshi, for the great experience at the Institut de Medicina Predictiva i Personalitzada del Càncer, IMPPC, of Badalona-Barcelona, Spain.

Finally, this thesis is dedicated to my parents and to my sister Simona, the most important person in my life. Thanks for your care, love, encouragement and continuous support for all these years.

SUMMARY

Ischemic heart disease, the main cause of mortality and morbidity in industrialized countries, is a metabolic phenomenon due to an inadequate oxygenation of heart tissue caused by the closing or narrowing of the coronary arteries. However, the ischemic condition and the subsequent tissue reperfusion, lead to several functional and metabolic changes that globally define the so-called “ischemia/reperfusion injury”. This injury leads to metabolic and functional alterations, in particular due to the production of the Oxygen Reactive Species (ROS) that are able to promote cell damage. Because iron is involved in the ROS production by the Haber-Weiss-Fenton reaction, the aim of this study was to elucidate the molecular mechanisms underlying the iron metabolism during the cardiac ischemia/reperfusion. To this aim it has been analyzed the activity and the expression of the main proteins involved in iron homeostasis, such as the Iron Regulatory Proteins, Transferrin Receptor 1 (TfR1), and ferritin in an *in vivo* model of cardiac ischemia/reperfusion.

The results show that in rats hearts subjected to the ischemic/reperfusion injury, the activity of IRP1 was altered without changing its cellular content. The evaluation of the TfR1 levels showed an evident decrease of the expression of this protein during ischemia followed by a marked increase after the reperfusion phase, while regarding the ferritin expression it was observed a considerable decrease of the cytosolic levels of this protein only after the reperfusion phase.

Moreover, using rat cardiomyoblasts (H9c2 cell line) in an *in vitro* model of hypoxia and reoxygenation, it was evaluated the cellular levels of the “Labile Iron Pool” (LIP), showing a “free iron” increase after the reoxygenation phase, in accordance with the observed changes of the TfR1 and ferritin expression.

In addition, it was observed an increased ROS production after the hypoxia/reoxygenation damage and, using the iron chelator SIH (Salicylaldehyde Isonicotinoyl Hydrazone), it was showed that a significant part of these ROS depend by the higher levels of the LIP, strongly suggesting that iron is involved in the development of the cardiac damage induced by ischemia/reperfusion conditions.

Other aim of this study has been to evaluate the cytoprotective role of the cholesterol-lowering drug Simvastatin, during the ischemic/reperfusion injury, because of its anti-inflammatory and antioxidant effects (“pleiotropic effects”). Simvastatin, at concentration of 0,01 μ M, reduced the reactive nitrogen species levels and ROS productions in rat cardiomyoblasts (H9c2 cell line) subjected to hypoxia/reoxygenation conditions and also was able to reduce the cellular levels of the “Labile Iron Pool”, justifying the reduced production of the ROS and the resulting increased cell viability, observed after the drug treatment.

Moreover, Simvastatin increased the ferritin levels, in particular during hypoxia conditions, thus explaining the LIP reduction after treatment with this drug.

In conclusion, these results not only clarify the crucial role that iron plays in the progression of ischemic damage, but also show that proteins regulating the homeostasis of this metal, such as ferritin, may be a target of the Simvastatin, which could be used for the prevention of oxidative damage induced by cardiac ischemic conditions. Should this be the case, a new horizon as an antioxiodont opens for Simvastatin.

TABLE OF CONTENTS

ACKNOWLEDGMENTS	2
SUMMARY	3
I. INTRODUCTION	9
1.1 Anatomy of the heart	9
1.2 Heart functioning.....	12
1.3 Cardiac muscle tissue	14
1.4 The coronary circulation	17
1.5 The Coronary Artery Disease (CAD).....	19
1.6 Risk factors.....	20
1.7 Biochemical dysfunction in heart exposed to ischemia and reperfusion injury...	22
1.8 Metabolic changes in ischemia and reperfusion.....	22
1.9 The Reactive Oxygen Species (ROS)	26
1.10 The chemistry of ROS.....	27
1.11 ROS and antioxidant defense mechanisms	28
1.12 NO and Reactive Nitrogen Species (RNS).....	29
1.13 NO synthases and NO synthesis.....	30
1.14 Role of NO and NOS system in ischemia	31
1.15 Cell death: necrosis and apoptosis.....	32

1.15.1 Receptor-mediated death pathway	34
1.16 Cell response to ischemic injury: HIF-1 α	36
1.17 Role and pleiotropic effects of statins	38
1.18 The iron-heart disease connection	40
1.19 Iron toxicity	41
1.20 Biochemistry and physiology of iron	43
1.21 Dietary iron absorption.....	44
1.22 Regulation of systemic iron traffic: the role of hepcidin.....	46
1.23 Cellular iron up-take and role of Transferrin Receptor-1	48
1.24 Iron storage	51
1.25 The “Labile Iron Pool” (LIP)	53
1.26 The IRE/IRP regulatory sistem	54
1.26.1 Regulation of TfR and ferritin expression by IRPs	54
1.26.2 Expression of DMT1 and ferroportin is regulated by IRPs.....	56
1.26.3 Other IRE-containing mRNAs	56
1.27 IRPs: functional and structural features	59
1.28 Regulation of IRP1	62
1.29 Regulation of IRP2	63
II Aim of the study.....	65

III Materials and methods	68
3.1 Animals and <i>in vivo</i> ischemia/reperfusion model	68
3.2 Cell cultures and <i>in vitro</i> hypoxia/reoxygenation model	70
3.3 Preparation of cytosolic extracts	71
3.4 Western blot analysis.....	72
3.5 Electrophoretic Mobility-Shift Assay (EMSA).....	73
3.6 Cell viability assay (MTT)	73
3.7 Counting of viable and dead cells	74
3.8 Cellular energy status: dosage of ATP	76
3.9 Dosage of lactate dehydrogenase (LDH) release	77
3.10 Measurement of ROS	78
3.11 Lipid peroxidation assay (TBARS' test).....	79
3.12 Assessment of "Labile Iron Pool" (LIP)	80
3.13 Simvastatin activation by alkaline hydrolysis	82
3.14 Nitrites measurement.....	82
3.15 Statistical analysis	83
IV. Results	84
4.1 Validation of the <i>in vivo</i> model of ischemia.....	84
4.2 <i>In vivo</i> cardiac damage and <i>in vitro</i> cardiomyoblasts viability	86
4.3 Cellular death: necrosis or apoptosis?	89

4.4 Evaluation of oxidative stress.....	89
4.5 RNA-binding activity of IRPs.....	91
4.6 Ferritin and TfR1 expression.....	94
4.7 LIP evaluation in an <i>in vitro</i> model of hypoxia and reoxygenation conditions ...	97
4.8 <i>In vitro</i> Simvastatin effects on hypoxia/reoxygenation injury	100
4.8.1 Simvastatin cytotoxicity	101
4.8.2 Effects of Simvastatin on iNOS expression and NO production	102
4.8.3 Simvastatin effects on ROS production during hypoxia and reoxygenation conditions	104
4.8.4 Effect of Simvastatin on cell viability in the hypoxia/reoxygenation damage	105
4.8.5 Effects of Simvastatin on iron homeostasis	106
V. Discussion	109
VI. References.....	113

1. INTRODUCTION

1.1 Anatomy of the Heart

The **heart** is a myogenic muscular organ that is responsible for pumping blood throughout the blood vessels by repeated, rhythmic contractions. The heart is composed of cardiac muscle, which is an involuntary striated muscle tissue found only in this organ, and connective tissue. The average human heart, beating at 72 beats per minute, will beat approximately three billion times [Hamacher-Brady *et al.*, 2006] during an average 66 year lifespan, and weighs approximately 250 to 300 grams in females and 300 to 350 grams in males.

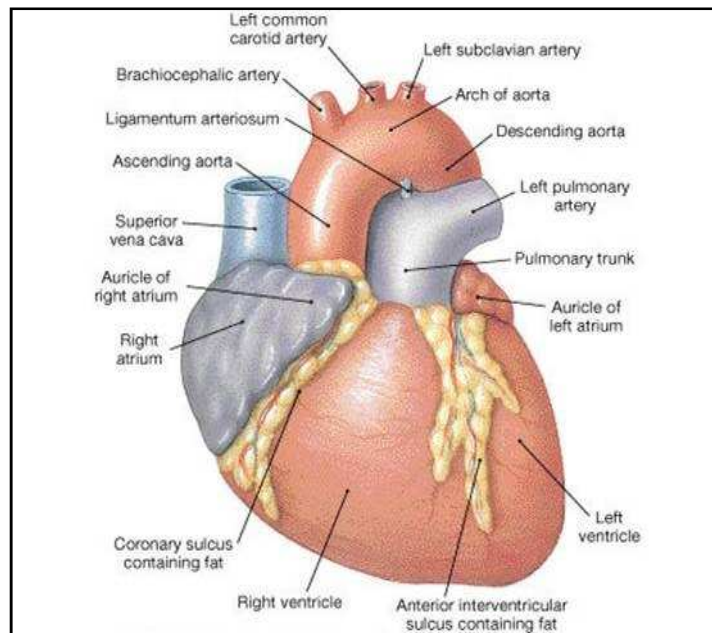


Figure 1. Human heart, anterior view.

The mammalian heart (figure 1) is derived from embryonic mesoderm germ-layer cells that differentiate after gastrulation into mesothelium, endothelium, and myocardium. Mesothelial pericardium forms the outer lining of the heart. The inner lining of the heart, lymphatic and blood vessels, develop from endothelium. Heart muscle is termed myocardium. In the human body, the heart is usually located in the mediastinum, situated in the middle of the thoracic cavity (figure 2), with the largest part of the heart slightly offset to the left, underneath the sternum. The heart is usually felt to be on the left side because the left heart (left ventricle) is stronger (it pumps to all body parts). The left lung is smaller than the right lung because the heart occupies more of the left hemithorax. The heart is fed by the coronary circulation and is enclosed by a sac known as the pericardium; it is also surrounded by the lungs. The pericardium comprises two parts: the fibrous pericardium, made of dense fibrous connective tissue, and a double membrane structure (parietal and visceral pericardium) containing a serous fluid to reduce friction during heart contractions.

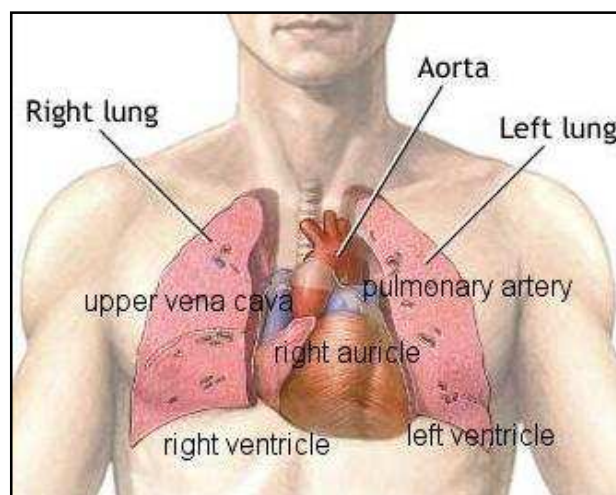


Figure 2. Position of the heart.

The outer wall of the human heart is composed of three layers. The outer layer is called the epicardium, or visceral pericardium since it is also the inner wall of the pericardium. The middle layer is called the myocardium and is composed of muscle which contracts. The inner layer is called the endocardium and is in contact with the blood that the heart pumps. Also, it merges with the inner lining (endothelium) of blood vessels and covers heart valves. The human heart is composed of four chambers, two superior atria and two inferior ventricles. The atria are the receiving chambers and the ventricles are the discharging chambers. The right ventricle discharges into the lungs to oxygenate the blood. The left ventricle discharges its blood toward the rest of the body via the aorta. The pathway of blood through the human heart consists of a pulmonary circuit and a systemic circuit. Blood flows through the heart in one direction, from the atria to the ventricles, and out of the great arteries, or the aorta for example. This is done by four valves (figure 3) which are the tricuspid valve, the mitral valve, the aortic valve, and the pulmonary valve.

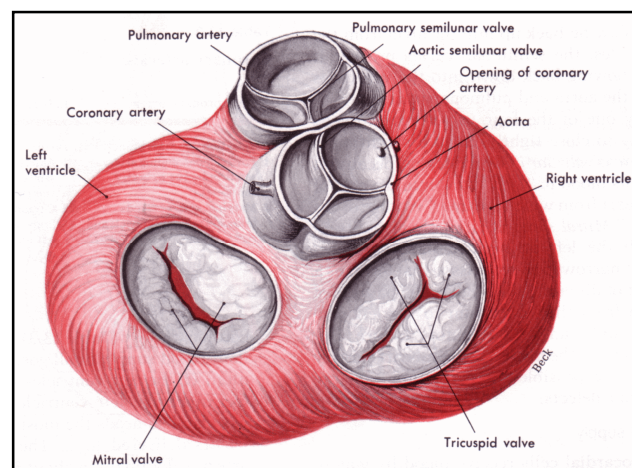


Figure 3. The valves of the heart viewed from above.

1.2 Heart functioning

In mammals, the function of the right side of the heart is to collect de-oxygenated blood, in the right atrium, from the body (via superior and inferior vena cavae) and pump it, through the tricuspid valve, via the right ventricle, into the lungs (pulmonary circulation) so that carbon dioxide can be dropped off and oxygen picked up (gas exchange). This happens through the passive process of diffusion. The left side, instead, collects oxygenated blood from the lungs into the left atrium. From the left atrium the blood moves to the left ventricle, through the bicuspid valve, which pumps it out to the body, via the aorta. In detail, starting in the right atrium, the blood flows through the tricuspid valve to the right ventricle. Here, it is pumped out the pulmonary semilunar valve and travels through the pulmonary artery to the lungs. From there, oxygenated blood flows back through the pulmonary vein to the left atrium. It then travels through the mitral valve to the left ventricle, from where it is pumped through the aortic semilunar valve to the aorta. The aorta forks and the blood is divided between major arteries which supply the upper and lower body. The blood travels in the arteries to the smaller arterioles and then, finally, to the tiny capillaries which feed each cell. The deoxygenated blood then travels to the venules, which coalesce into veins, then to the inferior and superior venae cavae and finally back to the right atrium where the process began (figure 4).

The heart is effectively a syncytium, a meshwork of cardiac muscle cells interconnected by contiguous cytoplasmic bridges. This relates to electrical stimulation of one cell spreading to neighboring cells. Some cardiac cells are self-excitabile, contracting without any signal from the nervous system. Each of these cells have their own intrinsic contraction rhythm.

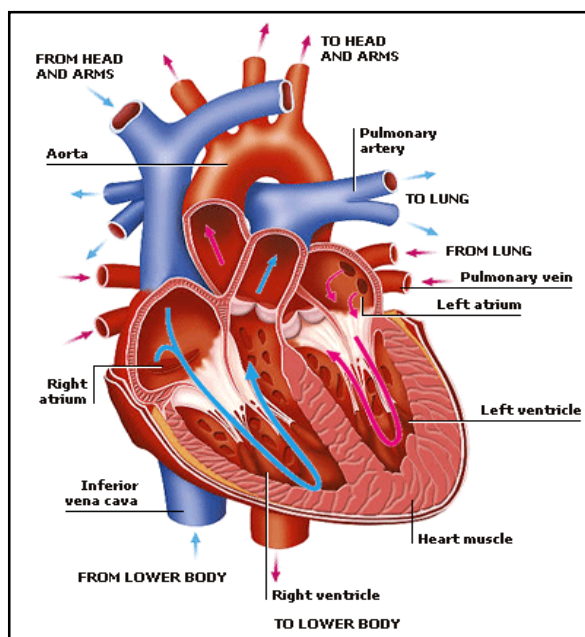


Figure 4. Illustration of normal blood flow through the heart.

A region of the human heart called the **sinoatrial node**, or pacemaker, sets the rate and timing at which all cardiac muscle cells contract. The SA node generates electrical impulses, much like those produced by nerve cells. Because cardiac muscle cells are electrically coupled by inter-calated disks between adjacent cells, impulses from the SA node spread rapidly through the walls of the atria, causing both atria to contract in unison. The impulses also pass to another region of specialized cardiac muscle tissue, a relay point called the **atrioventricular node**, located in the wall between the right atrium and the right ventricle. Here, the impulses are delayed for about 0.1s before spreading to the walls of the ventricle. The delay ensures that the atria empty completely before the ventricles contract. Specialized muscle fibers called Purkinje fibers then conduct the signals to the apex of the heart along and throughout the ventricular walls. The Purkinje fibres form conducting pathways called bundle branches (figure 5).

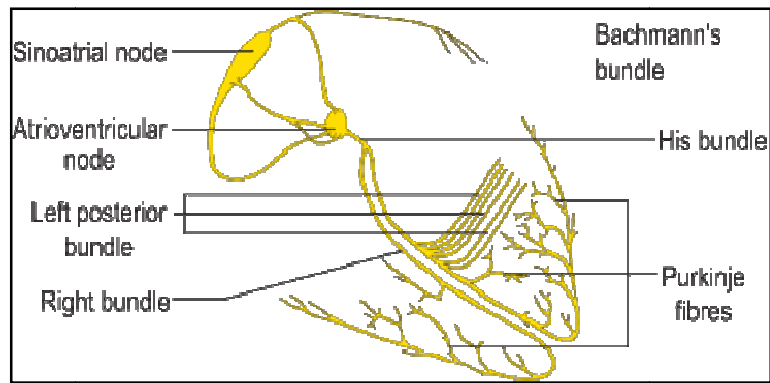


Figure 5. The conduction system of the heart.

This entire cycle, a single heart beat, lasts about 0.8 seconds. The impulses generated during the heart cycle produce electrical currents, which are conducted through body fluids to the skin, where they can be detected by electrodes and recorded as an electrocardiogram (ECG or EKG).

The events related to the flow or blood pressure that occurs from the beginning of one heartbeat to the beginning of the next can be referred to a cardiac cycle [Martini et al., Human Anatomy, 6th edition].

1.3 Cardiac muscle tissue

Cardiac muscle cells, also called *cardiomyocytes*, are relatively small, averaging 10–20 μm in diameter and 50–100 μm in length. A typical cardiac muscle cell (figure 6) has a single, centrally placed nucleus, although a few may have two or more. As the name implies, cardiac muscle tissue is found only in the heart.

As the skeletal muscle fibers, each cardiac muscle cell contains organized myofibrils, and the presence of many aligned sarcomeres gives it striations.

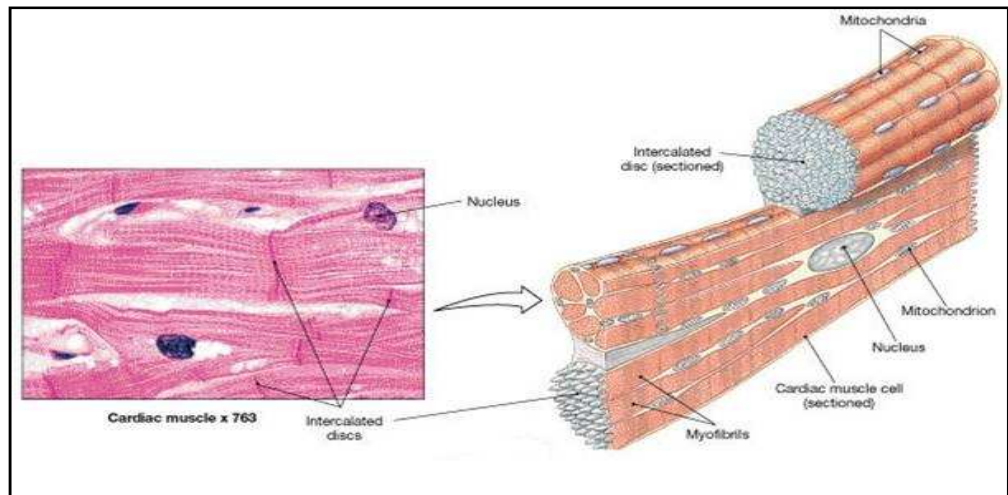


Figure 6. Schematic structure of cardiac muscle cell.

However, cardiac muscle cells are much smaller than skeletal muscle fibers, and significant structural and functional differences exist between the two types of cells.

Structural Differences:

- The T tubules in a cardiac muscle cell are short and broad, and there are no triads. The T tubules encircle the sarcomeres at the Z lines rather than at the zone of overlap.
- The SR of a cardiac muscle cell lacks terminal cisternae, and its tubules contact the cell membrane as well as the T tubules. As in skeletal muscle fibers, the appearance of an action potential triggers calcium release from the SR and the contraction of sarcomeres; it also increases the permeability of the sarcolemma to extracellular calcium ions.
- Cardiac muscle cells are almost totally dependent on aerobic metabolism to obtain the energy needed to continue contracting. The sarcoplasm of a cardiac

muscle cell thus contains large numbers of mitochondria and abundant reserves of myoglobin (to store oxygen). Energy reserves are maintained in the form of glycogen and lipid inclusions.

- Each cardiac muscle cell contacts several others at specialized sites known as **intercalated discs** that plays a vital role in the function of cardiac muscle. At an intercalated disc, the cell membranes of two adjacent cardiac muscle cells are extensively intertwined and bound together by gap junctions and desmosomes. These connections help stabilize the relative positions of adjacent cells and maintain the three-dimensional structure of the tissue. The gap junctions allow ions and small molecules to move from one cell to another. This arrangement creates a direct electrical connection between the two muscle cells. An action potential can travel across an intercalated disc, moving quickly from one cardiac muscle cell to another.

Functional Differences:

- Cardiac muscle tissue contracts without neural stimulation. This property is called **automaticity**.
- The timing of contractions is normally determined by specialized cardiac muscle cells called **pacemaker cells**.
- Innervation by the nervous system can alter the pace established by the pacemaker cells and adjust the amount of tension produced during a contraction.
- Cardiac muscle cell contractions last roughly 10 times longer than do those of skeletal muscle fibers. Myofibrils in the two interlocking muscle cells are firmly anchored to the membrane at the intercalated disc. Because their myofibrils are essentially locked together, the two muscle cells can "pull together" with

maximum efficiency. Because the cardiac muscle cells are mechanically, chemically, and electrically connected to one another, the entire tissue resembles a single, enormous muscle cell. For this reason, cardiac muscle has been called a *functional syncytium*.

1.4 The coronary circulation

The heart works continuously, and cardiac muscle cells require reliable supplies of oxygen and nutrients. The coronary circulation supplies blood to the muscle tissue of the heart. During maximum exertion, the demand for oxygen rises considerably. The blood flow to the myocardium may then increase to nine times that of resting levels. The coronary circulation includes an extensive network of coronary blood vessels. The left and right coronary arteries originate at the base of the ascending aorta, at the aortic sinuses. Blood pressure here is the highest in the systemic circuit. Each time the left ventricle contracts, it forces blood into the aorta. The arrival of additional blood at elevated pressures stretches the elastic walls of the aorta, and when the left ventricle relaxes, blood no longer flows into the aorta, pressure declines, and the walls of the aorta recoil. This recoil, called *elastic rebound*, pushes blood both forward, into the systemic circuit, and backward, through the aortic sinus and then into the coronary arteries. Thus, the combination of elevated blood pressure and elastic rebound ensures a continuous flow of blood to meet the demands of active cardiac muscle tissue.

The right coronary artery, which follows the coronary sulcus around the heart, supplies blood to the right atrium, portions of both ventricles, and portions of

the conducting system of the heart, including the *sinoatrial (SA)* and *atrioventricular (AV) nodes*. The cells of these nodes are essential to establishing the normal heart rate. Inferior to the right atrium, the right coronary artery generally gives rise to one or more marginal arteries, which extend across the surface of the right ventricle.

The left coronary artery supplies blood to the left ventricle, left atrium, and interventricular septum. As it reaches the anterior surface of the heart, it gives rise to a circumflex branch and an anterior interventricular branch. The circumflex artery curves to the left around the coronary sulcus, eventually meeting and fusing with small branches of the right coronary artery. The much larger anterior interventricular artery, or *left anterior descending artery*, swings around the pulmonary trunk and runs along the surface within the anterior interventricular sulcus. The anterior interventricular artery supplies small tributaries continuous with those of the posterior interventricular artery. Such interconnections between arteries are called arterial anastomoses.

Because the arteries (figure 7) are interconnected in this way, the blood supply to the cardiac muscle remains relatively constant despite pressure fluctuations in the left and right coronary arteries as the heart beats.

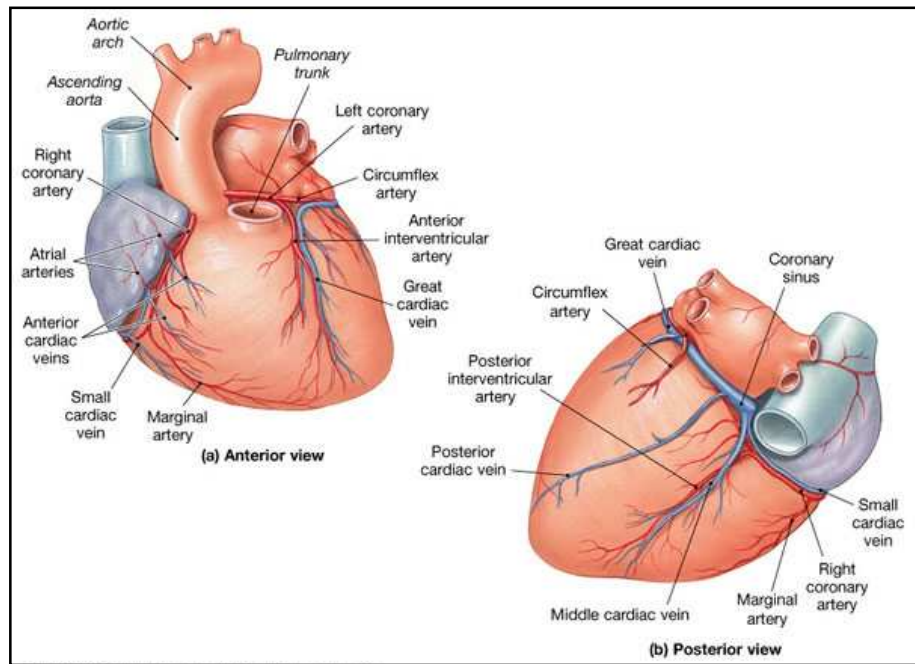


Figure 7. Coronary arteries. (a) anterior view; (b) posterior view.

1.5 The Coronary Artery Disease (CAD)

The Coronary Artery Disease (CAD) is the most common type of heart disease [Kumar, Abbas, Fausto: Robbins and Cotran Pathologic Basis of Disease, 7th Ed.]. It's the principal cause of death in the developed Countries. Only in the United States, each year, more than half a million Americans die from CAD. The term **coronary artery disease** refers to areas of partial or complete blockage of coronary circulation. Such reduced circulatory supply, known as **coronary ischemia**, generally results from partial or complete blockage of the coronary arteries that supply the heart muscle with oxygen-rich blood. The usual cause is the formation of a fatty deposit, or *plaque*, in the wall of a coronary vessel. The plaque (that is made up of fat, cholesterol, calcium, and other substances found in the blood) or an associated thrombus (clot), then

narrows the passageway and reduces blood flow to the heart muscle. Blood clots can partially or completely block blood flow. When the coronary arteries are narrowed or blocked, oxygen-rich blood can't reach the heart muscle, causing angina or a heart attack (figure 8).

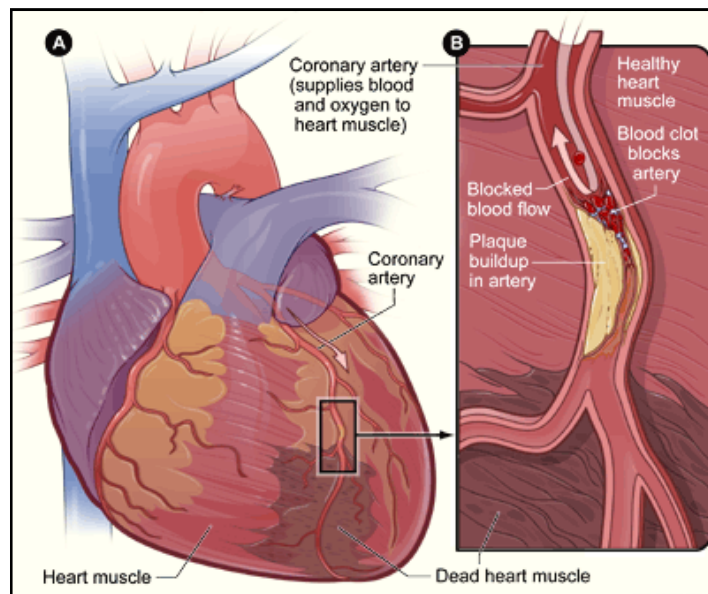


Figure 8. **A** is an overview of a heart and coronary artery showing damage (dead heart muscle) caused by a heart attack. **B** is a cross-section of the coronary artery with plaque buildup and a blood clot.

1.6 Risk factors

Many factors raise the risk of developing CAD. [Bhalli *et al.*, 2011; Poulter, 2003]

- Blood cholesterol levels. The ATP III study indicates as high a level of cholesterol > 240 mg/dL and such as high a level LDL cholesterol > 160 mg/dL.
- High blood pressure. Blood pressure is considered high if it stays at or above 140/90 mmHg over a period of time.

- Smoking. This can damage and tighten blood vessels, raise cholesterol levels, and raise blood pressure.
- Insulin resistance. This condition occurs when the body can't use its own insulin properly. Insulin is a hormone that helps move blood sugar into cells where it's used.
- Diabetes.
- Overweight or obesity.
- Metabolic syndrome. Metabolic syndrome is the name for a group of risk factors linked to overweight and obesity that raise your chance for heart disease and other health problems, such as diabetes and stroke.
- Lack of physical activity. Lack of activity can worsen other risk factors for CAD.
- Genetic or lifestyle factors cause plaque to build in the arteries as the age.
 - In men, the risk for CAD increases after age 45.
 - In women, the risk for CAD risk increases after age 55.
- Family history of early heart disease. The risk increases if the father or a brother was diagnosed with CAD before 55 years of age, or if the mother or a sister was diagnosed with CAD before 65 years of age.
- High levels of a protein called C-reactive protein (CRP) in the blood may raise the risk for CAD and heart attack. High levels of CRP are proof of inflammation in the body. Inflammation is the body's response to injury or infection. Damage to the arteries inner walls seems to trigger inflammation and help plaque grow. [*Abd et al., 2011*]

1.7 Biochemical dysfunction in heart exposed to ischemia and reperfusion injury

Heart tissue is remarkably sensitive to oxygen deprivation. Although heart cells, like those of most tissues, rapidly adapt to anoxic conditions, the ischemia and subsequent reperfusion lead to extensive tissue death during cardiac infarction [Solaini and Harris, 2005].

Two distinct types of damage occur to the heart: ischemic injury and reperfusion injury. The first results from the initial loss of blood flow and the second upon the restoration of oxygenated blood flow.

The heart can tolerate a brief exposure to ischemia as the inherent mechanisms to preserve energy levels prevent injury. These include switching the metabolism to anaerobic glycolysis and fatty acid utilization, increasing glucose uptake, and decreasing contractility.

If ischemia persists, the myocardium can develop a severe ATP deficit, which results in irreversible injury and culminates in cell death (ischemia/reperfusion injury) [Budas et al., 2007].

1.8 Metabolic changes in ischemia and reperfusion

Cardiac muscle, under normal conditions, obtains virtually all its energy from oxidative metabolism, showed in figure 9A.

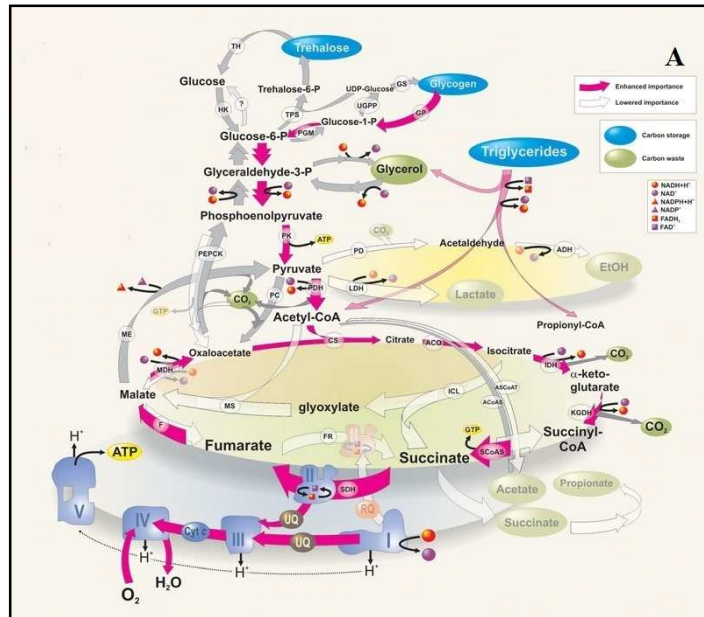


Figure 9 A. Schematic aerobic metabolism.

During hypoxia or ischaemia, the supply of O_2 to the respiratory chain fails. Non-esterified fatty acid levels rise, probably as a result of lipid breakdown rather than the concomitant cessation of fatty acid oxidation. The tricarboxylic acid cycle is blocked, and no energy is available from oxidative phosphorylation. This leads to an accumulation of cytoplasmic NADH, with the NADH/NAD⁺ ratio increasing several fold. In anoxia, ATP levels can still be maintained by glycolysis, but in ischaemia this is accompanied by an accumulation of lactate and a decrease in cytoplasmic pH (5.5–6 after 30 min of ischaemia), and glycolysis is also inhibited. The energy charge of the cardiomyocyte during ischaemia has been well investigated. Typically, creatine phosphate concentration falls precipitately (to less than 10% after 10 min of ischaemia), reflecting a sharp increase in free [ADP]. ATP levels fall rather more slowly, with 40–50% of [ATP] remaining after 30 min of ischemia (figure 9B).

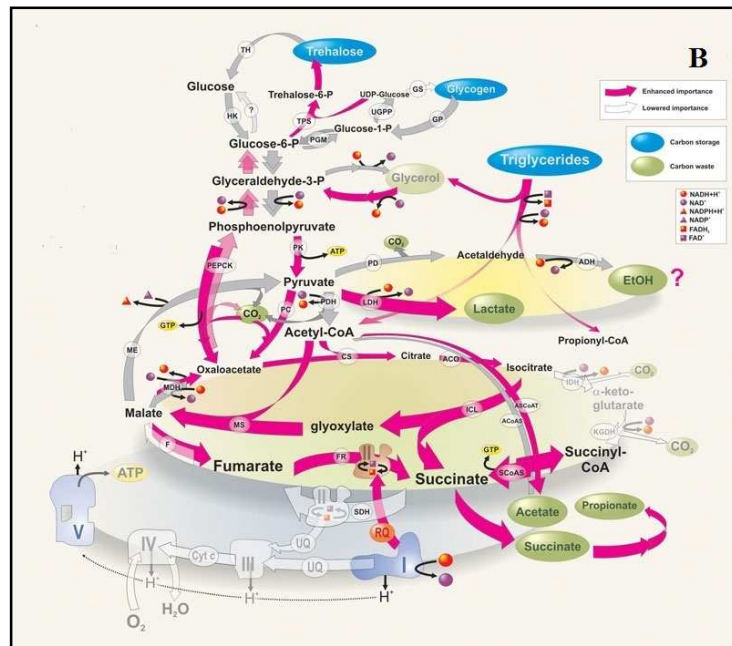


Figure 9 B. Schematic microaerobic metabolism (hypoxia).

During ischemia, the levels of total pyridine nucleotides seem to be roughly maintained, although there have been reports of significant loss (up to 30%) of total nucleotides from the cell. Their redox state, however, changes markedly, with [NADH] increasing sharply (as described above) [Ceconi *et al.*, 2000]. The cytoplasmic [NADPH], in contrast, declines by approx. 30%, resulting in a significant decrease in the NADPH/NADP⁺ ratio. While at first this may appear surprising, the fall in [NADPH] could be due to the action of glutathione reductase, which is particularly active under conditions of oxidative stress. In addition, a contributory effect may come from the activation of aldose reductase, a member of the ald-keto reductase family that utilizes NADPH to reduce carbonyl compounds, including glucose, in the metabolism of polyols. Inhibition of this enzyme promotes glycolysis and improves recovery from ischemia.

The ionic content of the sarcoplasm also changes markedly in ischemia. Owing

to low [ATP], the sarcolemmal Na^+/K^+ -ATPase and the sarcoplasmic reticulum Ca^{2+} -ATPase become ineffective, and cytoplasmic $[\text{Na}^+]$ and $[\text{Ca}^{2+}]$ rise [Piper *et al.*, 2004]. Prolonged lack of mitochondrial oxidation will lead to abolition of $\Delta\mu_{\text{H}^+}$, and this leads to (i) a decreased activity of the mitochondrial Ca^{2+} uniport, with decreased uptake of Ca^{2+} into mitochondria, and (ii) the operation of the ATP synthase, in reverse, as an ATPase. This ATPase activity is thought to contribute significantly (35–50%) to ATP loss in ischemia.

Over longer periods of ischemia, DNA and protein synthesis are suppressed [Casey *et al.*, 2002], although some specific proteins e.g. HSP (heat-shock protein) 70, PKC (protein kinase C) ϵ , and iNOS (inducible nitric oxide synthase) may be induced [Damy *et al.*, 2003; Ping *et al.*, 2002].

On reperfusion, electron transfer and ATP synthesis restart, and the internal cytoplasmic pH is restored to 7. However, this leads in some way to a further deterioration of cell function. While ATP and creative phosphate levels recover to some extent, the myocytes undergo further shortening (hypercontracture) and membrane damage, followed by cell death [Piper *et al.*, 2004]. Many explanations for this deterioration are linked to abnormal Ca^{2+} movements. $[\text{Ca}^{2+}]_{\text{c}}$ rises further, as indicated by hypercontracture probably because of the reverse of the normal direction of the sarcolemmal $\text{Na}^+/\text{Ca}^{2+}$ exchanger. This increased cytoplasmic Ca^{2+} , coupled with the restoration of mitochondrial membrane potential, leads to the accumulation of mitochondrial Ca^{2+} via the electrophoretic uniport, which has highly deleterious effects on mitochondrial function [Solaini and Harris, 2005]. However it is widely accepted that in the ischemia/reperfusion injury the overproduction of ROS is the main source of cell damage. It might be expected that ischemia, caused by low partial pressure

of O₂, would decrease ROS production, but this is paradoxically increased, with a further increase occurring on reperfusion. Cardiac ischemia, therefore, induces ROS production and subsequent reperfusion can result in toxic ROS overproduction that damages mitochondrial function and thus impaired recovery of physiological function and cell death [Misra *et al.*, 2009].

1.9 The Reactive Oxygen Species (ROS)

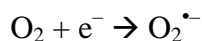
Oxidative stress induced by Reactive Oxygen Species (ROS) is considered to play an important role not only in the etiology of stroke, but also in the onset and development of cardiac damage following ischemia and reperfusion [Bordoni *et al.*, 2005]. ROS activity in the vessel wall, for example, is thought to contribute to the formation of oxidized LDL, a major contributor to the pathogenesis of atherosclerosis and is also involved in vessel plaque rupture, initiating coronary thrombosis and occlusion [Giordano, 2005]. Cell damage, instead, can occur through mechanisms involving:

- DNA alterations. ROS can contribute to mutagenesis of DNA by inducing strand breaks, purine oxidation, and inducing alterations in chromatin structure that may significantly affect gene expression;
- covalent modification of protein (particularly on –SH groups);
- lipid peroxidation, that damages membranes and profoundly affects membrane-associated proteins, including enzymes, receptors, and transporters, altering cell membrane properties.

These events may lead to the oxidative destruction of the cell.

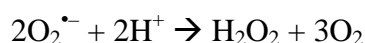
1.10 The chemistry of ROS

Free radicals can be formed in a molecule by gaining an additional electron, for example in the reduction of molecular oxygen (O_2) to the superoxide anion radical ($O_2^{\bullet-}$):

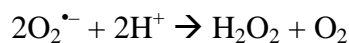


The superoxide ($O_2^{\bullet-}$) produced during the first reaction is a short-lived ROS ($\sim 2\text{--}4 \mu\text{s}$) and readily diffusible. In the cellular environment, $O_2^{\bullet-}$ may cause lipid peroxidation, thus weakening cell membrane. The most important free radicals in biological systems are derivatives of oxygen. The complete reduction of O_2 by the univalent pathway results in the formation of superoxide, anion hydrogen peroxide (a relatively long-lived and stable form of ROS) and other products such as triplet O_2 ($3O_2$), singlet O_2 , hydroxyl radical ($\bullet OH$), and hydrogen radical ($H\bullet$), as shown below:

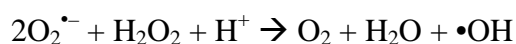
SOD



Spontaneous



Metal catalyst



Hydrogen peroxide is an oxidizing agent, but not especially reactive. It can diffuse through membranes and can therefore reach cellular components distant

from its site of synthesis. Its main significance lies in its being a source of hydroxyl radicals. In the absence of metal catalysts, superoxide and hydrogen peroxide are readily removed and are virtually harmless.

The hydroxyl radical is an extremely reactive oxidizing radical that will react with most biomolecules at diffusion-controlled rates and is therefore the most harmful form of ROS [Misra *et al.*, 2009].

1.11 ROS and antioxidant defense mechanisms

In the heart, mitochondria are the principal source of ROS, as the respiratory chain deals with most of the electrons potentially capable of reducing O₂.

The redox components of the respiratory chain have also been shown to produce ROS. Complexes I, and III are impaired during ischemia/reperfusion and may be considered as a major site of ROS production during ischemia [Gao *et al.*, 2008].

Cells are equipped with excellent antioxidant defense mechanisms to detoxify the harmful effects of ROS, i.e. superoxide (O₂^{•-}), H₂O₂, and hydroxyl radical (•OH). The antioxidant defenses can be non-enzymatic (e.g. glutathione, vitamins C, A, E, and thioredoxin) or enzymatic (e.g. superoxide dismutase, catalase glutathione peroxidase, and glutathione reductase).

In the mitochondrial matrix, most O₂^{•-} is dismutated by manganese-superoxide dismutase (MnSOD) to H₂O₂, which readily diffuses through mitochondrial membranes. Some of the O₂^{•-} goes to the cytoplasm and is converted into H₂O₂ by itself or after interaction with copper superoxide dismutase (CuSOD). The resultant H₂O₂ is removed by catalase, glutathione peroxidase and peroxiredoxin.

Overall, oxidative damage will occur only in situations in which the defense mechanisms are deficient or the production of ROS exceeds the capability of the defense mechanisms to handle them or a combination of both, than a fine balance between oxygen free radicals and a variety of endogenous antioxidants is crucial for avoiding myocardial injury [Misra et al., 2009].

1.12 NO and Reactive Nitrogen Species (RNS)

An important role in the ischemia/reperfusion injury is played by nitric oxide. NO, by virtue of its unpaired outer shell electron, is a reactive molecule. This molecule is an endogenous mediator of several important physiological processes, and it is very important in the heart tissue.

NO, indeed, does react and interact with ROS, and this crosstalk can also have significant effects on cardiac function.

NO can mediate the *S*-nitrosylation of proteins at specific cysteine residues. This process also occurs in the heart and has significant functional implications, especially with regard to calcium flux and excitation-contraction coupling.

S-nitrosylation is facilitated by $O_2^{\bullet-}$ when $O_2^{\bullet-}$ is present at “physiologic” levels. When levels of $O_2^{\bullet-}$ increase, however, it becomes inhibitory to normal *S*-nitrosylation. Increased $O_2^{\bullet-}$ levels also facilitate interaction of $O_2^{\bullet-}$ with NO to form deleterious reactive molecules, including peroxynitrite (ONO_2^-).

Thus, at an optimal NO/ $O_2^{\bullet-}$ stoichiometry, the crosstalk between these two reactive species facilitates essential cellular processes, a relationship termed nitroso-redox balance. In the African American Heart Failure Trial, combined therapy with hydralazine, a vasodilator that inhibits generation of $O_2^{\bullet-}$ and isosorbide dinitrate improved quality-of life scores and decreased mortality by

approximately 45% in African Americans with severe heart failure.

A compelling argument has been made that the effectiveness of this therapy is due in part to restoration of nitroso-redox balance [Taylor et al., 2004].

1.13 NO synthases and NO synthesis

Nitric oxide (NO) plays an important role in maintaining cardiovascular homeostasis through multiple biological actions [Tsutsui et al., 2009].

NO is formed from its precursor L-arginine by a family of NO synthases (NOSs) with stoichiometric production of L-citrulline, as shown in the figure 10.

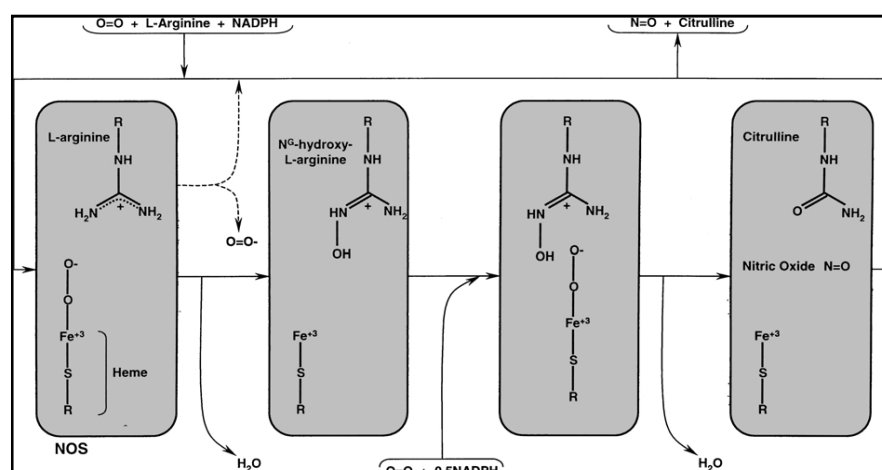


Figure 10. NO synthesis by Nitric Oxide Synthase (NOS).

The NOS system consists of three distinct isoforms, including neuronal (nNOS or NOS-1), inducible (iNOS or NOS-2), and endothelial NOS (eNOS or NOS-3) [Shimokawa and Tsutsui, 2010]. The NOS enzymes contain a NADPH-dependent cytochrome P-450 reductase motif at the C-terminus. The NOS C-terminus shuttles electrons from NADPH to FAD, FMN and then to a heme-

coordinated iron (Fe^{3+}) within the NOS N-terminal oxygenase domain. While the activities of the C and N-terminals may be functionally independent, the conversion of L-arginine to NO requires both domains and homodimerization through a N-terminal interface, requiring heme and stabilized by BH4 (tetrahydrobiopterin), L-arginine, and Zinc. The reaction catalyzed by the N-terminus proceeds via a stable intermediate, and thus consists of at least two steps. The first step involves binding of oxygen (O_2) to the heme moiety, and oxidation of a guanido N molecule of L-arginine to form NG-hydroxy-L-arginine. A second O_2 molecule is then combined with this intermediate leading to the production of NO and citrulline [Mungrue *et al.*, 2002].

1.14 Role of NO and NOS system in Ischemia

It was demonstrated that nNOS and eNOS are constitutively expressed mainly in the nervous system and the vascular endothelium, respectively, synthesizing a small and physiological amount of NO in a calcium-dependent manner both under basal conditions and upon stimulation, whereas iNOS is induced by several proinflammatory stimuli, producing a greater amount of NO in a calcium independent manner [Shimokawa and Tsutsui, 2010].

Several data show a decreased expression of eNOS during ischemia in contrast to an increased iNOS expression in cardiomyocytes in several heart disease, as ischemia, and in the development of heart failure [Di Napoli *et al.*, 2001].

The high levels of NO produced by iNOS, indeed, can interact with $\text{O}_2^{\bullet-}$ to form peroxynitrite, a potent mediator of cell damage [Pacher *et al.*, 2007].

1.15 Cell death: necrosis and apoptosis

Depending on the extent and duration of the ischemic loss, cardiomyocytes may die by necrosis or apoptosis [Vohra *et al.*, 2005]. Necrosis and apoptosis are characterized by distinct biochemical, morphological and functional changes, shown in figure 11.

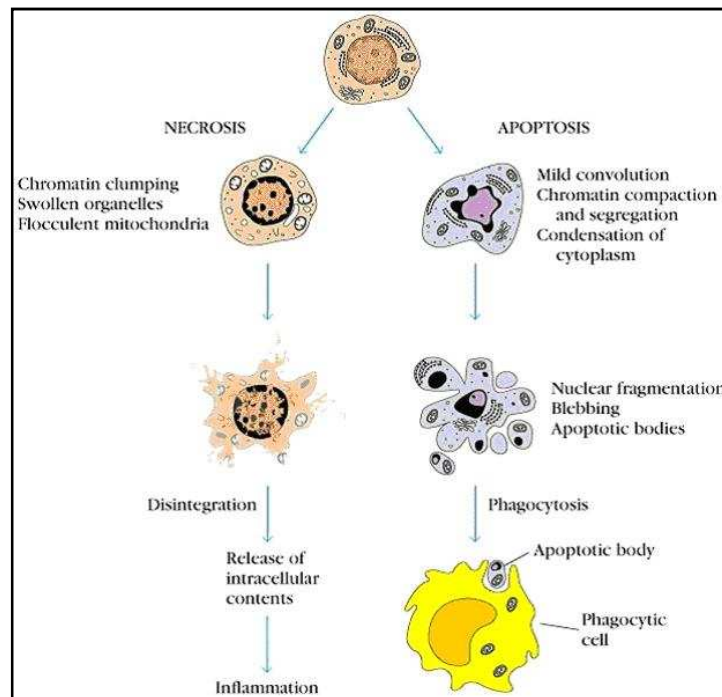


Figure 11. Difference between Necrosis and Apoptosis.

Necrosis is a rapid process that leads to destruction of subcellular and nuclear components. In particular, necrosis causes the loss of the cell membranes and nucleus integrity, with consequent release of their contents, up to cell lysis and nonspecific degradation of DNA and provokes an inflammatory response with cytokine release by macrophages. Morphologically nucleus and cytoplasm of necrotic cell are darkest and more wrinkled, and plasma and nuclear membranes are irregular. During necrosis the cell dimensions are significantly increased for

the presence in the cytoplasm of large vacuoles, some of which are swollen mitochondria. In contrast, apoptosis (also termed programmed cell death) is a highly regulated, genetically determined mechanism that does not provoke an inflammatory response. Apoptosis plays a role in pathophysiological conditions but is also essential in normal tissue homeostasis, allowing the organ or tissue to rid itself of cells which are dysfunctional or no longer needed. Apoptotic cell death is characterized by cell shrinkage, membrane blebbing, and nuclear condensation and degradation. The cell is eventually broken into small membrane-enclosed pieces (apoptotic bodies), which in vivo are removed by macrophages, or taken up by neighboring cells. This prevents the release of cellular compounds and thus ensures that an inflammatory response is not provoked [Hamacher-Brady *et al.*, 2006]. Apoptosis is mediated by two central pathways, the receptor-mediated (extrinsic) and the mitochondrial (intrinsic) pathway [Crow *et al.*, 2004] both of which are depicted in figure 12.

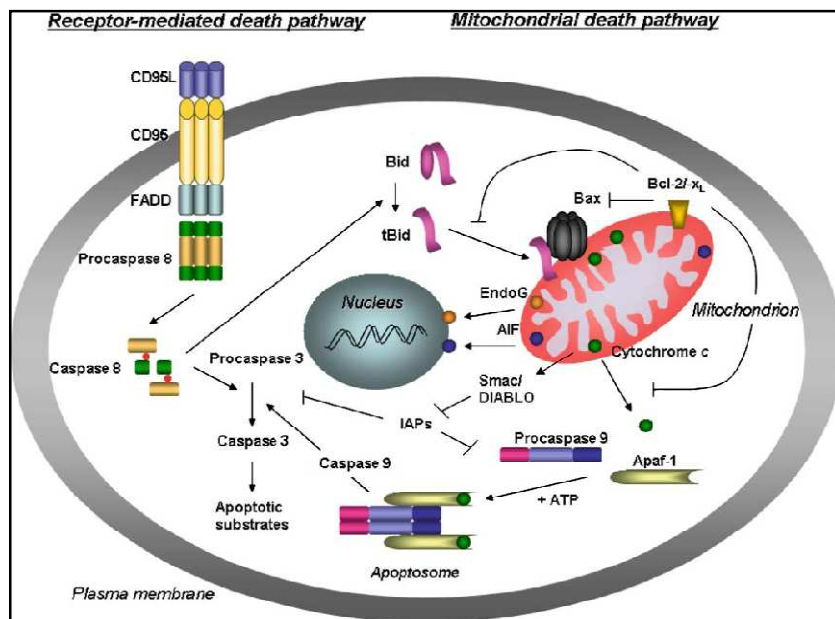


Figure 12. Schematic representation of extrinsic and intrinsic apoptotic pathways.

So-called caspases, a family of cysteine aspartate proteases, are the main effectors of, and allow for crosstalk between, both pathways [*Stennicke and Salvesen, 2000*]. Caspases are synthesized as inactive precursors and generally activated by proteolytic cleavage of the procaspase form to the catalytically active heterotetramer [*Shi, 2002*].

1.15.1 Receptor-mediated and mitochondrial death pathways

The receptor-mediated (extrinsic) pathway is initiated by the binding of a death ligand (e.g., CD95/Fas ligand, TNF- α) to its cognate cell surface death receptor (e.g., CD95/Fas, TNF- α receptor) [*Schmitz et al., 2000*]. Consequently, death adapter molecules such as FADD (Fas-associated death domain) and TRADD (TNF receptor-associated death domain) form homotrimers which are recruited to the cytoplasmic tail of the death receptor through interactions between “death domains” present in both proteins. Subsequently, procaspase 8 is recruited to the complex, resulting in proximity-induced processing. Once activated, caspase 8 initiates the apoptotic cascade via processing of downstream effector caspases such as caspase 3, as well as the proapoptotic Bcl-2 family member, Bid, leading to the death of the cell [*Hamacher-Brady et al., 2006*].

Under pathophysiological conditions (e.g., enhanced oxidative stress and/or calcium overload) mitochondria participate in the apoptotic pathway [*Desagher and Martinou, 2000*]. Death signals transmitted to the mitochondria lead to the release of pro-apoptotic proteins from the mitochondrial intermembrane space to the cytosol, through pathways which are still subject to investigation.

The majority of studies focused on the release of cytochrome c, which normally

functions as part of the mitochondrial electron transport chain. Two main models have been proposed to describe the mechanism(s) of cytochrome c release to the cytosol. The first model describes a non-specific mode of release in which opening of the mitochondrial permeability transition pore (MPTP) leads to the swelling of mitochondria due to the osmotic influx of water into the protein- and metabolite-dense mitochondrial matrix. The highly convoluted inner mitochondrial membrane is able to expand while the outer mitochondrial membrane ruptures, releasing cytochrome c into the cytosol [*Hamacher-Brady et al., 2006*].

The second model describes specific modes of release, where Bcl-2 family proteins form pores either directly via oligomerization, regulate the pore size of pre-existing pores, or indirectly by causing membrane instability which gives rise to lipidic pores. In the cytosol, cytochrome c binds to Apaf1 (apoptotic protease activating factor 1) and in the presence of dATP, procaspase 9 is recruited to the complex, now termed the apoptosome, leading to the activation of procaspase 9 [*Acehan et al., 2002*]. Activated caspase 9 can activate downstream effector caspases, and thus determine the cell to death. Cytochrome c-dependent activation of caspase 9 is supported by Smac/DIABLO which is likewise released from the mitochondrial intermembrane space and removes the anti-apoptotic activity of IAPs (inhibitor of apoptosis proteins) [*Verhagen et al., 2000*]. In addition, mitochondria release endonuclease G and AIF (apoptosis-inducing factor) which translocate to the nucleus and promote chromatin condensation and large-scale DNA fragmentation [*Sharpe et al., 2004*].

1.16 Cell response to ischemic injury: HIF-1 α

In mammalian cells, many compensatory mechanisms occur in response to changes in oxygen tension. Until recently, the means by which cells sense alterations in oxygen tension remained relatively obscure.

The first insight into an oxygen-sensing pathway in higher organisms came with the discovery of a family of oxygen-dependent enzymes responsible for the regulation of the hypoxia-inducible transcription factors (HIFs), that are activated by hypoxia. The HIF transcription factors are composed of two subunits: the hypoxia-regulated alpha subunit HIF-1 α (or its homologs, HIF-2 α and HIF-3 α), and the oxygen insensitive HIF-1 β subunit (also known as the aryl-hydrocarbon receptor nuclear translocator, or ARNT). Under normal oxygen conditions (normoxia), HIF-1 α is constitutively expressed. However, this subunit is rapidly targeted for proteasome-mediated degradation through a protein-ubiquitin ligase complex containing the product of the von Hippel Lindau tumor suppressor protein (pVHL). Recently, it has been reported that degradation of HIF-1 α under normoxic conditions is triggered by post-translational hydroxylation of conserved proline residues within a polypeptide region known as the oxygen-dependent degradation domain (ODD). The hydroxylated proline residues in this sequence are recognized by pVHL, leading to subsequent HIF-1 α degradation via the ubiquitin ligase pathway (figure 12). This modification is inherently oxygen-dependent, because the oxygen atom of the hydroxyl group is derived from molecular oxygen. Moreover, this reaction requires cofactors such as vitamin C, 2-oxoglutarate, and iron. The requirement of this last cofactor suggests that the oxygen-sensing factor is iron-dependent. Thus, this critical regulatory event is carried out by a family of iron (II)-

dependent dioxygenase prolyl hydroxylase enzymes that use O_2 as a substrate to catalyze hydroxylation of the target proline residues. Under hypoxic conditions, degradation of HIF-1 α is prevented, and thus HIF-1 α is able to accumulate within the nucleus allowing it to bind with its partner HIF-1 β . In addition to the ODD domain, the HIF-1 α subunit isoforms contain two transactivation domains responsible for recruiting transcriptional coactivators essential for gene expression, the N-terminal transactivation domain (NTAD), which overlaps the ODD and the C-terminal transactivation domain (C-TAD), which is able to recruit coactivator complexes such as p300/CBP only under hypoxic conditions (figure 13).

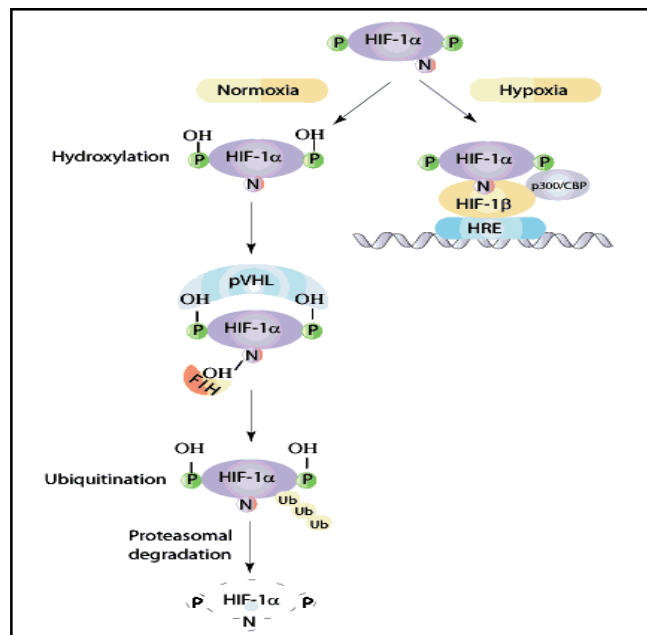


Figure 13. The scheme shows the HIF-1 α activation during hypoxia and the degradation pathway in normoxic conditions.

The C-TAD activity is also regulated by an oxygen-dependent hydroxylation event; however, in this case, the targeted residue appears not to be a proline but rather a conserved asparagine residue.

The heterodimeric complex thus formed, is able to recognize HIF-responsive elements (HREs) transactivating downstream target genes involved in the longer-term response to hypoxia. In particular is activated the transcription of erythropoietin (EPO), involved in erythropoiesis, and VEGF (vascular endothelial growth factor), implicated in angiogenesis/vasculogenesis, allowing an increase of oxygen delivery; on the other side, the HIF-1 pathway leads to transcription of IGF2 (insulin growth factor 2) and glucose transporter (GLUT) that promote adaptive prosurvival responses by metabolic adaptations and inhibition of apoptosis [*Chi and Karliner, 2004*].

1.17 Role and pleiotropic effects of statins

As explained above, the major mediators of ischemic damage are represented by ROS, RSN and inflammatory mediators, such as pro-inflammatory cytokines, cell adhesion molecules and C-reactive protein. In the last years many studies were conducted on the preventive effects of some drugs on the ischemia/reperfusion injury. Our attention was focused, in particular, on cardioprotective effects of statins. Several clinical trials, such as Scandinavian Simvastatin Survival Study (4S), Long-term Intervention with Pravastatin in Ischemia Disease (LIPID), and Heart Protection Study (HPS), have demonstrated the beneficial effects of statin therapy for primary and secondary prevention of cardiovascular disease.

The 3-hydroxy-3-methylglutaryl-CoA reductase inhibitors, or statins, are

principal therapeutic agents for the treatment of hypercholesterolemia. These drugs, indeed, inhibit 3-hydroxy-3-methylglutaryl-CoA (HMG-CoA) reductase, the enzyme that converts HMG-CoA in mevalonic acid, a cholesterol precursor. The inhibition of this enzyme by statins results in a dramatic reduction in circulating low density lipoprotein (LDL)-cholesterol. In addition, reduction of LDL-cholesterol leads to up-regulation of the LDL receptor and increased LDL clearance. The lowering of serum cholesterol levels is therefore the primary mechanism underlying the therapeutic benefits of statin therapy in cardiovascular disease [Wang *et al.*, 2008].

However, in relation to ischemia/reperfusion injury, more interesting are the cholesterol-independent effects of statins, also called “pleiotropic effects”.

In detail, it was shown that statins can:

- reduce oxidative stress, decreasing ROS production. In part this effect, induced by statins, is associated with a reduction of NADPH oxidase activity, since NADPH oxidase is an important source of ROS.

Importantly, it was shown that simvastatin can reduce the levels of superoxide anion, one of the key molecules involved in oxidative stress damage [Adam and Laufs, 2008; Mathur *et al.*, 2008];

- interfere with nitric oxide metabolism. During ischemia, the lower NO levels (< 100 nM) produced by the endothelial isoform of nitric oxide synthase (eNOS) exert a vasodilatory effect, whereas the higher NO levels (> 1 μ M) produced by the inducible isoform (iNOS) cause cell damage [Schulz *et al.*, 2004] by free radical production, such as peroxynitrite. It has been that statin administration during ischemia causes a decrease of iNOS expression, accompanied by a reduction of

the dangerous peroxynitrite, and an increase in eNOS expression, which is associated with an increase in blood flow and a decrease in infarct volume [Kirmizis and Chatzidimitriou, 2009];

- have an anti-inflammatory effect. Several studies have found that statins decrease the expression of inflammatory mediators such as C-reactive protein, IL-1, IL-6 and TNF- α . It has been also observed that statins reduce inflammatory mechanisms through a decrease in NF κ B activation [Holschermann *et al.*, 2006] and modulation of cytokine production.

On this basis, further studies are needed to evaluate the potential role of this drugs in the treatment and/or prevention of ischemia/reperfusion damages.

1.18 The iron-heart disease connection

A possible connection between body iron stores and the risk of heart disease was first put forward as a theory in 1981 by Dr. Jerome Sullivan (1981) to explain the differences in Cardiac Heart Disease (CHD) incidence and mortality between men and women. According to this theory, the lower iron stores of females protect them for developing CHD during the premenopausal years. This protection is diminished once the menopause sets in and body iron stores begin to rise. In 1992, Finnish investigators from the Kupio Ischemic Heart Disease Risk Factor (KIHD) Study presented some intriguing data indicating that in men with an elevated, but still apparently normal, serum ferritin (SF>200 μ g/L) were at a two-fold risk of developing a myocardial infarction. During the last years, the question of the importance of iron stores in the development of CHD has been hotly debated and still remains a topic of investigation [Wood 2004].

1.19 Iron toxicity

Iron is an essential nutrient playing a critical role in the body in terms of oxygen transport via hemoglobin and myoglobin, electron transport via iron-containing cytochromes, thus it is involved in cellular respiration; and it is implicated in DNA synthesis and other various critical enzymatic reactions where iron is a constituent of metallo-enzymes (figure 14).

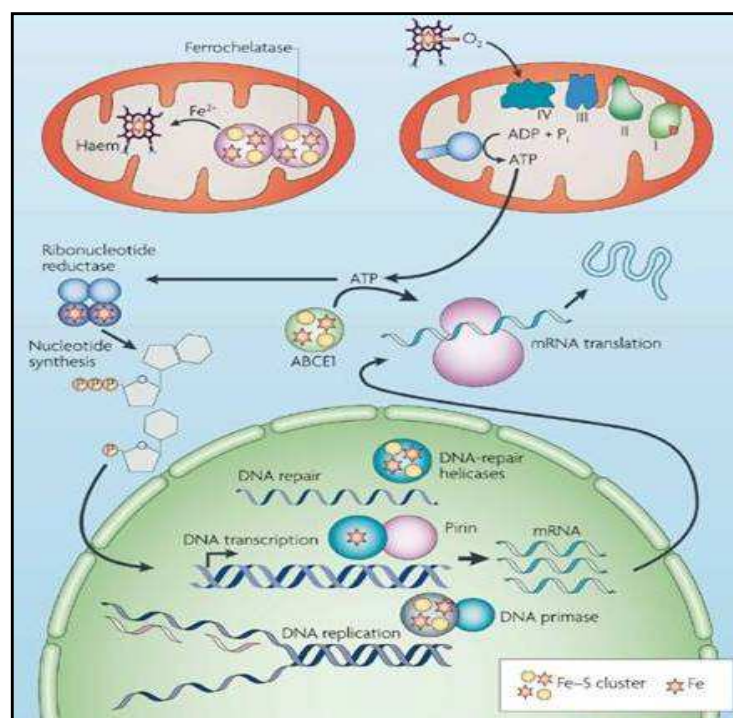
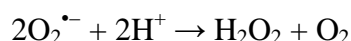
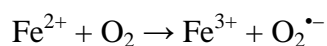


Figure 14. Representation of the main processes in which iron is involved: DNA synthesis, oxygen transport and cellular respiration.

On the other hand, potential harmful effects wrought by iron in the body have led to its consideration as the proverbial two-edged sword. The redox capability of iron is the basis of potential toxicity resulting from the Haber Weiss–Fenton sequence.

Haber–Weiss–Fenton reactions



that lead to the generation of hydroxyl radical (OH•) subsequent to the formation of superoxide (O₂^{•-}) following the one-electron reduction of dioxygen (O₂) by ferrous (Fe²⁺) iron. The hydroxyl radical can attack proteins, nucleic acids, and carbohydrates and initiate chain-propagating lipid peroxidation. Therefore, there is a biological imperative to balance the potential deleterious effects of free iron and the importance of maintaining a ready, but controlled, supply of this essential mineral nutrient. To achieve this needed equilibrium, various cellular mechanisms have evolved in organisms to control free iron concentrations in cells. One of the important biochemical modes of control relevant to this discussion is the iron-dependent translational control of ferritin protein production. Cellular ferritin is a cytosolic protein that acts to oxidize and sequester within its core excess cellular ferrous (Fe²⁺) iron.

The relative concentration of ‘chelatable’ iron in the cytosol is sensed by an iron–sulfur cluster found in the cytosolic iron regulatory protein (IRP). High iron conditions promote the transition of the iron–sulfur cluster to a cubane Fe₄–S₄ configuration that reduces the affinity of IRP for a regulatory binding site on the ferritin mRNA allowing more ferritin to be synthesized, thereby lowering the potentially harmful cytosolic Fe²⁺ concentration. Outside of the cell, iron is maintained in the less chemically reactive oxidized state as ferric iron (Fe³⁺) by the plasma ferroxidase activity of ceruloplasmin, a copper-dependent metalloenzyme. Ferric iron is carried in the extracellular space bound

to the protein transferrin. Interestingly, iron remains bound to transferrin until it is transported along with transferrin into cells by the cell surface transferrin receptor. Once safely compartmentalized inside endosomal vesicles, iron is then freed from transferrin and presumably reduced to Fe^{2+} prior to transport out of the endosome where it can enter the cytosolic iron pool and be available for free radical-generating Fenton reactions, or 'deactivated' by incorporation into iron-containing proteins or sequestered within the ferritin core. When iron is bound to either ferritin or transferrin it is catalytically inactive and will not participate in Fenton chemistry reactions. The regulation of iron movement and reactivity is an elegantly evolved metabolic system that allows for the harnessing of the redox power of iron and the minimization of iron's potentially harmful effects. In large part, the iron heart disease hypothesis rests on the supposition that high body iron burdens are a risk factor for increase oxidative stress, and oxidative stress is a risk factor for chronic disease, including heart disease. The root of this logical supposition appears to have merit given the capacity of free iron to act as an oxidant under physiological conditions. It is the presumed underlying supposition of the iron-heart disease hypothesis that there is some 'leakage' in the iron control system that allows iron-dependent damage that increases the susceptibility to or rate of pathological progression of coronary heart disease. This leakage-induced damage can be due presumably to some inefficiency of the iron control system [Wood, 2004].

1.20 Biochemistry and physiology of iron

With minor exceptions, almost all cells employ iron as a cofactor for fundamental biochemical activities, such as oxygen transport, energy

metabolism and DNA synthesis. This is due to the flexible coordination chemistry and redox reactivity of iron, which allow it to associate with proteins and bind to oxygen, transfer electrons or mediate catalytic reactions. However, as previously described, iron is also potentially toxic because it catalyses the propagation of ROS and the generation of highly reactive radicals (such as the hydroxyl radical) through Fenton chemistry, inducing damage of cellular macromolecules, tissue injury and disease. Thus the acquisition, usage and detoxification of iron pose a considerable challenge to cells and organisms, which have evolved sophisticated mechanisms to satisfy their metabolic needs and concomitantly minimize the risk of toxicity [De Domenico *et al.*, 2008; Hentze *et al.*, 2010]. The vast majority of body iron (at least 2.1 g in humans) is distributed in the hemoglobin of red blood cells and developing erythroid cells and serves in oxygen transport. Significant amounts of iron are also present in macrophages (up to 600 mg) and in the myoglobin of muscles (~300 mg), whereas excess body iron (~1 g) is stored in the liver. Other tissues contain lower, but not negligible, quantities of iron. Mammals lose iron from sloughing of mucosal and skin cells or during bleeding, but do not possess any regulated mechanism for iron excretion from the body. Therefore balance is maintained by the tight control of dietary iron absorption in the duodenum [Wang and Pantopoulos, 2011].

1.21 Dietary iron absorption

The uptake of nutritional iron involves reduction of Fe^{3+} in the intestinal lumen by ferric reductases such as Dcytb (duodenal cytochrome *b*) and the subsequent transport of Fe^{2+} across the apical membrane of enterocytes by DMT1 (divalent

metal transporter 1), a member of the SLC (solute carrier) group of membrane transport proteins, also known as SLC11A2 [Wallander *et al.*, 2006].

Dietary haem can also be transported across the apical membrane by a yet unknown mechanism and subsequently metabolized in the enterocytes by HO-1 (haem oxygenase 1) to liberate Fe^{2+} (figure 15).

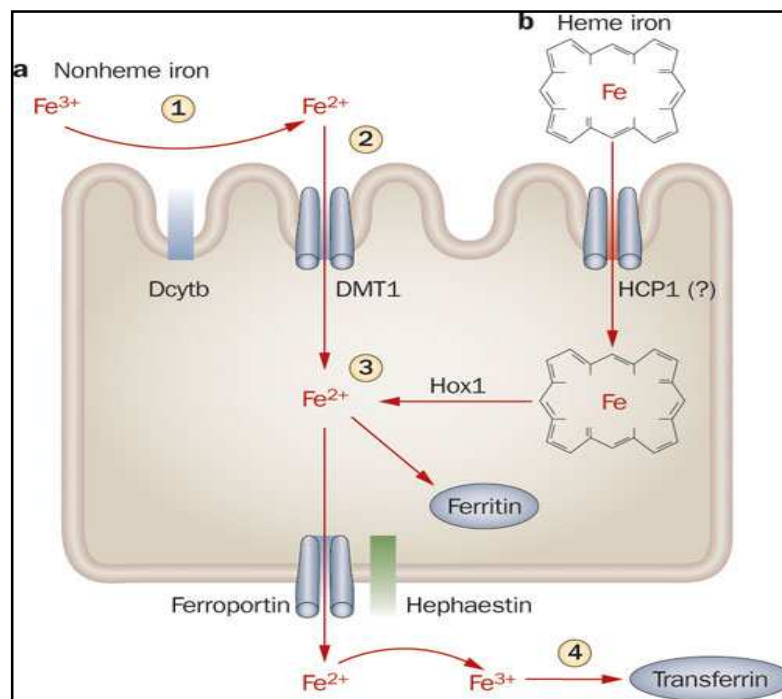


Figure 15. Mechanisms of dietary iron absorption.

Directly internalized or haem-derived Fe^{2+} is processed by the enterocytes and eventually exported across the basolateral membrane into the bloodstream via the solute carrier and Fe^{2+} transporter ferroportin (also known as SLC11A3). The ferroportin-mediated efflux of Fe^{2+} is coupled by its re-oxidation to Fe^{3+} , catalysed by the membrane-bound ferroxidase hephaestin that physically interacts with ferroportin, and possibly also by its plasma homologue ceruloplasmin. Exported iron is scavenged by transferrin (Tf), which maintains

Fe^{3+} in a redox-inert state and delivers it into tissues [Yeh *et al.*, 2009]. The vertebrate transferrin is an 80-KDa glycoprotein with homologous N-terminal and C-terminal iron-binding domains that is synthesized in the liver, retina, testis and brain. At the neutral pH of blood, transferrin can bind two atoms of Fe^{3+} , but only in the presence of an anion, usually carbonate, that bridges iron to transferrin [De Domenico *et al.*, 2008]. The Tf iron pool is replenished mostly by iron recycled from effete red blood cells and, to a lesser extent, by newly absorbed dietary iron.

Senescent red blood cells are cleared by reticuloendothelial macrophages, which metabolize haemoglobin and haem, and release iron into the bloodstream. By analogy to intestinal enterocytes, macrophages export Fe^{2+} from their plasma membrane via ferroportin, in a process coupled by re-oxidation of Fe^{2+} to Fe^{3+} by ceruloplasmin and followed by the loading of Fe^{3+} to transferrin [Wang and Pantopoulos, 2011].

1.22 Regulation of systemic iron traffic: the role of hepcidin

The ferroportin-mediated efflux of Fe^{2+} from enterocytes and macrophages into the plasma is critical for systemic iron homeostasis. This process is negatively regulated by hepcidin, a liver-derived peptide hormone that binds to ferroportin and promotes its phosphorylation, internalization and lysosomal degradation [Nemeth and Ganz, 2009]. Hepcidin is primarily expressed in hepatocytes as a precursor pro-peptide. Pro-hepcidin undergoes proteolytic processing to yield a bioactive molecule of 25 amino acids that is secreted into the bloodstream. Recently it was found that hepcidin is also expressed in the heart and, in

contrast to what happens in the liver, cardiac hepcidin expression is significantly up-regulated in response to hypoxia [Merle *et al.*, 2007].

Hepcidin accumulates following iron intake and under inflammatory conditions, resulting in decreased dietary-iron absorption and iron retention in macrophages. Conversely, hepcidin levels drop in iron deficiency or phlebotomy-induced anaemia, and this response promotes intestinal iron absorption and iron release from macrophages.

The disruption of hepcidin is associated with systemic iron overload (haemochromatosis) [Lee and Beutler, 2009], whereas pathological elevation of hepcidin levels contributes to the development of the anaemia of chronic disease [Weiss and Goodnough, 2005]. The expression of hepcidin is controlled transcriptionally by several mechanisms. Basal hepcidin transcription requires C/EBP α (CCAAT/enhancerbinding protein α) [Courselaud *et al.*, 2002].

Iron-dependent induction of hepcidin requires BMP (bone morphogenetic protein) signalling. Iron triggers the expression of BMP6 in the liver [Kautz *et al.*, 2008] and the intestine [Arndt *et al.*, 2010], which is thought to be secreted into the plasma for binding to a BMP receptor on the surface of hepatocytes. BMP6 signalling leads to phosphorylation of SMAD1/5/8 and translocation of SMAD4 to the nucleus, where it promotes hepcidin transcription upon binding to proximal and distal sites on its promoter [Meynard *et al.*, 2009; Andriopoulos *et al.*, 2009]. It has also been proposed that hepcidin responds to increased Tf saturation [Gao *et al.*, 2009], possibly by a mechanism requiring a cross-talk between BMP and MAP (mitogen-activated protein kinase) signalling [Ramey *et al.*, 2009]. Further cofactors are required for iron-dependent activation of hepcidin, even though their exact mode of action is not yet clear. These include

the haemochromatosis protein HFE, Tfr2 (Transferrin receptor 2) and the BMP co-receptor HJV (haemojuvelin). Mutations in these proteins impair hepcidin expression and lead to hereditary haemochromatosis [Lee and Beutler, 2009]. The pro-inflammatory cytokine IL-6 (interleukin-6) induces hepcidin transcription via STAT3 (signal transducer and activator of transcription 3) phosphorylation and translocation to the nucleus for binding to a proximal promoter element [Fleming, 2008] whereas, IL-1 β activates hepcidin via the C/EBP α and BMP/SMAD pathways [Matak et al., 2009]. Hepcidin transcription, instead, is suppressed by hypoxia and oxidative stress. The role of HIFs (hypoxia-inducible factors) in the hypoxic pathway of hepcidin is debatable [Volke et al., 2009], whereas oxidative stress promotes histone deacetylation and decreases binding of C/EBP α and STAT3 to the hepcidin promoter [Miura et al., 2008]. There is no doubt that hormonal regulation of iron efflux from cells via the hepcidin/ferroportin axis is of paramount importance for systemic iron homeostasis. However, it should be noted that the expression of ferroportin is also subjected to transcriptional [Ludwiczek et al., 2003] and post-transcriptional control.

1.23 Cellular iron up-take and the role of transferrin receptor-1

The transferrin-(Fe³⁺) complex in plasma is transported into cells through one of two cell-surface transferrin receptors. Transferrin receptor-1 (TfR1) is expressed on all cells, including cardiomyocytes, and is particularly enriched on precursors of the erythron because these cells show the highest demand for iron [Matak et al., 2009]. Transferrin receptor-2 (TfR2) is expressed primarily in the

liver and binds the transferrin-(Fe³⁺) complex at a much lower affinity than TfR1 does [De Domenico et al., 2008]. Transferrin receptor 1 is a membrane protein of ~90 KDa. It is a homodimer of two identical transmembrane subunits linked by disulphide bonds. Each subunit consists of a large extracellular C-terminal domain, an hydrophobic membrane-spanning domain and a small cytoplasmic N-terminal domain (figure 16).

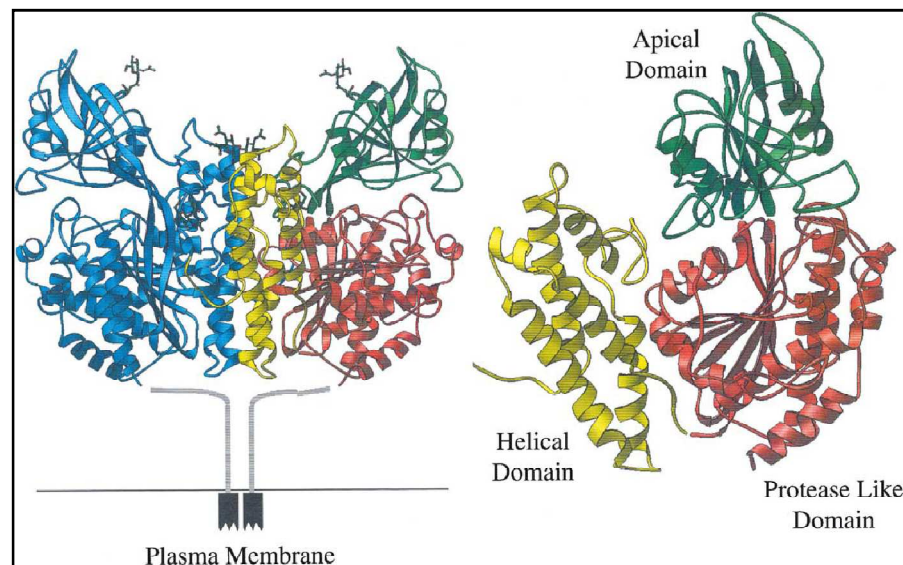


Figure 16. Crystal structure of the Transferrin Receptor.

Human TfR1 bears one O-linked and three N-linked oligosaccharides; N-linked glycosylation is particularly important for proper folding and transport of the protein to the cell surface. The extracellular domain binds one molecule of transferrin per subunit, forming the multimeric Tf-TfR1 complex. TfR1 knockout mice display embryonic lethality, showing the importance of this protein in iron metabolism [Aisen et al., 2004]. The Tf-TfR1 complex is the main process by which the uptake of transferrin bound iron from plasma to cells of peripheral tissues is mediated (figure 17).

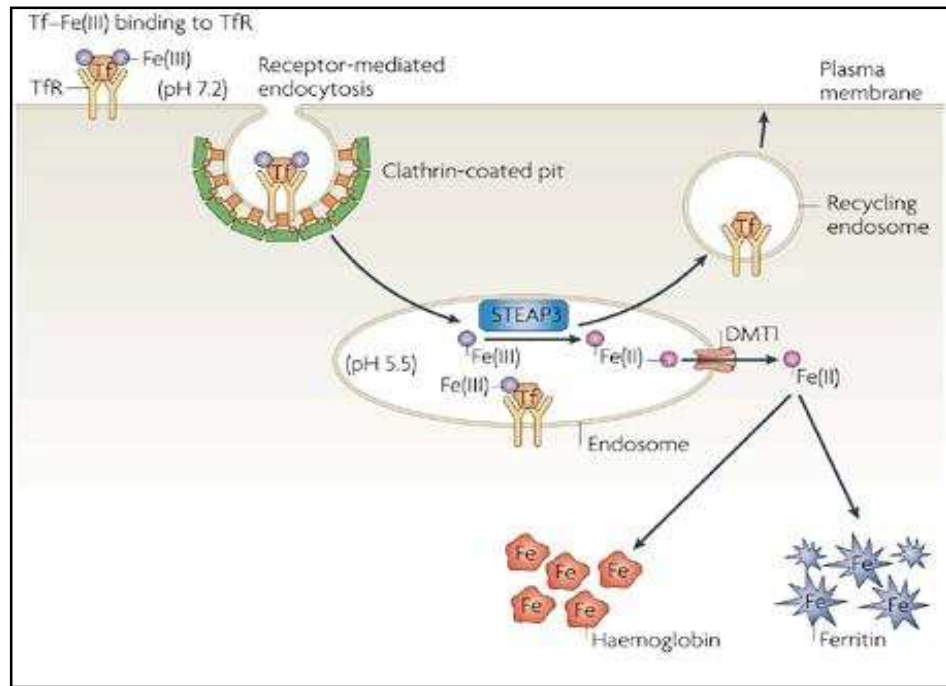


Figure 17. Representation of cellular iron up-take.

After binding to its receptor, the complex of $(\text{Fe}^{3+})-(\text{Tf}-\text{TfR1})$ is rapidly internalized by receptor-mediated endocytosis through clathrin-coated pits.

Inside the cells, the internalized complex localizes to an endosome that is acidified by an ATP-dependent proton pump that lowers the luminal pH to ~ 5.5 . Acidification produces a conformational change in both transferrin- (Fe^{3+}) and TfR1 with the consequent release of iron. The endosomal (Fe^{3+}) is converted into (Fe^{2+}) by a ferrireductase that has been identified as STEAP3, and then the endosomal DMT1 transports the product of the STEAP3-catalysed reaction from the endosome to the cytosol.

At acidic pH, apotransferrin remains bound to TfR1 and the complex is recycled to the cell surface. At the more neutral pH of plasma (pH 7,4), apotransferrin dissociates from TfR1 and is free to bind iron and initiate further rounds of receptor-mediated endocytosis [De Domenico, 2008].

1.24 Iron storage

Cells may eliminate excess intracellular iron by secretion of Fe^{2+} via ferroportin or by secretion of haem through the putative haem exporter FLVCR (feline leukaemia virus, subgroup C, receptor) [Keel *et al.*, 2008], but cells can mainly store and detoxify excess intracellular iron in the cytosol within ferritin, a conserved protein consisting of 24 H and L subunits, encoded by distinct genes (figure 18).

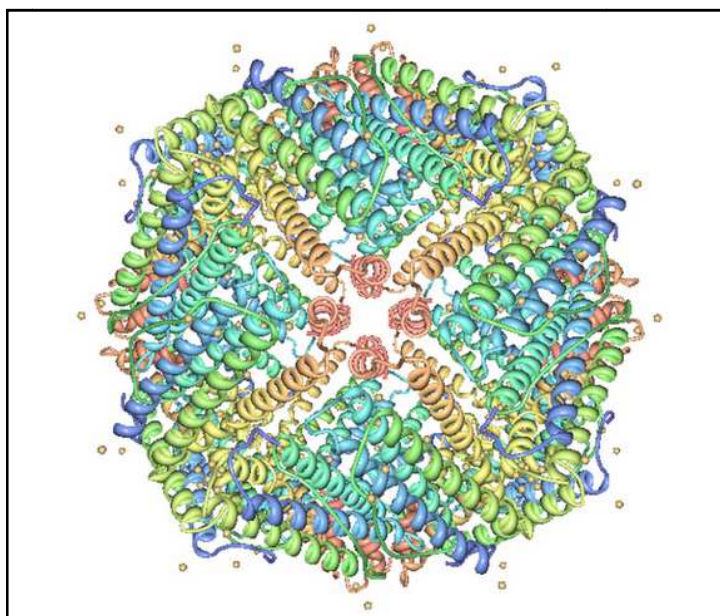


Figure 18. Cristal structure of ferritin.

The levels of H-ferritin and L-ferritin differ among various tissues; the former is enriched in the heart and the latter in the liver. The H (for heavy or heart) subunit is 21 kDa, whereas the L (for light or liver) subunit is 19 kDa [Arosio *et al.*, 2009].

Ferritin assembles into a shell-like structure with a cavity of $\sim 80 \text{ \AA}$ ($1 \text{ \AA} = 0.1 \text{ nm}$) that provides storage space for up to 4500 Fe^{3+} ions in form of ferric oxy-

hydroxide phosphate. Iron may enter ferritin with the aid of PCBP1 [poly(rC)-binding protein 1], which appears to function as an iron chaperone [*Shi et al., 2008*]. The incorporation of iron into holo-ferritin also requires the ferroxidase activity of H-ferritin, whereas L-ferritin chains are associated with iron nucleation, mineralization and long-term iron storage. Since H-ferritin can bind to and release iron more easily than L-ferritin, it plays a key role in rapid detoxication of iron and intracellular iron transport. [*You and Wang, 2005*].

A secreted glycosylated isoform of predominantly L-ferritin circulates in the bloodstream. It contains very low amounts of iron, suggesting that it does not play an essential role in iron storage or traffic, but it is used as a clinical marker for body iron stores [*Cohen et al., 2010*].

Intracellular iron deposits may also be detected within haemosiderin, a structure consisting of ferritin degradation products and iron oxide clusters. Iron stored within ferritin is considered to be bioavailable and may be mobilized for metabolic purposes during its lysosomal turnover [*Zhang et al., 2010*] and, possibly, also following dynamic structural rearrangements of the ferritin subunits. The induction of ferroportin promotes mobilization and export of ferritin-derived iron, followed by mono-ubiquitination and degradation of apoferritin by the proteasome [*De Domenico et al., 2006*]. Thus ferritin can be degraded by two different pathways, the lysosomal and the proteasomal pathways, which appears to require prior depletion of its iron [*De Domenico et al., 2009*]. The iron-storage function of ferritin is crucial for health. Ferritin can act as a critical anti-oxidant by sequestering unbound or “free” iron, thereby limiting its participation in oxidative reactions. The conditional disruption of this gene, indeed, promotes damages due to oxidative stress [*Darshan et al.,*

2009]. Recently an isoform of ferritin was found in the mitochondria [Levi and Arosio, 2004]. Mitochondrial ferritin derives from an unusual intronless gene and is synthesized in the cytosol as a precursor polypeptide that is targeted to mitochondria by an N-terminal leader sequence. The mature protein possesses ferroxidase activity and assembles into functional ferritin nanocages. Mitochondrial ferritin is normally expressed at low levels and does not appear to have any major function in normal mitochondrial iron utilization. Its expression, however, is significantly induced in iron-loaded ring erythroblasts (sideroblasts) of sideroblastic anaemia patients and may serve as a sink for iron deposition [Cazzola et al., 2003].

1.25 The “Labile Iron Pool” (LIP)

The amount (< 5%) of iron that is not bound to ferritin or other proteins form a transient cytosolic pool, named “Labile Iron Pool” (LIP). This LIP is redox-active and comprises both ionic forms of iron (Fe^{2+} and Fe^{3+}), presumably associated to low-molecular mass intracellular chelates, such as citrate, various peptides, ATP, AMP or pyrophosphate [Kaklon and Cabantchik, 2002].

The cytosolic LIP reflects the cellular iron content and its fluctuations trigger homeostatic adaptive responses. In particular, LIP levels are maintained homeostatically for cells, not only to meet the metabolic demands for iron, but especially to minimize its potential engagement in ROS formation [Breuer et al., 2008]. On these bases, a critical aspect of the maintenance of cellular iron homeostasis is the control of the expression of genes encoding proteins required for the uptake (TfR1, DMT1), storage (H and L ferritin) or export (FPN) of iron [Goforth et al., 2010]. Iron regulatory proteins (IRPs) are central components of

a sensory and regulatory system required for the maintenance of iron homeostasis in vertebrates.

1.26 The IRE/IRP regulatory system

1.26.1 Regulation of TfR and ferritin expression by IRPs

The expression of TfR1 and ferritin are co-ordinately regulated post-transcriptionally upon binding of IRP1 or IRP2 to IREs in the UTRs (untranslated regions) of their respective mRNAs [Recalcati *et al.*, 2010]. IREs are evolutionarily conserved hairpin structures of 25–30 nt [Piccinelli and Samuelsson, 2007]. A typical IRE stem consists of variable sequences that form base pairs of moderate stability ($\Delta G \approx -7$ kcal/mol), and folds into an α -helix that is slightly distorted by the presence of a small bulge in the middle (an unpaired C residue or an asymmetric UGC/C bulge/loop commonly found in the ferritin IRE). The loop contains a conserved 5'-CAGUGH-3' sequence (H denotes A, C or U), where the underlined C and G residues form a base pair [Wallander *et al.*, 2006], as shown in figure 19.

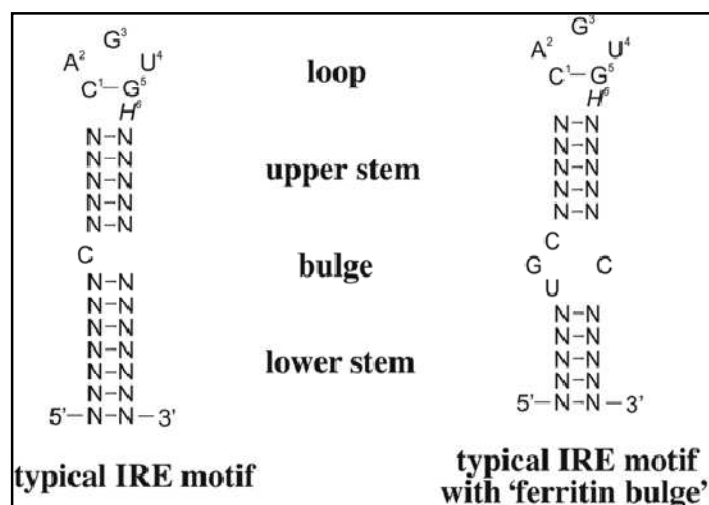


Figure 19. Representation of a typical IRE motif.

TfR1 mRNA contains multiple IREs within its long 3'-UTR, whereas the mRNAs encoding H and L ferritin contain a single IRE in their 5'-UTRs.

In iron-starved cells, IRPs bind with high affinity to cognate IREs. The IRE-IRP interactions stabilize TfR1 mRNA and, moreover, impose a steric blockade to ferritin mRNA translation. As a result, increased TfR1 levels stimulate acquisition of iron from plasma Tf to counteract iron deficiency. The inhibition of *de novo* ferritin synthesis leads to decreased abundance of this protein, as iron storage becomes obsolete under these conditions.

Conversely, in cells with high iron content, both IRP1 and IRP2 become unavailable for IRE binding, allowing TfR1 mRNA degradation and ferritin mRNA translation. Thus when iron supply exceeds cellular needs, the IRE-IRP switch minimizes further iron uptake via TfR1, and favours the storage of excess iron in newly synthesized ferritin.

The IRE-IRP system was initially defined as a relatively simple and ubiquitous post-transcriptional regulatory circuit that maintains cellular iron homeostasis in vertebrates by orchestrating co-ordinated iron uptake by TfR1 and storage in ferritin. The identification of additional IRE-containing mRNAs and the ongoing biochemical and physiological characterization of IRPs added considerable complexity and uncovered a functional significance for the IRE-IRP system that exceeds the narrow boundaries of cellular iron uptake and storage [Wang and Pantopoulos 2011].

1.26.2 Expression of DMT1 and ferroportin is regulated by IRPs

The mRNAs encoding the iron transporters DMT1 and ferroportin are expressed in alternatively spliced isoforms, some of which are furnished with a translation-type IRE. Two out of four DMT1 transcripts contain a single IRE in their 3'-UTR that presumably operates as a stability control element and accounts for the higher DMT1 expression in iron-deficient conditions [Hubert and Hentze, 2002]. Ferroportin mRNA is expressed in two alternatively spliced transcripts, one of which contains a single translation-type IRE in its 5'-UTR [Zhang *et al.*, 2009] that is consistently associated with high ferroportin expression in iron-sufficient state [Abboud and Hail, 2000]. Conversely, the lack of IRE in the alternative ferroportin transcript, which is enriched in duodenal enterocytes and erythroid precursor cells, allows the accumulation of ferroportin in these tissues during iron deficiency [Mckie *et al.*, 2000] by evading the translational blockade imposed by active IRPs. In an iron-deficient state, the bypass of the IRE-IRP system contributes to homeostatic adaptation by (i) probably facilitating dietary-iron absorption in the duodenum, and (ii) possibly also permitting efflux of iron from erythroid cells in the bloodstream to restrict erythropoiesis and to make the metal available to iron-starved non-erythroid cells.

1.26.3 Other IRE-containing mRNAs

The biochemical characterization of IREs and the establishment of a canonical IRE motif prepared the way for the discovery of further IRE-containing

mRNAs, some of them bearing atypical, yet functional, IREs [Rouault, 2006].

A functional IRE (an IRE that confers translational regulation) was found in the 5'-UTR of ALAS2 mRNA. Considering that ALAS2 (δ -aminolevulinate synthase) catalyses the initial reaction for heme biosynthesis in erythroid cells, the translational repression of its mRNA by IRPs associates the IRE-IRP system with systemic iron utilization and homeostasis [Cairo and Recalcati, 2007].

A single IRE was also found in the 5'-UTR of the mRNAs encoding mammalian m-aconitases (mitochondrial aconitases) and the *Drosophila* iron-containing protein succinate dehydrogenase subunit b (SDHb), which are both iron-sulfur enzymes of the citric acid cycle, and then link the IRE-IRP system with energy metabolism [Cairo and Recalcati, 2007].

More recently, a high-throughput biochemical screen revealed an atypical IRE in the 5'-UTR of HIF-2 α mRNA that functions as a translational control element [Sanchez et al., 2007]. The Hypoxia-Inducible Factor, (HIF)-2 α , is a transcription factor that is activated by lack of oxygen or iron. This finding represents a new link between iron and oxygen homeostasis.

A single IRE motif was found also in the 3'-UTR of mRNA splice variants encoding MRCK α [myotonic dystrophy kinase-related Cdc42 (cell division cycle 42)-binding kinase α] [Cmejla et al., 2006] and human Cdc14A phosphatase [Sanchez et al., 2006]. Preliminary biochemical characterization suggests that these IRE motifs contribute to the regulation of mRNA stability, linking the IRE-IRP system with cytoskeletal remodelling and the cell cycle.

The mRNA encoding β -APP harbours a non-canonical IRE motif with a conserved 5'-CAGAG-3' sequence (the underlined C and G residues form a base pair) as part of an extended loop in its 5'UTR, which preferentially

interacts with IRP1 and functions as a translational control element [Cho *et al.*, 2010]. Interestingly, α -synuclein mRNA also contains a predicted IRE-like motif [Friedlich *et al.*, 2007] that awaits functional characterization. Aberrant expression of β -APP and α -synuclein is associated with Alzheimer's and Parkinson's diseases respectively; thus validation of the regulatory function of their IREs may couple the IRE–IRP system with human neurodegenerative conditions.

Recently, Mayka Sanchez and colleagues (Sanchez *et al.*, 2011) following a genome-wide strategy identified 35 novel mRNAs that bind both IRP1 and IRP2. Some of these mRNA are implicated in cancer progression and metastasis, including the chemokine CXCL16, that contains a predicted IRE motif at its 3'-UTR, and FXYD5, also named Dysadherin, which contains a predicted IRE in 5'-UTR. Further work is needed to elucidate if these proteins can alter iron homeostasis, but their abnormal expression in several human cancers, may represent a novel link between iron metabolism and cancer.

Overall, as illustrated in the figure 20, functional IRE motifs have thus far been identified in mRNAs encoding proteins of iron uptake (TfR1), storage (H and L ferritin), erythroid utilization (ALAS2) and transport (DMT1 and ferroportin), as well as energy metabolism (m-aconitase and *Drosophila* SDH), hypoxic regulation (HIF-2 α), cytoskeletal reorganization (MRCK α), cell cycle control (Cdc14A) and neuronal function (β -APP and α -synuclein).

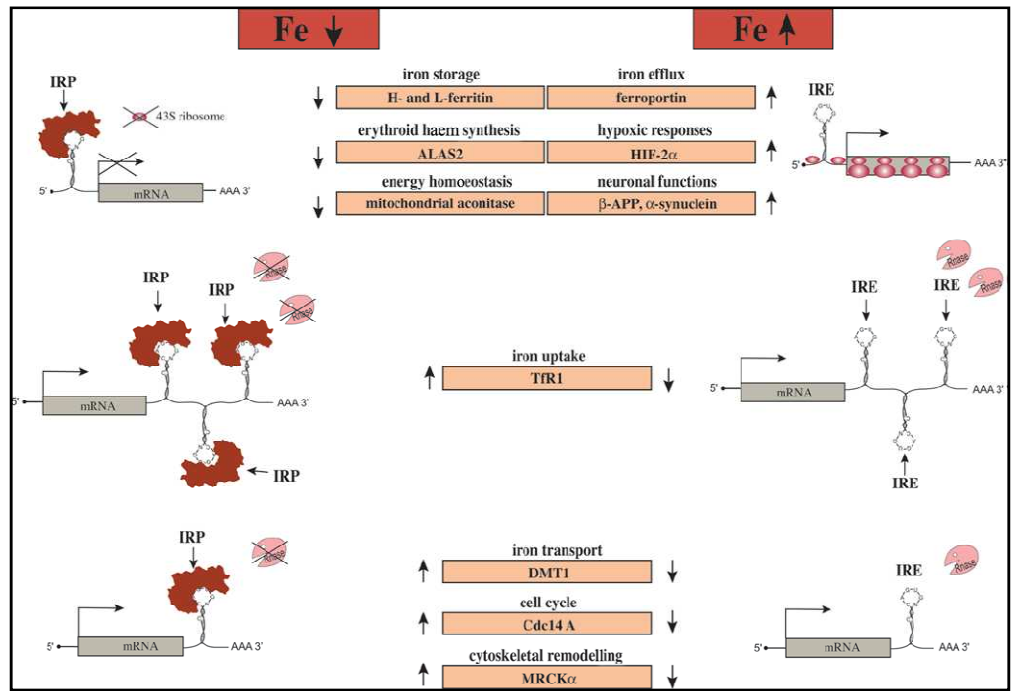


Figure 20. Post-transcriptional control by the IRE-IRP regulatory system.

The expanded list of IRE-containing mRNAs emphasizes the role of the IRE–IRP system as a master post-transcriptional iron regulatory switch, but also implies further regulatory potential outside the context of iron metabolism in a strict sense.

1.27 IRPs: functional and structural features

IRP1 and IRP2 do not share sequence similarities with known RNA-binding proteins and do not contain any established RNA-binding motifs. They both belong to the family of Iron-Sulfur Cluster (ISC) isomerases, which includes m-aconitase. This enzyme catalyses the isomerization of citrate to iso-citrate via the intermediate *cis*-aconitase during the citric acid cycle, and contains a cubane $[4\text{Fe-4S}]^{2+}$ ISC in its active site. Three of the iron atoms are attached to cysteine residues of the polypeptide, whereas the fourth iron remains free and mediates

catalytic chemistry [Muckenthaler *et al.*, 2008]. IRP1 assembles an analogous to m-aconitase ISC that converts it to a c-aconitase (cytosolic aconitase). However, in contrast with m-aconitase, IRP1 only retains its ISC and its enzymatic function in iron-replete cells. In iron deficiency, holo-IRP1 is converted into apo-protein that possesses IRE-binding activity. Thus IRP1 is bifunctional and its mutually exclusive activities are reversibly regulated by an unusual ISC switch. IRP1 probably evolved independently of m-aconitase following an early duplication event that allowed it to acquire IRE-binding activity. A second duplication event led to the evolution of IRP2 in higher eukaryotes [Wang and Pantopoulos, 2011]. IRP2 shares extensive homology with IRP1; however, it neither assembles an ISC nor retains aconitase active-site residues. Consequently, IRP2 only exhibits an IRE-binding activity and does not have any enzymatic function. A feature of IRP2 that distinguishes it from IRP1 is the presence of a conserved cysteine and proline-rich stretch of 73 amino acids close to its N-terminus. This sequence is encoded by a separate exon and appears to be unstructured [Dycke *et al.*, 2007]. IRP2 is regulated in an irreversible manner, at the level of protein stability. The crystal structure of IRP1 has been solved in both the c-aconitase-binding and IRE-binding [Walden *et al.*, 2006] forms (figure 21), although the structure of IRP2 has not yet been determined. It was shown that the site for catalysis and RNA-binding overlap, and the switch between the enzymatic and RNA-binding forms is associated with extensive conformational rearrangements. The folding of holo-IRP1 follows the pattern of m-aconitase [Dupuy *et al.*, 2006], despite relatively limited sequence identity (22%), but consistently with the conservation of active-site residues. The protein is composed of four globular domains.

Domains 1–3 are compact and join domain 4 through a surface linker. The ISC is located centrally at the interface of the four domains.

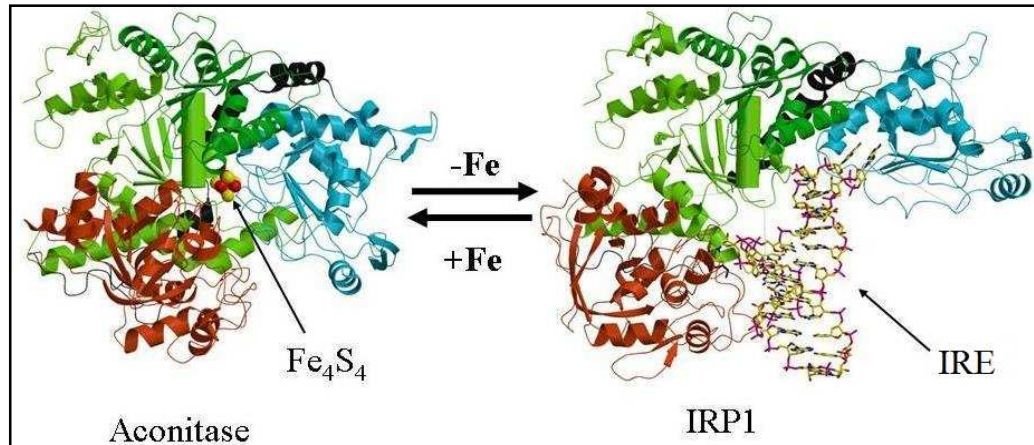


Figure 21. Crystal structure of IRP1. On the right the c-Aconitase form; on the left the IRE-binding form.

The topology of the ISC and the surrounding environment are fairly conserved between c- and m-aconitases. Nevertheless, the overall structure of holo-IRP1, a protein of 889 amino acids, (~98 KDa), also shows differences to that of m-aconitase, which is smaller (780 amino acids). The short IRP1 fragments that do not superimpose with m-aconitase are exposed on the surface of the protein. As a result, the shapes and surface topologies of holo-IRP1 and m-aconitase diverge substantially, which may explain the fact that only the former can acquire IRE-binding activity.

How do the IRPs recognize IREs?

The structure of IRP1 in a complex with ferritin IRE uncovered the details of the protein reorganization upon loss of its ISC. The main features are a rotation of domain 4 by 32°, but also an unpredicted extensive rearrangement of domain

3 by 52° that creates a hydrophilic cavity and allows access to the IRE. The RNA–protein interaction requires two crucial segments at the interface of domain 2 (residues 436–442) and domain 3 (residues 534–544). Thr⁴³⁸ and Asn⁴³⁹ make direct contacts with the IRE. The terminal residues of the IRE loop, A15, G16 and U17, interact with Ser³⁷¹, Lys³⁷⁹ and Arg²⁶⁹ respectively within a cavity between domains 2 and 3. A second binding site is formed around the unpaired-C-bulge residue between the upper and lower stem, which occupies a pocket within domain 4, sandwiched between Arg⁷¹³ and Arg⁷⁸⁰. The IRE–IRP1 complex is stabilized by additional bonds, ionic interactions and van der Waals contacts. This structural studies offered detailed insights into the dual function of IRP1 as a c-aconitase and an IRE-binding protein [Walden *et al.*, 2006].

As regards IRP2, the resolution of its structure, especially in a complex with IRE, will be necessary to precisely map the RNA–protein interaction and to understand the topology of the IRP2-specific 73 amino acid insert and its possible role in IRE binding [Zumbrennen *et al.*, 2009].

1.28 Regulation of IRP1

The iron-sulfur cluster of IRP1 is the major site for its regulation. Within cells, the conversion of apo- to holo-IRP1 requires several cofactors, such as the mitochondrial proteins Nfs1 (ISCS) [Biederbick *et al.*, 2006], frataxin [Seznec *et al.*, 2005], ISCU [Tong and Rouault, 2006], Grx5 [Ye *et al.*, 2010], ISD11 [Shi *et al.*, 2009] or Abcb7 [Pondarre *et al.*, 2006], showing an active role of mitochondria in the assembly of holo-IRP1.

Many factors can interpose with the ISC of IRP1, in particular:

- The ISC of IRP1 exhibits also sensitivity to oxidants, in particular to superoxide anion and peroxynitrite that can attack the ISC of cytoplasmic aconitase, inducing its disassembly to form IRP1 [Zimmer *et al.*, 2008], whereas hypoxia favours its stabilization, accompanied by a rise in aconitase activity [Deck *et al.*, 2009].
- Iron starvation leads to conversion of holo-IRP1 (cytosolic aconitase) into an IRE-binding apo-protein following depletion of its ISC. This process is relatively lengthy (8–12 h) and does not require *de novo* protein synthesis.
- In contrast, in iron-loaded state the apo-IRP1 is converted in holo-IRP1.

IRP1 is a fairly stable protein (half-life of ~24 h) and, under normal circumstances, its stability remains unaffected by iron levels. However, when ISC biogenesis is impaired by either inactivation of ISC assembly cofactors or phosphorylation of IRP1 at Ser¹³⁸, iron leads to ubiquitination and slow degradation of apo-IRP1 by the proteasome [Wang *et al.*, 2007; Deck *et al.*, 2009]. IRP1 can be phosphorylated by PKC (protein kinase C) at the conserved Ser¹³⁸ and Ser⁷¹¹ residues [Clarke *et al.*, 2006]. Ser¹³⁸ is located in proximity to the ISC and its phosphorylation appears to interfere with the ISC stability [Deck *et al.*, 2009]. This backup mechanism prevents accumulation of excessive apo-IRP1 that may disrupt iron homeostasis by its unregulated IRE-binding activity.

1.29 Regulation of IRP2

IRP2 is synthesized *de novo* in response to low iron and remains stable under iron starvation or hypoxia. In iron replete cells, however, IRP2 becomes

destabilized and undergoes rapid ubiquitination and degradation by the proteasome [Wang and Pantopoulos, 2011].

It was recently demonstrated that IRP2 are substrates of FBXL5 (F-box and leucine-rich repeat protein 5), a member of an E3 ubiquitin ligase complex that also includes Skp1 (S-phase kinase-associated protein 1), Cul1 (Cullin 1) and Rbx1 (Ring-box 1) [Vashisht *et al.*, 2009; Salahudeen *et al.*, 2009].

FBXL5 contains an N-terminal haemerythrin domain with a characteristic Fe–O–Fe centre. In iron-replete and oxygenated cells, FBXL5 accumulates and interacts with IRP2, mediating its ubiquitination and subsequent degradation (figure 22). In contrast, in iron-deficient or hypoxic cells, FBXL5 itself undergoes proteasomal degradation by a yet unknown mechanism upon the loss of its Fe–O–Fe centre, which allows the stabilization of IRP2.

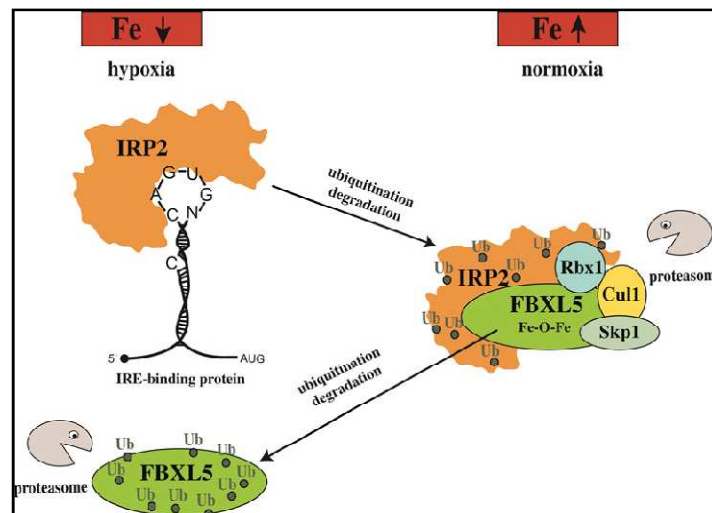


Figure 22. Iron and oxygen-dependent regulation of IRP2 stability by FBXL5

Hence, FBXL5 senses iron and oxygen levels through the Fe–O–Fe centre of its haemerythrin domain and emerges as a novel regulator of cellular iron homeostasis.

2. AIM OF THE STUDY

Ischemic heart disease, the main cause of mortality and morbidity in industrialized countries, is a metabolic phenomenon due to an inadequate oxygenation of heart tissue caused by the closing or narrowing of the coronary arteries.

Regardless of the cause that led to the ischemic conditions, there is an impairment of oxygen and oxidizable substrates to a part of myocardial tissue. The early reperfusion of ischemic myocardium restores cellular functions altered by ischemia and contrasts cell death. However, the ischemic condition and the subsequent tissue reperfusion, lead to several functional and metabolic changes that globally define the so-called “ischemia/reperfusion injury”. It is widely accepted that in the ischemia/reperfusion injury the overproduction of ROS is the main source of cell damage. The Reactive Oxygen Species (ROS), indeed, are highly reactive molecules that can cause lipid peroxidation, protein oxidation and nucleic acid alterations, playing an important role in the genesis and progression of ischemic damage.

A pivotal role in the ROS production is played by iron. This metal, for its redox properties, can quickly give and accept electrons and thus promote the ROS production through the Haber-Weiss-Fenton reaction.

It is well known that iron is an essential element for the growth and metabolism of all living organisms, because it is involved in many cellular functions, such as the synthesis of the DNA and cellular respiration. However, an excess of this metal can be toxic for all cell types, then the iron metabolism must be finely regulated to prevent dangerous excess or deficiencies of this essential

metal. At cellular level the main proteins involved in the regulation of iron metabolism are represented by the Transferrin Receptor 1 (TfR1) and the Divalent Metal Transporter (DMT1), that mediate the iron up-take, the ferroportin that is the only known cellular iron exporter in mammals and ferritin which is able to sequester iron in a non-toxic form. Other important proteins involved in the control of iron metabolism are the Iron Regulatory Proteins (IRPs), that are able to regulate at post-transcriptional level the expression of proteins such as Transferrin Receptor 1, DMT1, ferroportin and ferritin.

On this basis, the aim of my study was to analyze, in both *in vivo* and *in vitro* models of ischemia/reperfusion injury (for the model details, see Materials and Methods section) the molecular mechanisms that regulate the cellular iron homeostasis, as well as assess the potential oxidative damages caused by this metal during the complex phenomenon of ischemic heart disease. In particular, it was investigated the effect of ischemia/reperfusion conditions on the cell viability and ROS production, and the effects on the activity and expression of the principal proteins implicated in the iron metabolism, such as IRPs, TfR1, and ferritin. My study was focused also on the so-called “pleiotropic” effects of statins, in particular on the anti-inflammatory and antioxidant activities, that could protect cardiac tissue from ischemia/reperfusion injury.

In detail, it was investigated the cytoprotective effects of Simvastatin, one of the most common statins used in the treatment of hypercholesterolemia, on the expression of protein such as iNOS, (involved in the production of nitric oxide, that can interact with $O_2^{\bullet-}$ to form peroxynitrite, a potent mediator of cell damage), on the ROS production and then on the cell viability in rat cardiomyoblasts subjected to hypoxia and reoxygenation conditions.

Moreover, considering the close relationship between the ROS production and iron, it was also evaluated the effects of Simvastatin on the iron metabolism, in particular assessing the LIP extension and the expression of protein such as ferritin and Transferrin Receptor 1.

3. MATERIALS AND METHODS

3.1 Animals and *in vivo* ischemia/reperfusion model

All animal experiments complied with the Italian legislative decree (D.L.) no.116 of January 27, 1992 and associates guidelines in the European Communities Council Directive of November 24, 1986 (86/609/ECC).

Male Wistar rats (250–280 g; Harlan Nossan, Correzzana, MI, Italy), were divided in different groups: (1) Sham group; animals underwent to the surgical intervention without the LAD ligation, (2) ischemic group; animals were subjected to ischemia 30-90 minutes, (3) reperfused group; animals subjected to 24 hours of reperfusion after ischemia.

Animals were anaesthetized with an intraperitoneal injection of a solution of ketamine (100 mg/kg) and xylazine (10 mg/kg) placed on a surgical table and artificially ventilated through a tracheal cannula connected to a ventilation pump for small animals (Ugo Basile, Comerio, VA, Italy).

Myocardial infarction was produced by ligation of left anterior descending coronary artery (LAD), according to a method previously described in Wistar rats [Guerra *et al.*, 2006]. Briefly, the left side of the thorax was opened between the fourth and fifth intercostal space. The heart was gently exteriorized and the pericardium dissected out. The LAD was occluded (figure 23) near its anatomical origin by a 5.0 silk suture (Ethicon, Johnson-Johnson) at different times (30 and 90 minutes). At the end of the ischemia period, the ligature was removed to obtain the 24 hours reperfusion phase, and a blood sample was withdrawn from abdominal aorta.

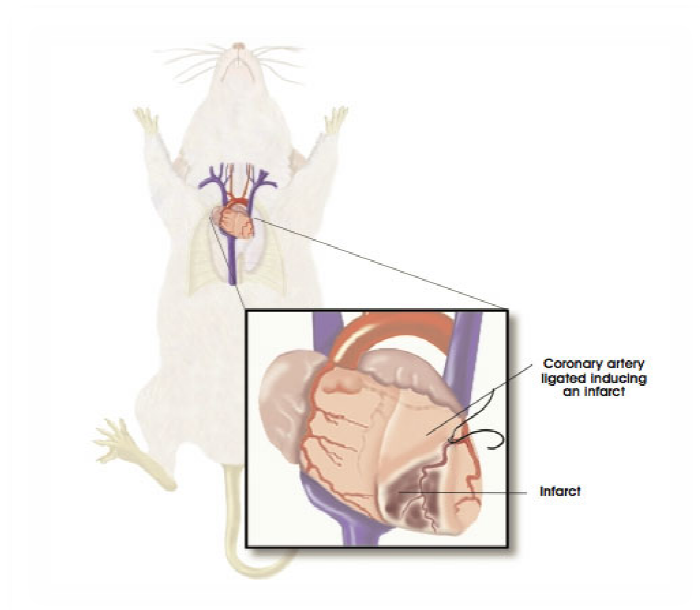


Figure 23. *In vivo* model of cardiac ischemia. The figure shows the ligation of left anterior descending coronary artery.

The serum was obtained 24 hours thereafter, following centrifugation at 3000 rpm for 15 minutes and then kept at -80°C until the measurement day. Harvested hearts after ischemia phases was placed into a Petri dish containing potassium chloride and cut into 5–6-mm thick transverse slices from the apex to the basis. Slices were incubated for 30 minutes at 37°C in a 1% solution of 2,3,5-triphenyltetrazolium chloride in 1% phosphate-buffered solution (PBS) then washed with PBS and stored in PBS with 0.01% sodium azide (PBS-A) at 4°C , as described in Pitts et al. [2007]. Infarct size was calculated as percentage of necrotic area compared with the total area, using a computerized program (Leica).

Histological Analysis. To assess the model, morphological analysis of tissues obtained from sham and ischemic animals was performed. Heart slices were fixed in 10% (vol/vol) buffered formalin for 48 hours. Sections were then embedded in paraffin and cut (10- μm thick) and stained with hematoxylin and

eosin for tissue morphological evaluation. The sections were analyzed by using a standard light microscope (320 objective) and photographed by a digital camera (Leica).

Determination of Biochemical Parameters. Quantitative determinations of serum cardiac troponin I (cTnI) and myoglobin (MYO) were performed by immune enzymatic assays (AxSYM System; Abbott).

3.2 Cell cultures and *in vitro* hypoxia/reoxygenation model

The rat cardiomyoblasts line H9c2, obtained from European Collection of Cell Cultures, were grown in Dulbecco's modified Eagle's medium supplemented with 10% fetal bovine serum (Bio-Whittaker), penicillin (100 U/ml) and streptomycin (100 µg/ml). The cells were grown at 37°C in a humidified 5% CO₂ atmosphere.

Combined oxygen and glucose deprivation and reoxygenation. H9c2 cells were exposed to oxygen, glucose and serum deprivation (OGSD) for various times (0,5-12h) according to a previously reported protocol [Irace *et al.*, 2005]. Briefly, the culture medium was replaced with deoxygenated (saturated for 20 minutes with 95% N₂ and 5% CO₂), glucose- and serum-free medium containing NaCl 116 mM, KCl 5.4 mM, MgSO₄ 0.8 mM, NaHCO₃ 26.2 mM, NaH₂PO₄ 1 mM, CaCl₂ 1.8 mM, glycine 0.01 mM and 0.001 % (w/v) phenol red. Cultures were then placed in an humidified 37°C incubator within an anaerobic chamber (Billups-Rothenberg, Inc., Del Mar, CA, USA) containing a gas mixture of 95% N₂ and 5% CO₂. The final oxygen concentration in the medium in these experimental conditions, measured by an oxygen-sensitive

electrode (OxyLite 2000, Oxford Optronix, Oxford, UK), was 5 mmHg. Reoxygenation was achieved by replacing the OGSD medium with oxygenated regular medium containing glucose, and returning cultures to normoxic conditions (37°C in a humidified 5% CO₂ atmosphere) for 3 hours (brief period of reoxygenation) and 24 hours (long period of reoxygenation).

3.3 Preparation of cytosolic extracts

Heart tissues were homogenized through polytron system at 6000 rpm/min with lysis buffer containing 10 mM HEPES, pH 7.5, 3 mM MgCl₂, 40 mM KCl, 5% glycerol, 1 mM DTT 10 mM EDTA, inhibitor proteases and 0.2% Nonidet P-40 at 4°C. Cell debris and nuclei were pelleted by centrifugation at 13 000 x g for 15 min at 4°C, and supernatants were stored at -80°C.

Cells were washed and detached with PBS containing 1 mM EDTA. To obtain cytosolic extracts for electrophoretic mobility shift assay (EMSA) and ferritin and IRP1 Western Blot analysis, cells were treated with lysis buffer containing of 10 mM HEPES, pH 7.5, 3 mM MgCl₂, 40 mM KCl, 5% glycerol, 1 mM DTT and 0.2% Nonidet P-40 at 4°C. Cell debris and nuclei were pelleted by centrifugation at 13 000 x g for 15 min at 4°C, and supernatants were stored at -80°C. For Western blot analysis of TfR1, cell pellets were lysed in 20 mM Tris.HCl pH 7.4, 150 mM NaCl, 5 mM EDTA, 5% (v/v) glycerol, 10 mM NP-40 and proteases inhibitors tablets (Roche, Mannheim, Germany) at 4°C. The supernatant fraction, obtained by centrifugation at 13000 x g for 15 min, was stored at -80°C [Mattace Raso *et al.*, 2009]. The protein concentration was determined by the Bio-Rad protein assay according to the supplier's manual (Bio-Rad, Milan, Italy).

3.4 Western blot analysis

Lysates aliquots containing 50-100 µg of proteins were denatured, separated on a 12% (for ferritin) or 8% (for IRP1, Tfr1, iNOS) SDS-polyacrylamide gel and transferred onto a nitrocellulose membrane (Amersham Biosciences, Little Chalfont, Buckinghamshire, UK) using a Bio-Rad Transblot. Protein were visualized on the filters by reversible staining with Ponceau-S solution (Sigma Aldrich, St. Louis, MO, USA) and destained in PBS. Filters were blocked in milk buffer (1X TBS, 5% non fat dry milk, 0.1 % Tween 20) and incubated for 2 hr at room temperature or overnight at 4°C with 1:1000 rabbit polyclonal antibody to human ferritin cross-reactive with rat protein (Dako Cytomation, Glostrup, Denmark), or with 1:1000 mouse antibody to human transferrin receptor 1 crossreactive with rat Tfr1 (Zymed Laboratories Inc., CA, USA), or with 1:250 goat antibody to human IRP1 cross-reactive with rat IRP1 (Santa Cruz Biotechnology, Inc., Santa Cruz, CA, USA), or with 1:2000 mouse antibody to human iNOS crossreactive with rat iNOS (BD Transduction Laboratories). Subsequently, the membranes were incubated for 90 minutes at room temperature with peroxidase-conjugated goat anti-mouse IgG + IgM, or peroxidase-conjugated rabbit anti-goat IgG, or peroxidase-conjugated goat anti-rabbit IgG (all the secondary antibodies were purchased from Jackson ImmunoResearch Laboratories, Baltimore Pike, West Grove, PA). The resulting complex was visualized using chemiluminescence Western blotting detection reagents (ECL, Amersham) in an Image Quant (GE Healthcare). The optical density of the bands was determined by a GS-800 imaging densitometer (Bio-Rad). Normalization of results was ensured by incubating the nitrocellulose membrane in parallel with the α -tubulin and/or β -actin antibody.

3.5 Electrophoretic Mobility-Shift Assay (EMSA)

Plasmid pSPT-fer, containing the sequence corresponding to the IRE of the H-chain of human ferritin, was linearized at the *Bam* HI site and transcribed *in vitro* as previously described [Santamaria *et al.*, 2011].

For band shift analysis, 5 µg of protein extracts were incubated for 30 min at room temperature with 0.2 ng of *in vitro* transcribed ³²P-labelled IRE RNA. The reaction was performed in lysis buffer (10 mM Hepes, pH 7.5, 3 mM MgCl₂, 40 mM, KCl, 5% (v/v) glycerol, 1 mM DTT and 0.07% (v/v) Nonidet P-40) in a final volume of 20 µl. To recover total IRP1 binding activity, 2-mercaptoethanol was added to the binding reaction before the addition of ³²P labelled IRE RNA. To degrade unbound probe, the reaction mixture was incubated with 1 unit of RNase T₁ (Roche) for 10 min and non specific RNA-protein interaction was displaced by the addition of 5 mg/ml heparin for 10 min. After the addition of 10 µl of loading buffer containing 30 mM Tris-HCl, pH 7.5, 40 % (w/v) sucrose and 0.2 % bromophenol blue, the reaction mixtures were electrophoresed for 2 h at 200 V in a 6% non denaturing polyacrylamide gel. After electrophoresis the gel was dried and autoradiographed at -80°C. The IRP-IRE complexes were quantified with a GS-800 imaging densitometer (Bio Rad, Milan). The results are expressed as the percentage of IRP binding activity versus 2-mercaptoethanol-treated samples.

3.6 Cell viability assay (MTT)

Cell viability was assessed by measuring the level of mitochondrial dehydrogenase activity using 3-(4,5-dimethyl-2-thiazolyl)-2,5-diphenyl-2H-

tetrazolium bromide (MTT) as substrate, as reported in Simeone et al. [2011, *Epub. ahead of print*]. The assay was based on the redox ability of living mitochondria to convert dissolved MTT into insoluble formazan (figure 24).

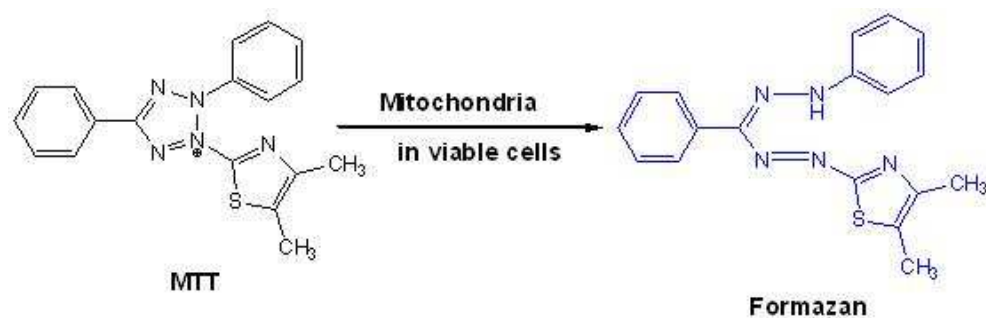


Figure 24. The figure shows the dehydrogenase-mediated reaction that converts MTT into insoluble formazan salt.

Briefly, after OGSD and OGSD/Reoxygenation, the medium was removed and the cells were incubated with the MTT solution (0.5 mg/mL) for 1 hour in a humidified 5% CO₂ incubator at 37°C. The incubation was stopped by removing the MTT solution and adding 100µL/well of dimethylsulfoxide (DMSO) to solubilize the formazan. The absorbance was monitored at 550 nm by using an iMark microplate reader spectrophotometer (Bio-Rad, Milan, Italy). The data were expressed as the percentage of cell viability, compared to control cultures.

3.7 Counting of viable and dead cells

The counting of viable and dead cells after exposure to OGSD/Reoxygenation conditions, for the appointed times, was realized using the commercial kit MultiTox-Fluor Multiplex Citotoxicity Assay (Promega Corporation). This method simultaneously measures the relative number of live and dead cells in

cell populations. The MultiTox-Fluor Assay simultaneously measures two protease activities: one is a marker of cell viability, and the other is a marker of cytotoxicity. The live-cell protease activity is restricted to intact viable cells and is measured using a fluorogenic, cell-permeant peptide substrate (glycyl-phenylalanyl-amino fluorocoumarin; GF-AFC). The substrate enters intact cells where it is cleaved by the live-cell protease activity to generate a fluorescent signal proportional to the number of living cells. This live-cell protease becomes inactive upon loss of cell membrane integrity and leakage into the surrounding culture medium. A second, fluorogenic, cell-impermeant peptide substrate (bisalanil-alanyl-phenylalanyl-rhodamine 110; bis-AAF-R110) is used to measure dead-cell protease activity, which is released from cells that have lost membrane integrity. Because bis-AAF-R110 is not cell-permeant, essentially no signal from this substrate is generated by intact, viable cells (figure 25).

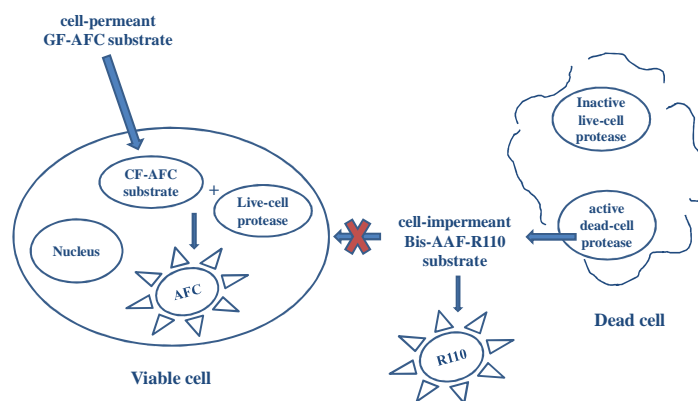


Figure 25. Summary diagram of the MultiTox-Fluor Assay.

The live- and dead-cell proteases produce different products, AFC and R110, which have different excitation and emission spectra (viability: Excitation 400 nm; Emission 505 nm - cytotoxicity: Excitation 485 nm; Emission 520 nm), allowing them to be detected simultaneously. The results were expressed as a percentage of live cells and dead cells, compared to control cultures.

3.8 Cellular energy status: dosage of ATP

The intracellular levels of ATP were determined by using the Bioluminescent somatic cell assay kit (Sigma Aldrich, St. Louis, USA). This method uses the enzyme luciferase, which catalyzes the oxidative decarboxylation of luciferin in the presence of ATP, producing a luminous signal whose intensity is proportional to the concentration of ATP.

In detail:



To perform this test, the cells were resuspended in PBS at a concentration of 10^6 cells/mL. 50 μL of this suspension were added to 50 μL of sterilized water and 100 μL of a buffer (Somatic Cell Releasing Reagent) to allow the immediate release of ATP from the cells. Subsequently, 100 μL of sample were added to 100 μL of ATP Mix Assay. After shaking, the intensity of light emission was measured by luminometer (EG&G Berthold).

The results were expressed as a percentage of control culture and were normalized for micrograms of protein and number of cells.

3.9 Dosage of lactate dehydrogenase (LDH) release

The Cyto Tox-ONE Assay kit (Promega Corporation) permits a rapid, fluorescent measure of the release of lactate dehydrogenase (LDH) from cells with a damaged membrane. This method, used to evaluate the fraction of damaged and/or necrotic cells exposed to OGSD/Reoxygenation conditions, is based on a coupled enzymatic reaction that allows to measure the release of the LDH, an enzyme that catalyzes the conversion of lactate to pyruvate with the concomitant production of NADH.

NADH in the presence of the diaphorase enzyme, permits the conversion of resazurin into the fluorescent substrate resorufin as shown in figure 26.

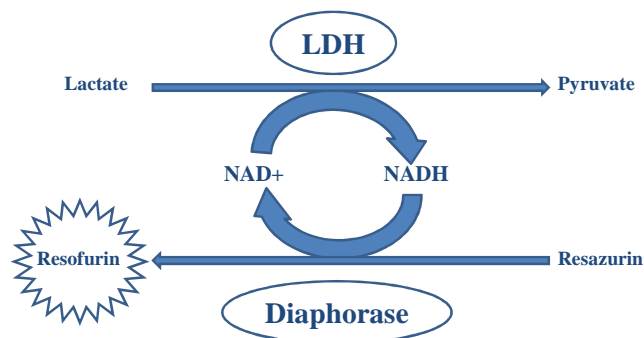


Figure 26. The figure shows coupled enzymatic reaction that allows to measure the release of the LDH

The fluorescence was monitored using an excitation wavelength of 560 nm and an emission wavelength of 590 nm in a Perkin-Elmer LS-55 Luminescence Spectrometer (Perkin-Elmer Ltd., Beaconsfield, England). The results were expressed as percentage of necrotic cells compared to control cultures.

3.10 Measurement of ROS

The formation of ROS was evaluated by means of the probe 2',7'-dichlorofluorescein-diacetate (H₂DCF-DA) as described in Santamaria et al. [2004]. Briefly, H9c2 cells were grown in DMEM containing 10% (v/v) fetal bovine serum, then were plated at a density of 10000 cells/well into 96-well dishes. Cells were allowed to grow for 48 hours and then incubated in the growth medium containing 50 μM of H₂DCF-DA (Sigma-Aldrich) for 1 h at 37 °C. H₂DCF-DA is a non-fluorescent permeant molecule that passively diffuses into cells, where the acetates are cleaved by intracellular esterases to form H₂DCF and thereby traps it within the cell. In the presence of intracellular ROS, H₂DCF is rapidly oxidized to the highly fluorescent 2',7'-dichlorofluorescein (DCF), as showed in figure 27.

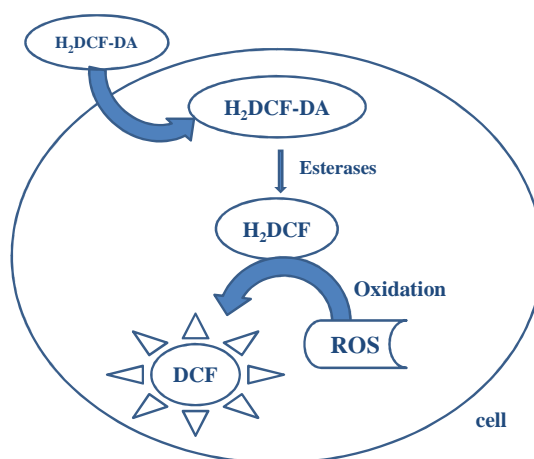


Figure 27. Summary diagram of the ROS assay.

Cells were washed twice with PBS buffer and were then subjected to hypoxia/reoxygenation conditions at different times. At the end of the

OGSD/reoxygenation experiments, ROS levels were measured in a fluorescent microplate reader (Perkin Elmer LS-55 Luminescence Spectrometer, Perkin-Elmer Ltd., England). Fluorescence was monitored using an excitation wavelength of 485 nm and an emission wavelength of 538 nm. The data were expressed as the percentage of ROS production, compared to control cultures.

3.11 Lipid peroxidation assay (TBARS' test)

Lipid peroxidation products from cells were measured by the thiobarbituric acid colorimetric assay. This method permits a quantitative evaluation of the lipid peroxidation of cell membranes by determining the malondialdehyde (MDA), one of the final products of oxidation of polyunsaturated fatty acids caused by the presence of free radicals, including ROS. The TBARS' test, therefore, is an indirect index of ROS production and cellular oxidative stress [Irace *et al.*, 2005]. The MDA reacts with thiobarbituric acid (TBA) in acidic media and at a temperature of 90-95°C resulting in a pink adduct that has a maximum absorption at a wavelength of 550 nm, and that is spectrophotometrically quantized.

Briefly, after OGSD and OGSD/Reoxygenation, cells were washed and collected in PBS $\text{Ca}^{2+}/\text{Mg}^{2+}$ -free medium containing 1 mM EDTA and 1.13 mM butylated hydroxytoluene (BHT). Cells were broken up by sonication. Trichloroacetic acid, 10% (w/v), was added to the cellular lysate and, after centrifugation at 1000 x g for 10 min, the supernatant fluid was collected and incubated with 0.5% (w/v) thiobarbituric acid at 80-100°C for 30 min. After cooling, malondialdehyde (MDA) formation was recorded at 550 nm in the iMark microplate reader spectrophotometer (Bio-Rad, Milan, Italy). Samples

were scaled for protein concentration determined by the Bio-Rad protein assay, and a standard curve of MDA was used to quantify the MDA levels formed during the experiments. The results are presented as percentage of MDA production versus a control obtained in untreated cultures.

3.12 Assessment of “Labile Iron Pool” (LIP)

The cellular labile iron content was estimated by a fluorimetric assay using the metal-sensitive probe calcein (CA) [*Santamaria et al., 2011*] and the strong membrane-permeant iron chelator SIH (salicylaldehyde isonicotinoyl hydrazone), generously provided by Prof. Prem Ponka (McGill University, Montreal, QC, Canada). H9c2 cells, plated at a density of 10×10^3 cells/well, were subjected to OGSD and OGSD/Reoxygenation conditions and then were loaded with 0.5 μ M CA-AM (calcein-acetomethoxy, Molecular Probes, Invitrogen, Eugene, OR) for 45 min at 37 °C in calcium- and bicarbonate-free modified Krebs Henseleit buffer (KHB), consisting of HEPES 20mM, pH 7.4, NaCl 119mM, KCl 4.9 mM, KH_2PO_4 0.96 mM and glucose 5 mM. CA-AM rapidly penetrates across the plasma membrane and is intracellularly hydrolysed to release free CA. After loading, the cultures were washed of excess CA-AM two times with KHB. Cellular CA fluorescence was recorded in a Perkin Elmer microplate reader (Perkin Elmer LS-55 Luminescence Spectrometer, Beaconsfield, UK) using a filter combination with an excitation wavelength of 485 nm and an emission wavelength of 530 nm (slits 5 nm). Cell cultures without CA-AM were used as blank to correct non-specific autofluorescence. Trypan blue was added in all experiments to eliminate extracellular fluorescence. Once hydrolyzed, calcein becomes trapped in the

cytoplasm and emits intense green fluorescence. The calcein-loaded cells have a fluorescence component (ΔF) that is quenched by intracellular iron and can be revealed by addition of 100 μM SIH (figure 28).

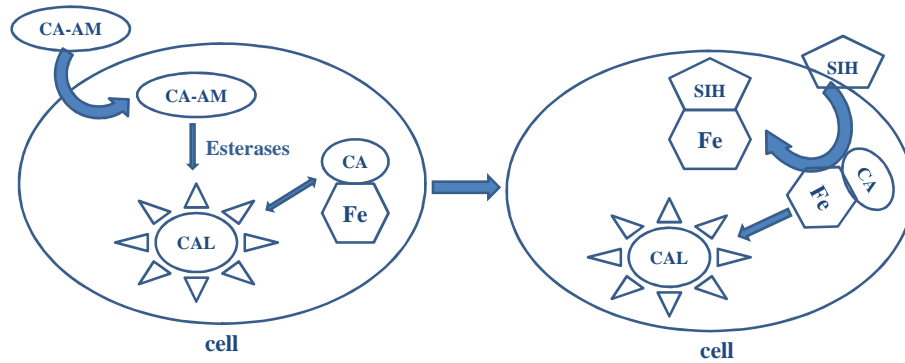


Figure 28. Summary diagram of the LIP assay.

The rise in fluorescence is equivalent to the change in calcein concentration or to the amount of cellular iron originally bound to CA. Thus, the changes in CA fluorescence intensity were directly proportional to the iron labile pool. To characterize the responsiveness of CA fluorescence toward different concentrations of intracellular iron, cells were preloaded with ferrous ammonium sulphate, ferric ammonium citrate or with the cell permeable ferrous iron chelator SIH. The data were expressed as the percentage of cellular labile iron pool, compared to control cultures.

3.13 Simvastatin activation by alkaline hydrolysis

Simvastatin obtained from Sigma-Tau was activated to its active form by alkaline hydrolysis before use. Briefly, Simvastatin prodrug was dissolved in an 0.1 N NaOH and 0.154 mol/liter NaCl solution and then incubated at 50 °C for 2 h. The pH was brought to 7.0 by HCl. The stock solution was stored at -20 °C [Madonna *et al.*, 2005].

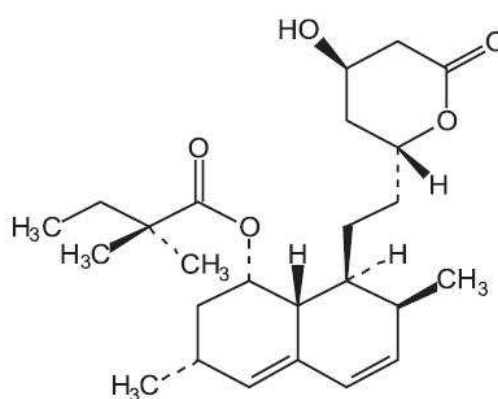


Figure 29. Molecular structure of Simvastatin.

3.14 Nitrites measurement

After release, NO reacts with O₂ to form the stable metabolite nitrite. Nitrite concentrations were measured by the Griess reaction to estimate the total amounts of NO in the media released from H9c2 cells, treated or not with Simvastatin and subjected to OGSD/reoxygenation conditions. To measure the nitrite levels, 100 µl of the medium in duplicate were removed and mixed with 100 µl of Griess reagent (1% sulfanilamide-0.1% naphthylethylenediamine-5% phosphoric acid; obtained by Sigma Aldrich) and incubated for 10 min at room temperature [Irace *et al.*, 2007]. Absorbance was measured at 550 nm by using

using an iMark microplate reader spectrophotometer (Bio-Rad, Milan, Italy). Nitrite concentrations were determined by comparison with NaNO₂ standards.

3.15 Statistical analysis

For the MTT assay, cell counting and ATP, LDH, ROS, MDA, LIP, nitrites determinations, results are expressed as mean of percentage \pm SEM of n observations respect to control cells (100%), where n represents the number of experiments performed on different days. The results were analyzed by one-way ANOVA followed by a Bonferroni post hoc test for multiple comparisons. A p-value ≤ 0.05 was considered significant.

The densitometric data from EMSA and Western blot analysis are reported as percentage of controls \pm SEM of n observations, where n represents the number of experiments performed on different days. Statistical significance among the results was determined by the ANOVA followed by the Newman–Keuls test. A p-value less than 0.05 was considered statistically significant.

4. RESULTS

4.1 Validation of the *in vivo* model of ischemia

To validate the *in vivo* model of heart ischemia, morphological analysis of cardiac tissues and dosage of myocardial infarction markers (Troponin I and myoglobin), obtained from sham and ischemic rats were performed.

Myocardial tissue from sham rats presented normal architecture, whereas tissue from ischemic rats presented edema between muscle fibers and erythrocyte infiltration, as showed in figure 30.

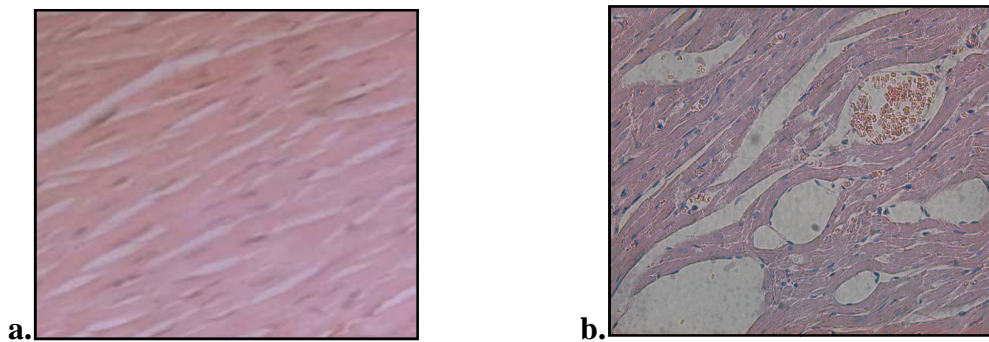


Figure 30. The figure **a** shows the normal myocardial tissue (sham) whereas the figure **b** shows the ischemic tissue, where there is clearly a loss of normal cell architecture, edema and erythrocyte infiltration.

The release of cTpI and MYO (figure 31) confirmed the tissue damage after ischemia.

Treatment	MYO (ng/ml)	cTnI (ng/ml)
SHAM	32.25 ± 11.02	1.25 ± 0.18
ISCHEMIA	46.86 ± 10.35	29.35 ± 12.32

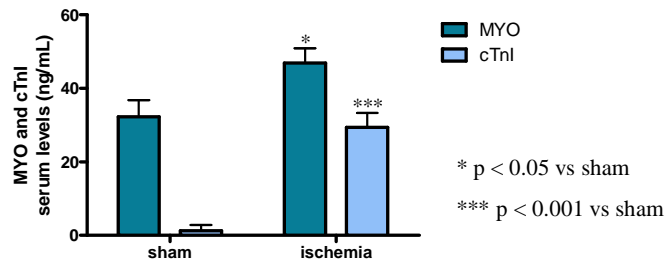


Figure 31. Graphic of the cTnI and MYO release. Data are expressed as mean ± SEM. * $p < 0,05$ vs sham; *** $p < 0,001$ vs sham.

Further validation of our model of cardiac ischemia was given by the increased expression of the transcription factor HIF1- α that, as we know, is stable during a state of oxygen deficiency (figure 32).

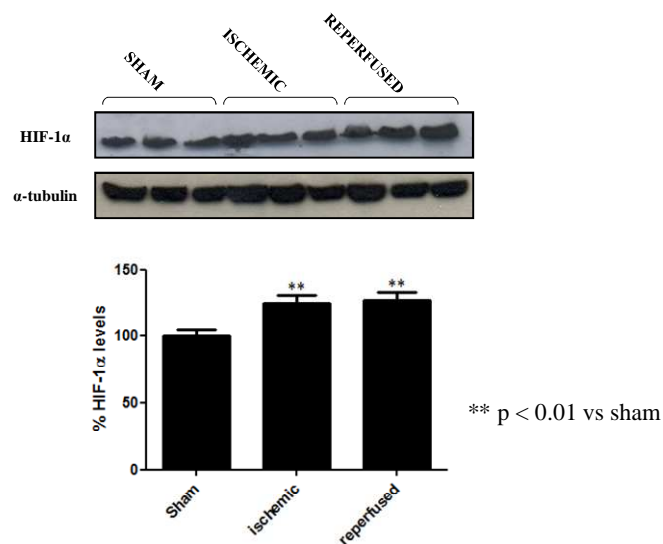


Figure 32. Expression, evaluated by Western blotting, of HIF-1 α after ischemia and subsequent reperfusion. Data are expressed as percentage compared to the sham. ** $p < 0,01$ vs sham.

4.2 *In vivo* cardiac damage and *in vitro* cardiomyoblasts viability

2,3,5-Triphenyltetrazolium chloride staining showed that left anterior descending coronary artery (LAD) ligation, lasting 30 to 90 minutes, produced an intramural infarction of the anterior wall of the left ventricle. As described in the Table 1, the percentage of damage after 90 minutes of ischemia was greater than obtained after 30 minutes. Furthermore, the damage after ischemia increased in reperfusion (24 hours).

TREATMENT	% DAMAGE
Sham	-
Ischemia 30 min.	4.41 ± 3.2
Ischemia 30 min + Reperfused	6.24 ± 2.5
Ischemia 90 min.	18.75 ± 2.8 ***
Ischemia 90 min + Reperfused	24.63 ± 3.0

Table 1. The tissue damage, induced at different times of ischemia and subsequent reperfusion, is expressed as percentage compared to the total tissue. Data are expressed as mean ± SEM; *** p < 0,001 vs sham.

These *in vivo* results were confirmed by *in vitro* data on cell viability (MTT assay and count of live and dead cells), allowing us to clarify some aspects of the damage caused by ischemia/reperfusion conditions.

The data obtained through hypoxia/reoxygenation experiments on cardiomyoblast (H9c2 cell line), that mimic ischemia/reperfusion conditions, shown that the cell viability was not affected during brief periods of OGSD (up to 3 hours), whereas 6 hours of OGSD reduced cell viability up to 50%.

However, these data have showed a recovery of cell viability in reoxygenation phase after the 6-hours OGSD. During long periods of OGSD (up to 12 hours), instead, the cell viability was dramatically reduced (up to 25%), and no recovery was observed during reoxygenation, as resumed in the Table 2.

OGSD (time)	OGSD	Rx 3 h	Rx 24 h
1 h	95 ± 3.5%	92 ± 4.5%	98 ± 4%
3 h	79 ± 2.1% **	88 ± 2.7% °	97 ± 2.5% °°
6 h	51 ± 3% ***	54 ± 3.5%	86 ± 3% °°°
12 h	29 ± 3.26% ***	23 ± 4.5%	31 ± 4.12%

Table 2. Cell viability, evaluated by MTT assay, at different times of hypoxia. Data are expressed as percentage of the mitochondrial dehydrogenase activity compared to the control. ** p < 0.01 vs CTRL; *** p < 0.001 vs CTRL; ° p < 0.05 vs OGSD; °° p < 0.01 vs OGSD; °°° p < 0.001 vs OGSD.

These results were also confirmed by the assessment of ATP levels, and the release of the enzyme lactate dehydrogenase (LDH), a classical marker of the damage of cell membranes, during OGSD/reoxygenation experiments.

Experiments for the evaluation of the cellular energy balance, conducted up to 6 hours of OGSD and subsequent reoxygenation, showed a reduction in ATP levels during hypoxia, in accordance with the alteration of the respiratory chain, followed by a recovery to the control levels when normoxic conditions were restored.

For long periods of OGSD (up to 12 hours), instead, the energy charge of the cardiomyocytes was nearly wiped during hypoxia and no recovery was observed during reoxygenation (Table 3).

OGSD (time)	OGSD	Rx 3 h	Rx 24 h
3 h	80 ± 2.5% *	126 ± 3% °°	135 ± 2.3% °°°
6 h	49 ± 3% ***	96.3 ± 3.5% °°°	112 ± 3.2% °°°
12 h	5 ± 2.96% ***	9 ± 4.5%	14 ± 4.62%

Table 3. Cellular energy balance evaluated as percentage of ATP levels at different times of hypoxia. Data are expressed as percentage compared to the control. * P < 0,05 vs CTRL; *** p< 0.001 vs CTRL; °° p < 0.01 vs OGSD; °°° p< 0.001 vs OGSD.

The data on LDH release (Table 4), finally, showed a strongly increase of the LDH levels in the culture medium, both in hypoxia and reoxygenation condition, only for long period of OGSD (12 hours).

OGSD (time)	OGSD	Rx 3 h	Rx 24 h
3 h	9.3 ± 2.5%	29.8 ± 3% °°°	29.4 ± 3% °°°
6 h	6.5 ± 2.8%	24 ± 3% °°°	27.5 ± 2.9% °°°
12 h	53.7 ± 2% ***	79.8 ± 3% °°°	94 ± 3.12% °°°

Table 4. Table of LDH release. Data are expressed as percentage compared to the control. *** p< 0.001 vs CTRL; °°° p< 0.001 vs OGSD.

Overall these results show that relatively short periods of hypoxia (up to 6 hours) and subsequent reoxygenation lead to a reversible damage, while for longer periods of hypoxia, up to 12 hours, the damage is irreversible, emphasizing (pointing out) that the 6 hours of hypoxia are the “no return point”, beyond which the damage sustained by cardiomyocytes is irreversible.

4.3 Cellular death: necrosis or apoptosis?

The LDH enzyme, is a marker of the damage of cell membranes and its release in the culture medium shown that the hypoxic damage leads to a necrotic death of the cardiomyocytes subjected to OGD/reoxygenation experiments, confirming the *in vivo* data regarding the release of cTnI and MYO, as a markers of necrosis, after ischemic injury. We have also evaluated by western blot the activation of Caspasi-3, as a marker of apoptotis (figure 33). In our experiments, no activation of this protein was observed confirming that the cell death, during hypoxia/reoxygenation conditions, not involved the apoptotic pathway.

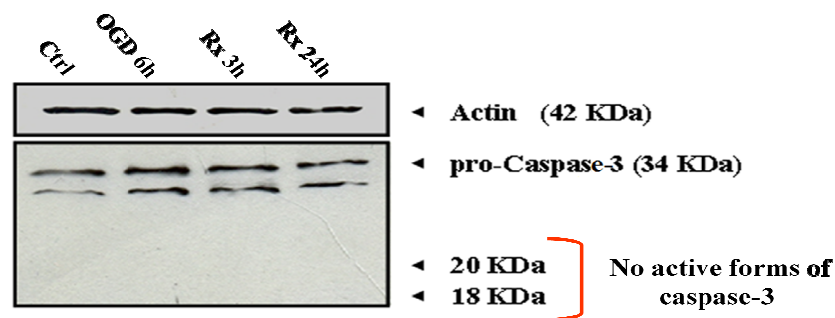


Figure 33. Western blot of the Caspasi-3. No active forms (18-20 KDa) of this protein was detected after hypoxia and subsequent reoxygenation phases.

4.4 Evaluation of oxidative stress

As known, ROS are involved in the pathogenesis and progression of ischemia/reperfusion injury, we have evaluated the levels of oxidative stress using for the *in vivo* model an indirect method based on the assessment of lipid peroxidation, and for the *in vitro* model the fluorescent probe 2',7'-dichlorofluorescein that consent a direct dosage of the ROS. The obtained data,

in accordance with the results on cell viability, showed a strong increase of lipid peroxidation after 90 minutes of ischemia and subsequent 24 hours of reperfusion, compared to the sham (4 and 5 folds respectively), whereas no significant variation was evidenced following 30 minutes of ischemia and successive reperfusion (figure 34).

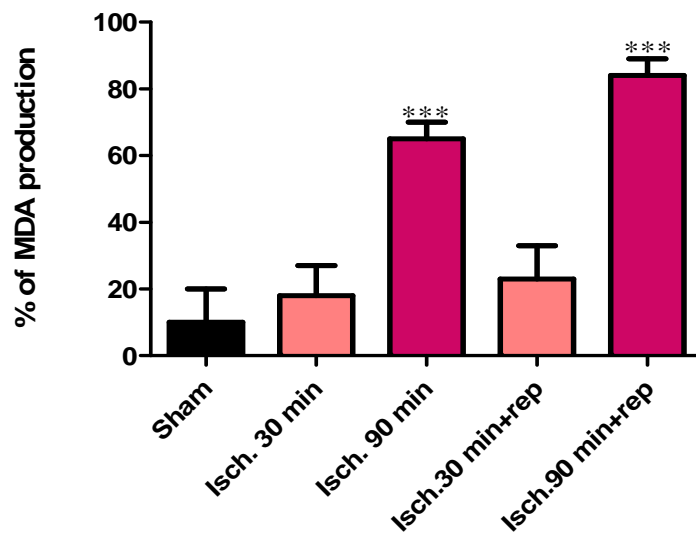


Figure 34. Evaluation of the oxidative stress by assessment of MDA production. Data are expressed as percentage compared to the sham. *** $p < 0.001$ vs sham.

These results were confirmed in the *in vitro* model which clearly showed an increase of ROS levels during OGSD and reoxygenation phases starting from long periods (6 hours) of hypoxia whereas no significant variation of ROS production were showed in cells subjected to short periods (up 3 hours) of hypoxia (figure 35).

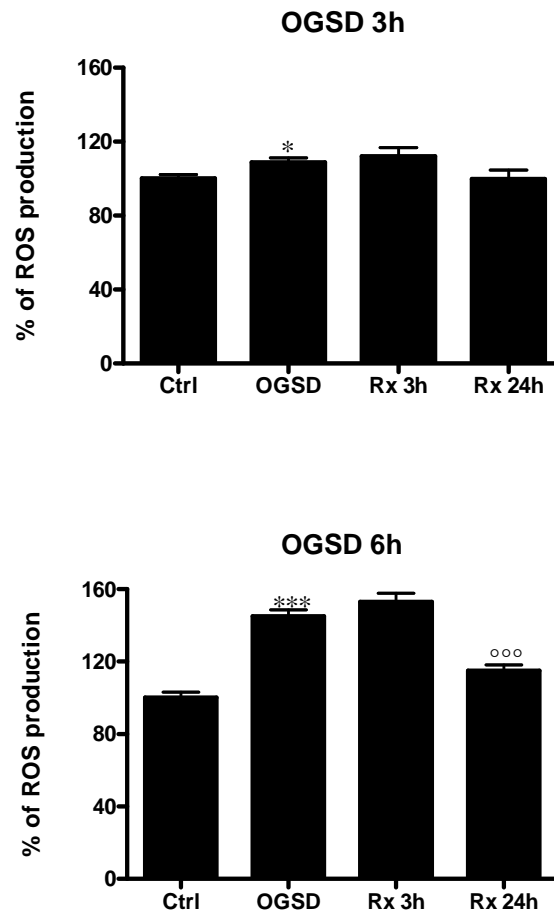


Figure 35. Evaluation of ROS production by 2',7'-dichlorofluorescein. Data are expressed as percentage compared to the control.
 * $p < 0.05$ vs CTRL; *** $p < 0.001$ vs CTRL; ooo $p < 0.001$ vs OGSD.

4.5 RNA-binding activity of IRPs

As previously described, the iron is involved in the ROS production, and for this reason we evaluated the activity and the expression of the main proteins implicated in the homeostasis of this metal, such as the Receptor of Transferrin 1 (TfR1), ferritin and the Iron Regulatory Proteins (IRPs). RNA-band shift experiments, conducted on protein samples from rat hearts subjected to ischemia for 30 and 90 minutes and subsequent 24 hours of reperfusion, showed a significant decrease (~50%, compared to the sham) of RNA-binding activity of IRP1 after 90 minutes of ischemia, followed by a remarkable

increase (~ 4 folds, compared to the ischemic samples) during the reperfusion phase, whereas no significant variation was showed during 30 minutes of ischemia and subsequent reperfusion (figure 36).

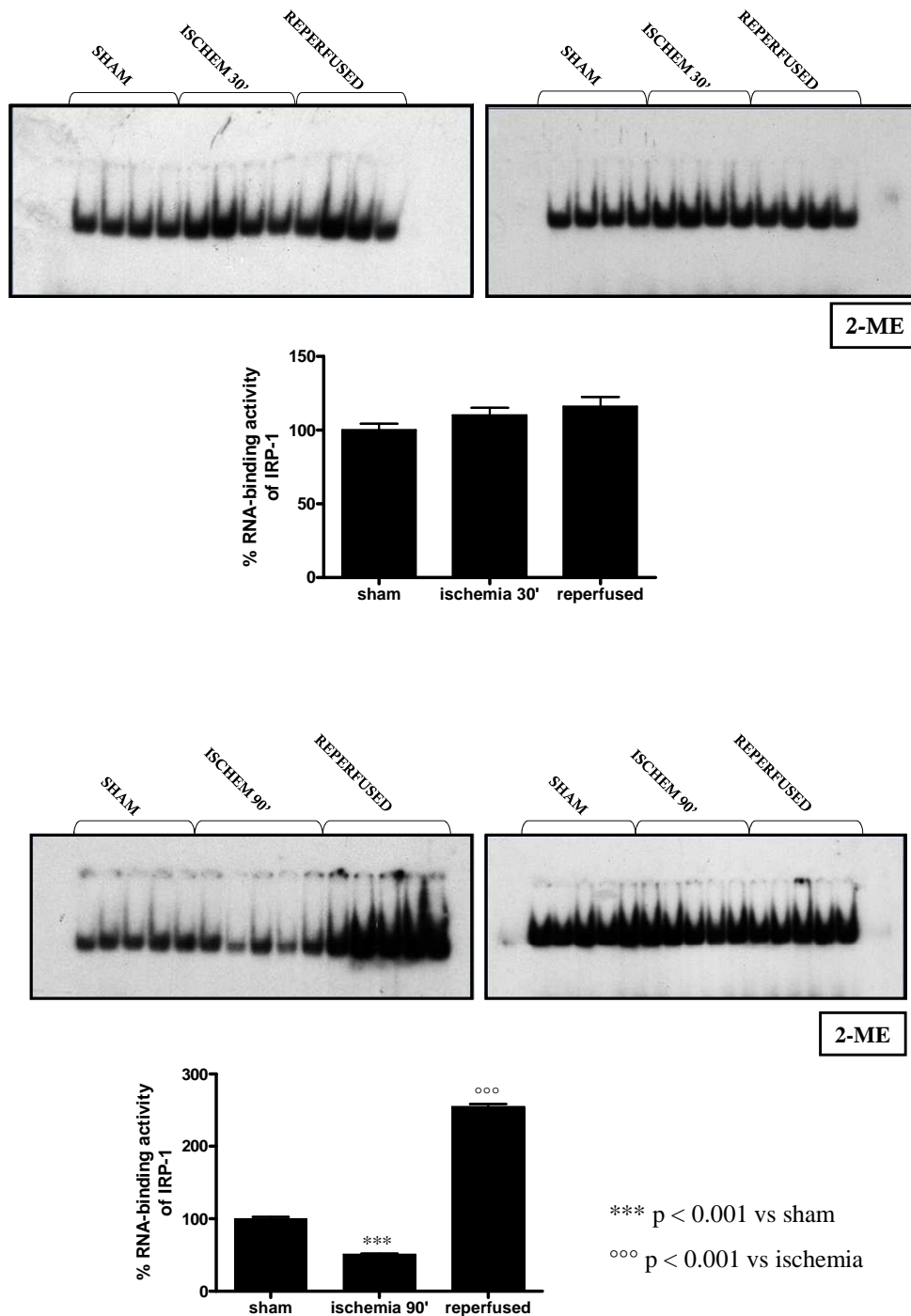


Figure 36. The RNA-binding activity of IRPs evaluated by EMSA. Data are expressed as percentage compared to the sham.
 *** p < 0,001 vs sham; °°° p < 0,001 vs ischemia.

To determine the total amount of IRP1 RNA-binding activity, 2-mercaptoethanol was added to the binding reaction before the addition of ^{32}P -labelled IRE to reveal ‘‘latent’’ IRP1 RNA-binding activity, thus giving the total amount of IRP1 activity (100% of IRE-binding). To evaluate whether the modulation of IRP1 RNA-binding activity was caused by a variation of IRP1 protein content after ischemia/reperfusion injury, we also analysed the cytosolic levels of this protein. As shown in figure 37, immunoblot analysis did not show any appreciable variations in the amounts of IRP1 protein in all the examined samples, suggesting that the ischemia/reperfusion injury caused a regulation of RNA-binding activity of IRP1 without affecting the protein expression.

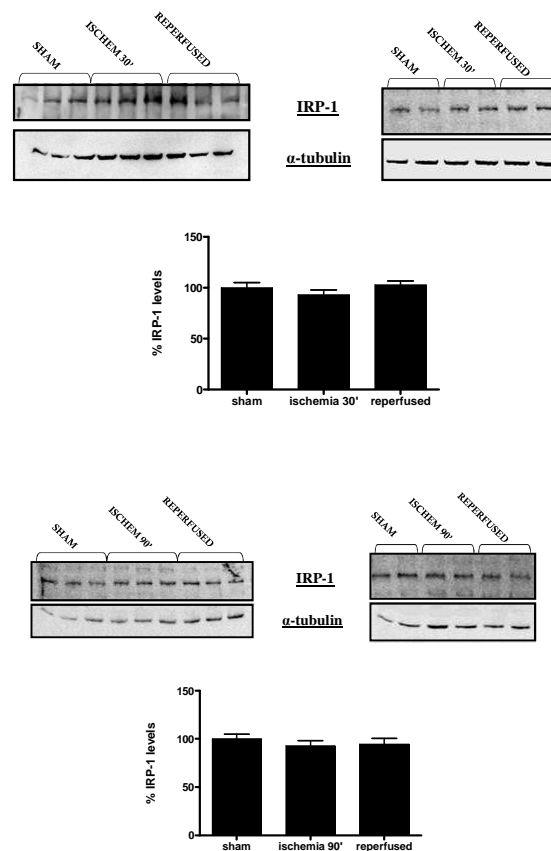


Figure 37. Expression, evaluated by Western blot, of IRP1 in heart rat samples exposed to 30 and 90 minutes of ischemia and subsequent 24 hours of reperfusion. Data are expressed as percentage compared to the control.

4.6 Ferritin and TfR1 expression

Based on the results of RNA-binding activity of IRPs, we analyzed under the same experimental conditions, the expression of the main proteins regulated at post-transcriptional level by the Iron Regulatory Proteins (IRPs), such as ferritin and Transferrin Receptor 1 (TfR1), shown in figure 38.

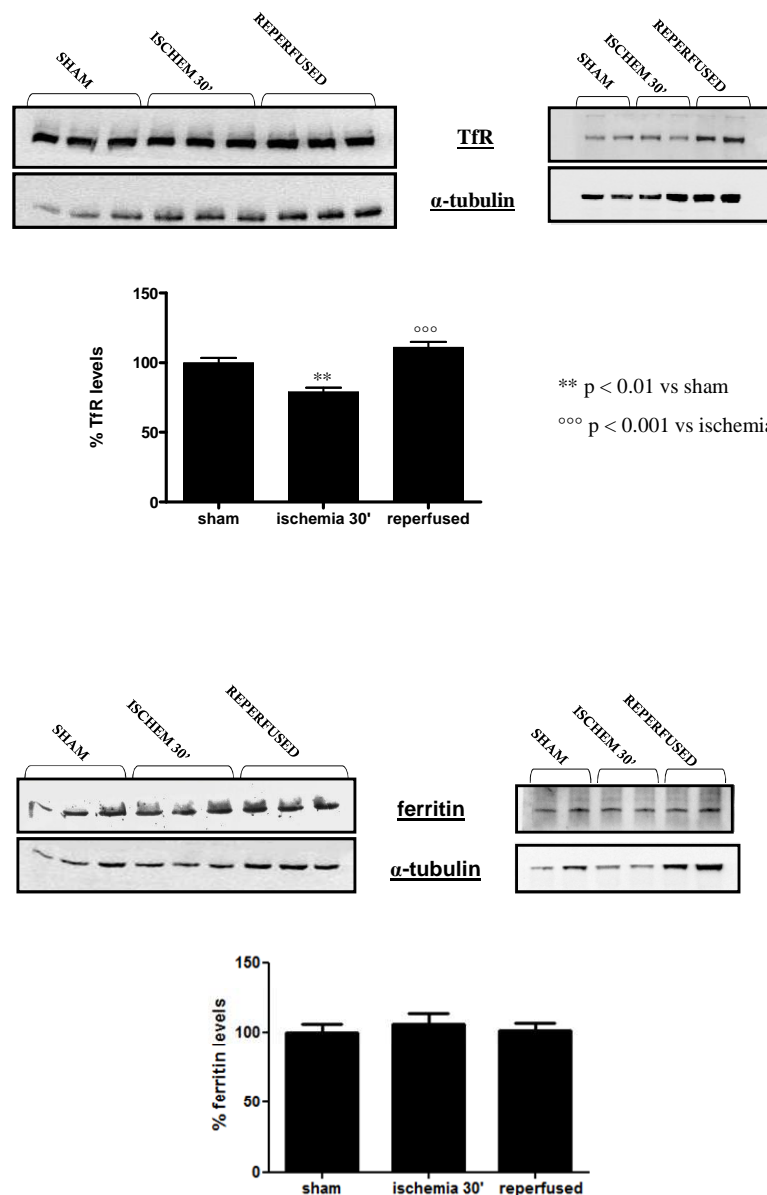


Figure 38. Expression of TfR1 and ferritin after 30 minutes of ischemia and subsequent reperused phase of 24 hours. Data are expressed as percentage compared to the sham. ** p < 0,01 vs sham; $^{\circ\circ\circ}$ p < 0,001 vs ischemia.

In rat hearts subjected to 30 minutes ischemia and subsequent 24 hours of reperfusion we observed slight decrease of TfR1 expression after ischemia, followed by a small increase during the reperfusion phase, whereas no alteration was shown in cytosolic levels of ferritin in both ischemic and reperfusion phases.

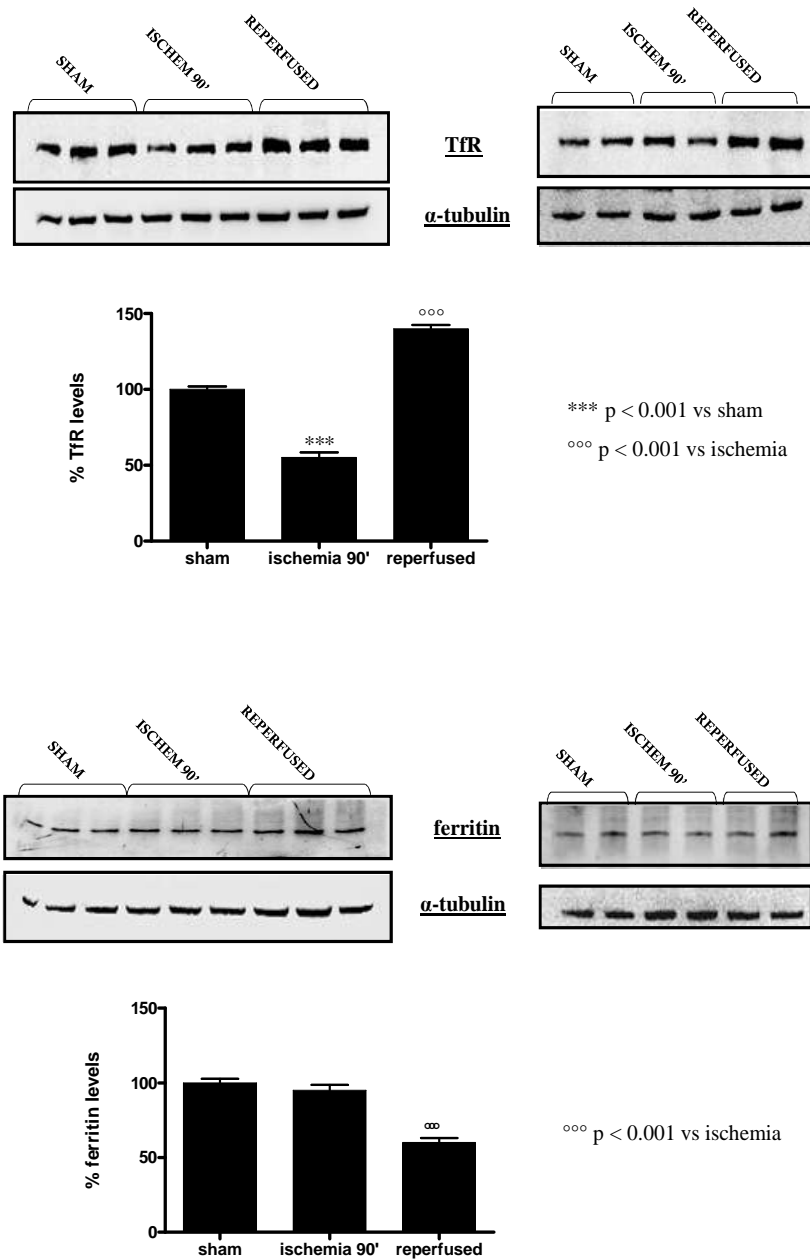


Figure 39. Expression of TfR1 and ferritin after 90 minutes of ischemia and subsequent 24 hours of reperfusion. Data are expressed as percentage compared to the sham. *** p < 0,001 vs sham; $\circ\circ\circ$ p < 0,001 vs ischemia.

On the contrary, in rat hearts subjected to 90 minutes of ischemia and subsequent reperfusion (figure 39), we observed a significant reduction of TfR1 levels after ischemia and a remarkable increase during reperfusion phase. Moreover, no variation was shown in cytosolic levels of ferritin after 90 minutes of ischemia, whereas a significant reduction of this protein was shown during the subsequent 24 hours reperfusion. These data are substantially consistent with changes in binding activity of IRP1 and suggest an increase in intracellular levels of iron, in particular during reperfusion after a period of 90 minutes of ischemia.

Moreover, in order to confirm that the possible changes in the expression of these proteins are effectively due to ischemic injury, we also evaluated possible alterations of the expression of TfR1, ferritin and IRP1 in the right ventricle, normally sprinkled with the blood flow. The results, shown in figure 40, did not reveal alterations in the expression of these proteins, thus demonstrating that the changes seen in the left ventricle can be attributed to ischemic damage.

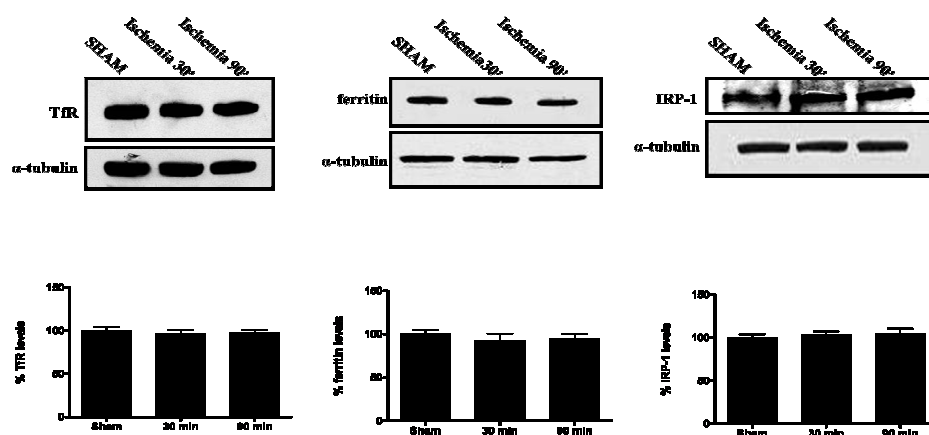


Figure 40. Evaluation of the TfR1, ferritin and IRP1 expression by Western blot in the right ventricle (no ischemic ventricle) after 30 and 90 minutes of ischemia. Data are expressed as percentage compared to the sham.

4.7 LIP evaluation in an *in vitro* model of hypoxia and reoxygenation conditions

On the basis of this results it is possible to speculate that the altered expression of ferritin and TfR1, observed after a prolonged ischemia/reperfusion phase, could lead to an increase of intracellular iron content. In order to confirm this hypothesis, using an *in vitro* model of hypoxia/reoxygenation, we evaluated the intracellular levels of the “Labile Iron Pool”. The data, depicted in the figure 41, shown a strong increase of the cellular levels of iron, in particular after the reoxygenation phase.

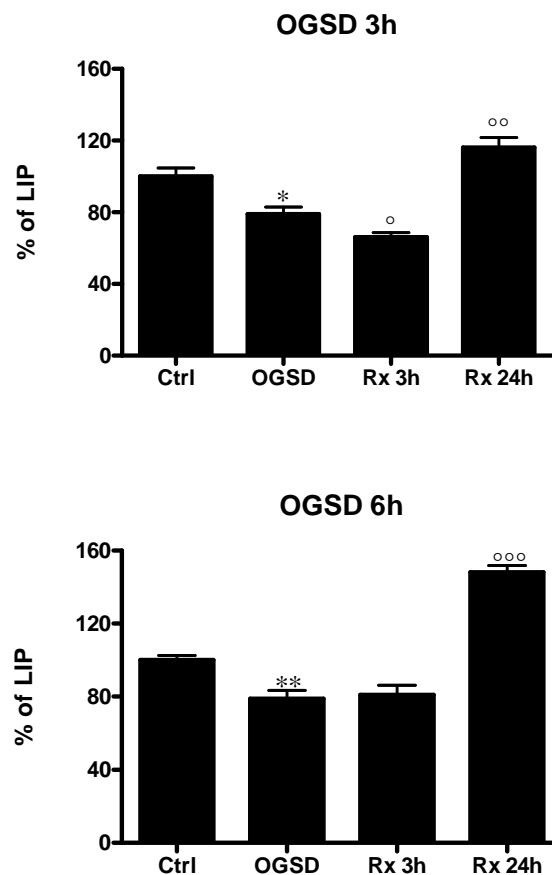


Figure 41. LIP extension in H9c2 cell line exposed to 3 and 6 hours of hypoxia/reoxygenation phase. Data are expressed as percentage compared to the control.

* $p < 0.05$ vs CTRL; ** $p < 0.01$ vs CTRL; ° $p < 0.05$ vs OGSD;
°° $p < 0.01$ vs OGSD; °°° $p < 0.001$ vs OGSD.

These results support the hypothesis of an increase in iron levels in cardiac cells, in particular during reperfusion subsequent to long periods of ischemia, and can explain the greatest damage suffered by cardiomyocytes after prolonged periods of ischemia. The increased availability of iron to participate in the Fenton reaction after long periods of ischemia/hypoxia, may explain the increased production of ROS, and the largest loss of cell viability observed in these conditions compared to that obtained after brief period of ischemia/hypoxia. In order to confirm the role of iron in the ROS production and then its role in the progress of hypoxic/ischemic injury, we conducted experiments in which H9c2 cells were treated with 100 μ M SIH (Salicylaldehyde Isonicotinoyl Hydrazone), as a strong iron chelator, and then exposed to 6 hours of hypoxia and subsequent reoxygenation phases, because is at this time that we observed a strong ROS increase and a greater reduction of cell viability. For these experiments we chose the concentration of 100 μ M, because it is the highest not toxic concentration of SIH, as it is evident through cell viability experiments conducted on H9c2 cells subjected for 1 hour to increasing concentrations of SIH shown in figure 42.

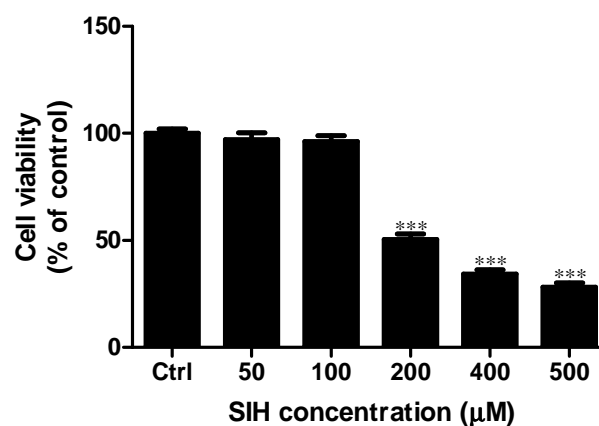


Figure 42. Evaluation of cell viability after treatment with different concentration of SIH. Data are expressed as percentage compared to the control. *** $p < 0,001$ vs CTRL.

As shown in the figure 43, we observed a significant reduction of ROS production in iron starved cells exposed to hypoxia/reoxygenation conditions, resulting in an improvement in cell viability (figure 44).

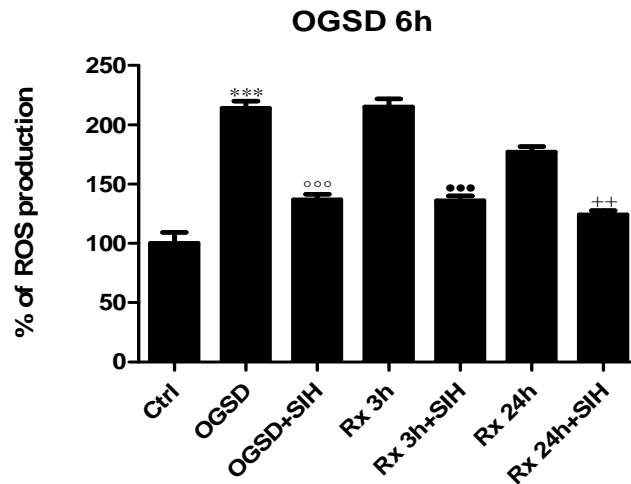


Figure 43. ROS production during hypoxia/reoxygenation conditions, with or without SIH 100 μ M. Data are expressed as percentage compared to the control.

*** $p < 0,001$ vs CTRL; °°° $p < 0,001$ vs OGSD;
 ••• $p < 0,001$ vs Rx 3h; ++ $p < 0,01$ vs Rx 24h.

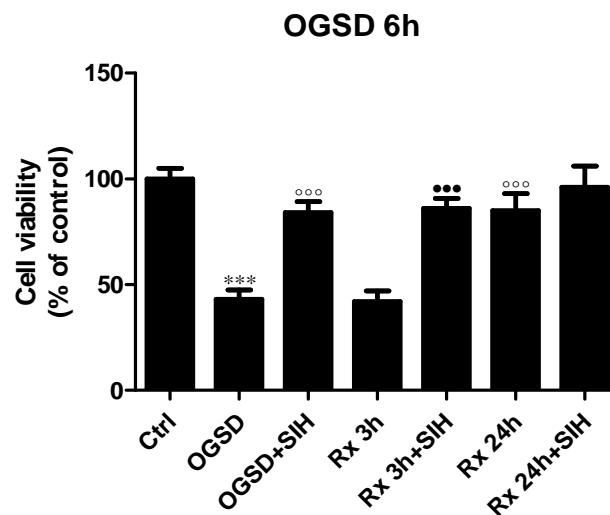


Figure 44. Cell viability after hypoxia and reoxygenation conditions, with or without SIH 100 μ M. Data are expressed as percentage compared to the control.

*** $p < 0,001$ vs CTRL; °°° $p < 0,001$ vs OGSD; ••• $p < 0,001$ vs Rx 3h.

These results demonstrate that a important portion of ROS, produced during hypoxia is iron-dependent, confirming still again that this metal is directly involved in the development of ischemia/reperfusion injury.

4.8 *In vitro* Simvastatin effects on hypoxia/reoxygenation injury

It has been suggested that statins may exert effects separate from their cholesterol-lowering actions, including promotion of endothelial NO synthesis (Vaughan *et al.*, 1996).

Therefore, we tested the hypothesis that a clinically relevant dose of a widely used statin could exert an ameliorating effect on reperfusion injury in our *in vitro* model of myocardial ischemia-reperfusion.

Based on the above considerations, it was evaluated the cytoprotective effects of Simvastatin on the expression of protein such as NOS, (involved in the production of nitric oxide, that can interact with $O_2^{\bullet-}$ to form peroxynitrite, a potent mediator of cell damage), on the ROS production and then on the cell viability in rat cardio-myoblasts subjected to hypoxia and reoxygenation conditions, as described in the Material and Methods section.

Considering the close relationship between the ROS production and iron, it was also evaluated the effects of Simvastatin on the iron metabolism, in particular assessing the LIP extension and the expression of protein such as Transferrin Receptor 1 and ferritin.

4.8.1. Simvastatin cytotoxicity

As reported in literature [Medina *et al.*, 2008], the treatment with Simvastatin induce a biphasic dose-related response. Medina and colleagues demonstrated that in retinal microvascular endothelial cells (RMECs) low concentrations (0,01-0,1 μ M) of Simvastatin, significantly promoting cell proliferation, whereas high concentration of Simvastatin (10 μ M) had the opposite effect, and that Simvastatin induced cell death at concentrations higher than 1 μ M. On these bases we evaluated the cytotoxic effect of Simvastatin on H9c2 cells, by MTT assay (figure 45).

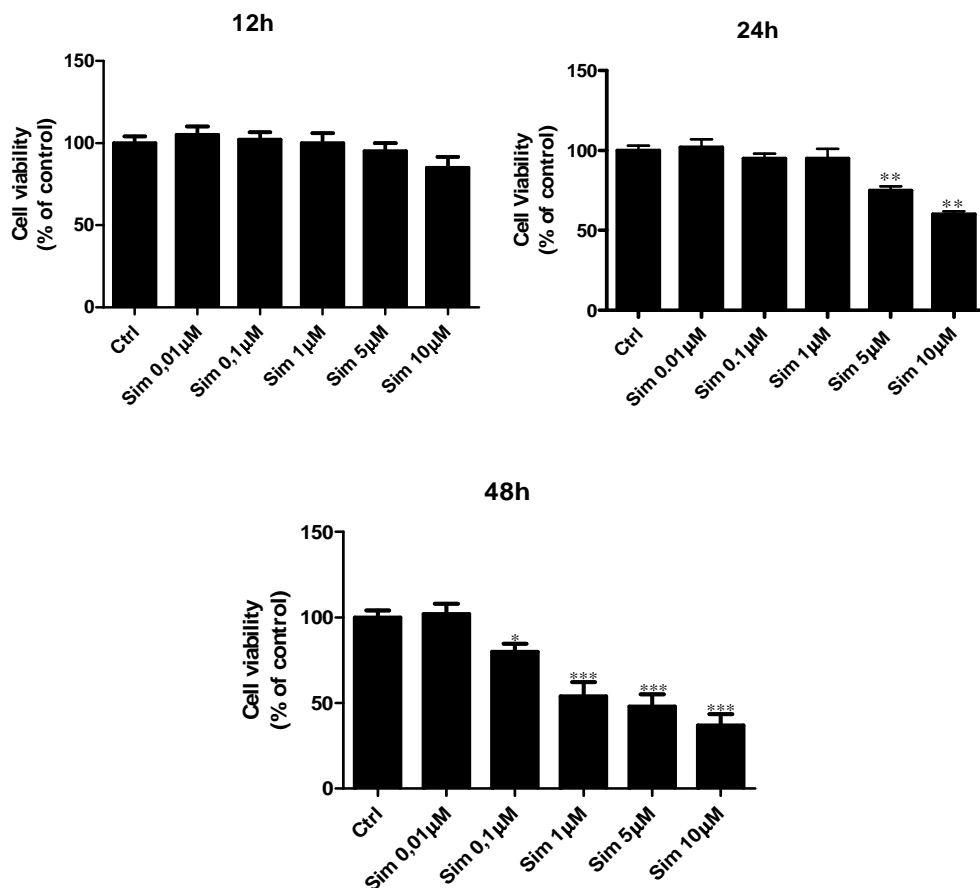


Figure 45. Cell viability after treatment with different concentrations of Simvastatin, at 12, 24 and 48 hours. Data are expressed as percentage compared to the control.

* $p < 0,05$ vs CTRL; ** $p < 0,01$ vs CTRL; *** $p < 0,001$ vs CTRL.

We treated H9c2 cells with 0,01-10 μ M Simvastatin for 12, 24 and 48 hours. The results, shown a reduction of cell viability at concentrations higher than 1 μ M after 24 and 48 hours of exposition with Simvastatin, whereas after 48 hours, Simvastatin was toxic at concentration higher than 0,1 μ M.

Therefore, to evaluate possible cytoprotective effects of Simvastatin during hypoxia and reoxygenation conditions, we chose to expose H9c2 cells with 0,01 μ M of Simvastatin for 24 hours, and then we subjected the same cells to 6 hours of hypoxia and subsequent reoxygenations, keeping constant the dose of the drug during hypoxia and reoxygenation phases.

4.8.2 Effects of Simvastatin on iNOS expression and NO production

Regarding the nitric oxide (NO) metabolism, it was evaluated, during hypoxia/reoxygenation conditions and after treatment with Simvastatin, the expression of iNOS that is able to produce high levels of NO.

The results shown that Simvastatin treatment strongly reduced the high levels of iNOS (figure 46), which expression, as reported in literature and confirmed in our conditions, is induced during hypoxia and the subsequent reoxygenation phases.

This result was reflected by the nitrites level (figure 47) that was increased after hypoxia/reoxygenation phases, and that was significantly reduced after treatment with Simvastatin, in accordance with the iNOS expression. In this experiments the H9c2 cells were treated also with LPS 100 μ M, as positive control, in order to show the higher concentration of nitrites in this cell line.

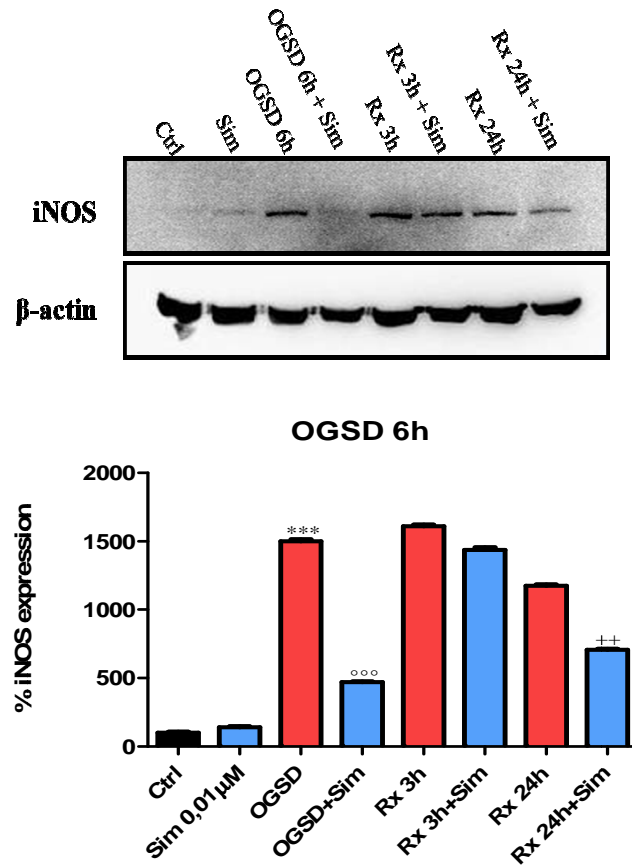


Figure 46. iNOS expression, evaluated by Western blot, during hypoxia and reoxygenation conditions, with or without Simvastatin 0,01 μM.
 *** p < 0.001 vs CTRL; °°° p < 0.001 vs OGSD; ++ p < 0.01 vs Rx 24h.

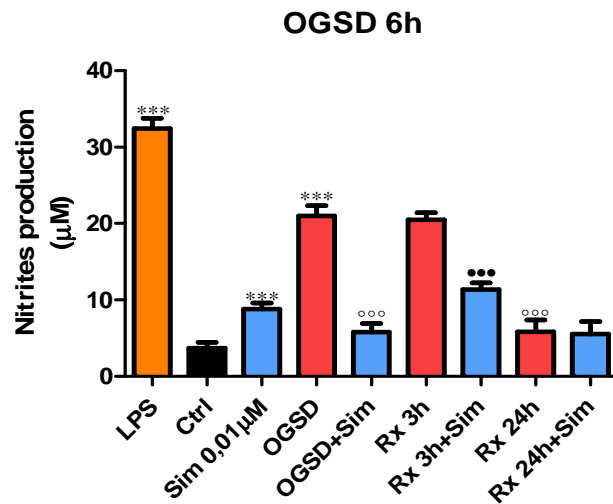


Figure 47. Nitrites dosage during hypoxia/reoxygenation conditions, with or without Simvastatin 0,01 μM. Data are expressed as μM of nitrites produced by the cells.
 *** p < 0.001 vs CTRL; °°° p < 0.001 vs OGSD; °°° p < 0.001 vs Rx 3h.

4.8.3 Simvastatin effects on ROS production during hypoxia/reoxygenation conditions

Because statins shown a “pleiotropic” effect that could reduce the oxidative stress, we evaluated the ROS production in H9c2 cells treated with Simvastatin and then exposed to hypoxia/reoxygenation conditions.

The obtained data shown a significant increase of ROS levels during hypoxia, as previously demonstrated, levels that remained elevated in the following reoxygenation phases (see figure 48).

Interestingly, the treatment with Simvastatin determined a decrease of ROS production, constantly observed either in hypoxia that in reoxygenation conditions.

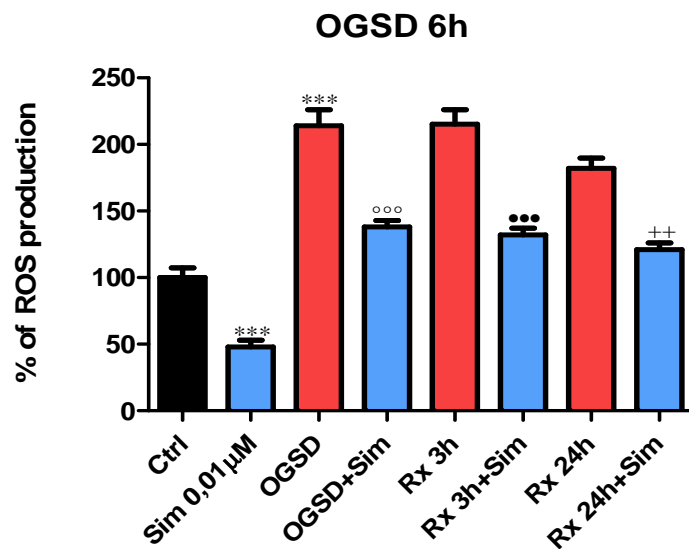


Figure 48. Evaluation of ROS production during hypoxia/reoxygenation condition, with or without Simvastatin 0,01 μM. Data are expressed as percentage compared to the control.

*** p < 0.001 vs CTRL; °°° p < 0.001 vs OGSD; ••• p < 0.001 vs Rx 3h; ++ p < 0,01 vs Rx 24h.

4.8.4 Effect of Simvastatin on cell viability in the hypoxia/reoxygenation damage

The results previously described, shown a reduction of the nitrites levels and ROS that are the principal mediators of the ischemic injury.

In this contest it was evaluated also the effects of Simvastatin on the cell viability. The data, shown an improvement of cell viability (figure 49), in agreement with the reduced production of nitrites and ROS.

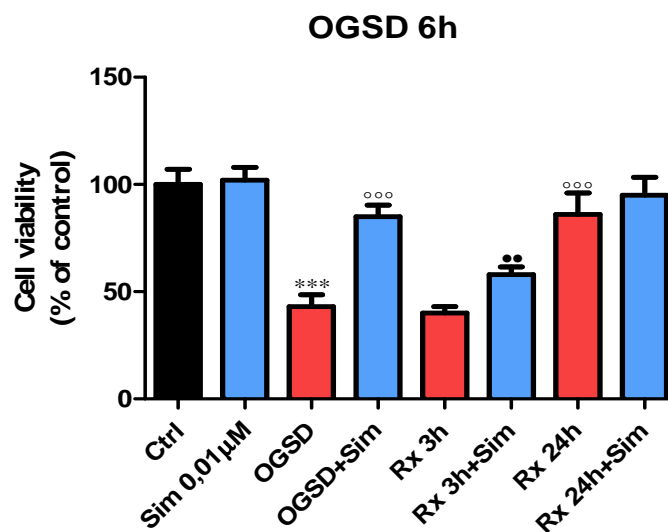


Figure 49. Cell viability during hypoxia and subsequent reoxygenation phase, with or without Simvastatin 0,01 μM. Data are expressed as percentage compared to the control.

*** $p < 0.001$ vs CTRL; °°° $p < 0.001$ vs OGSD; °° $p < 0.01$ vs Rx 3h.

In detail, it was observed a recovery of cell viability, in particular after hypoxia and during the 3 hours of reoxygenation phases, whereas a less evident recovery was observed during the 24 hours of reoxygenation phase. This result can be explained because during the 24 hours of reperfusion phase, subsequent to 6 hours of hypoxia, as previously described, the cells are still able to recover from the hypoxic damage.

4.8.5 Effects of Simvastatin on iron homeostasis

As demonstrated above, iron is involved in the progression of ischemia/reperfusion injury catalyzing the production of ROS. Because our results demonstrated that Simvastatin can reduce the ROS production in H9c2 cells subjected to hypoxia/reoxygenation conditions, we decided to investigate whether Simvastatin can affect the cellular iron homeostasis. In detail, it was examined the effect of Simvastatin on the expression of protein such as ferritin and TfR1, and also on the LIP extension. The obtained results shown not significant changes in TfR1 expression (figure 50), while of great interest are the effects of Simvastatin on the expression of ferritin.

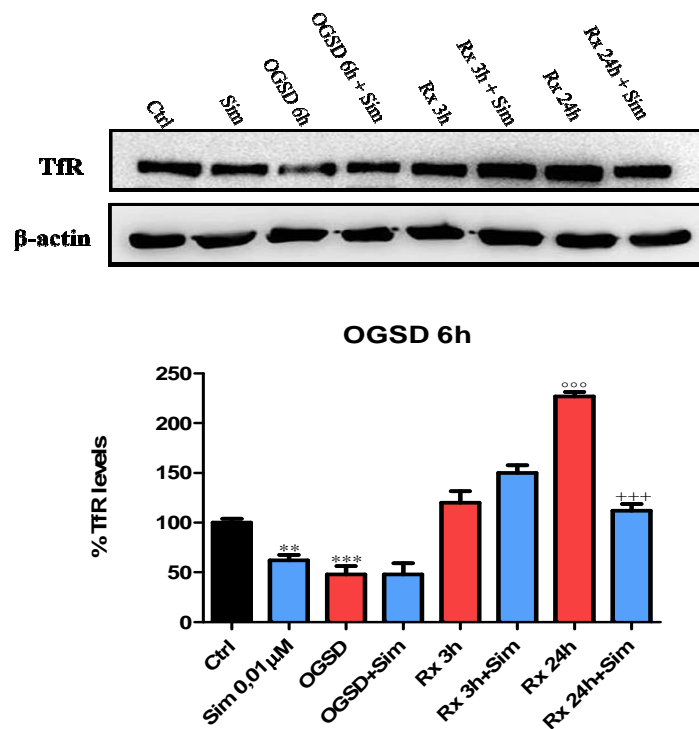


Figure 50. TfR1 expression after hypoxia/reoxygenation conditions, with or without Simvastatin 0,01 μ M. Data are expressed as percentage compared to the control.

** $p < 0,01$ vs CTRL; *** $p < 0,001$ vs CTRL; °°° $p < 0,001$ vs OGSD; +++ $p < 0,001$ vs Rx 24h.

In fact, it was observed a strong increase of ferritin levels exclusively in cells treated with Simvastatin and then exposed to hypoxia, whereas no significant changes were observed in all the other phases of the experiment (figure 51).

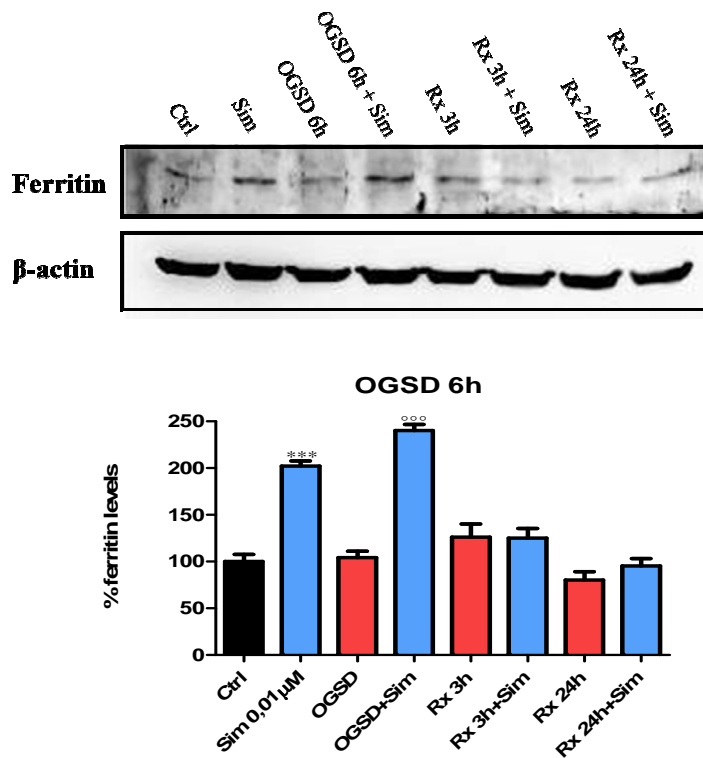


Figure 51. Ferritin expression after hypoxia/reoxygenation conditions, with or without Simvastatin 0,01 μM. Data are expressed as percentage compared to the control. *** $p < 0.001$ vs CTRL; ooo $p < 0.001$ vs OGSD.

These results are in accordance with the changes of the LIP extension, showing a reduction of the Labile Iron Pool in H9c2 cells subjected to hypoxia and treated with Simvastatin (figure 52).

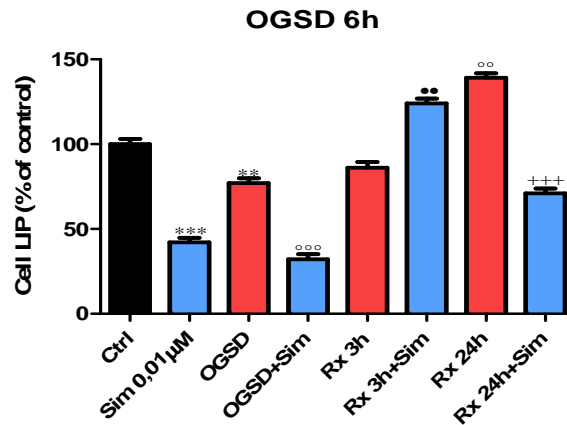


Figure 52. Dosage of LIP during hypoxia/reoxygenation damage, with or without Simvastatin 0,01 µM. Data are expressed as percentage compared to the control.

** p < 0,01 vs CTRL; *** p < 0.001 vs CTRL; °° p < 0,01 vs OGSD;
 °°° p < 0.001 vs OGSD; °° p < 0,01 vs Rx 3h; +++ p < 0,001 vs Rx 24h.

Overall these results demonstrated that the cytoprotective effects of Simvastatin, with a consequent improvement of cell viability observed in H9c2 cells subjected to hypoxia/reoxygenation and treated with Simvastatin, were due to:

- the reduction of peroxynitrite levels, related to the reduced expression of iNOS, induced by Simvastatin;
- a decrease of ROS production determined, at least in part, to a reduced LIP extension, and then to a reduced availability of iron to participate in the ROS production;
- finally, the observed reduction in the LIP was essentially related to the increased expression of ferritin, induced by the treatment with Simvastatin.

5. DISCUSSION

There is a growing body of evidence that increased oxidative stress and generation of ROS is one of the crucial mechanisms of ischemic cardiomyopathy [Asghar *et al.*, 2009; Smyth *et al.*, 2010]. In addition, it was indicated that the generation of ROS correlated with metal oxidants such as iron [Ward *et al.*, 2010]. The ischemic cardiac condition and the subsequent reperfusion, lead to several functional and metabolic changes that globally define the so-called “ischemia/reperfusion injury”, in which the overproduction of ROS is the main source of cell damage. A key role in the ROS production is played by iron through the Haber-Weiss-Fenton reaction. Iron is an essential element for the growth and metabolism of all living organisms, however, an excess of this metal can be toxic for all cell types, then the iron metabolism must be finely regulated.

To evaluate the role of iron and the molecular mechanisms that regulate the cellular iron homeostasis during the cardiac ischemia/reperfusion injury, an *in vivo* model of myocardial infarction/reperfusion was produced in rat by ligation of left anterior descending coronary artery, and successive ligature removal, at the end of the ischemia period, to obtain a reperfusion phase. We have demonstrated in this *in vivo* model that relatively short periods of ischemia lead to a minimum damage that not affects the functions of the cardiac tissue, while longer periods of ischemia induce greater damage that alters the normal architecture of myocardial tissue, showing edema between muscle fibers and erythrocyte infiltration.

Concerning the iron metabolism, we demonstrated that 90 minutes of ischemia alter IRP1 activity in *in vivo* model of ischemia/reperfusion injury. In particular, we

demonstrated a significant decrease of RNA-binding activity of IRP1 after 90 minutes of ischemia, followed by a remarkable increase during the reperfusion phase. Through the immunoblot analysis of IRP1 levels, that did not show any appreciable variations in the amounts of IRP1 protein, we demonstrated that the ischemia caused an up-regulation of RNA-binding activity of IRP1 without affecting the protein expression.

In agreement with the altered IRP1 activity, we observed a decrease of TfR1 expression after ischemia, followed by an increased levels of this protein during the reperfusion, especially in rats subjected to 90 minutes of ischemia and subsequent reperfusion phase. Respect to the expression of ferritin, no variation was shown in the cytosolic levels of this protein after 90 minutes of ischemia, whereas a significant reduction of ferritin was shown during the subsequent reperfusion, a result that is consistent with altered IRP1 activity. All these results suggest an increase of intracellular levels of iron, in particular during reperfusion after a period of 90 minutes of ischemia. To demonstrate this hypothesis, we decided to evaluate the extension of the “Labile Iron Pool” (LIP) in an *in vitro* model of hypoxia/reoxygenation. To this aim, rat cardiomyoblasts (line H9c2) were exposed to combined oxygen and glucose deprivation and then to a reoxygenation condition.

First, we determined the cell viability and ATP production in this model. The obtained results show that up to 6 hours of hypoxia and subsequent reoxygenation the damage is reversible, emphasizing that the 6 hours of hypoxia could be considered a “no return point”, beyond which the damage sustained by the cells becomes irreversible. Moreover, measuring the release of LDH enzyme, as a marker of the damage of cell membranes, and evaluating the activation of Caspase-3, as a marker of apoptosis, we demonstrated that hypoxia leads to a necrotic death of the

cells, confirming the *in vivo* obtained data on cTnI and MYO release, markers of necrosis, after ischemic injury.

Then, we evaluated the LIP extension and we found that the free intracellular iron content was strongly increased, in particular during the reoxygenation phase subsequent to hypoxia.

To assess the potential oxidative damages caused by iron, we determined the ROS content, both in the *in vivo* and in the *in vitro* cardiac models. The results were in accordance with increased LIP extension. In fact, we found a significant increase of ROS levels essentially during prolonged periods of ischemia, levels that remained elevated during the subsequent reperfusion.

Moreover, we conducted experiments in which H9c2 cells were treated with SIH, a strong iron chelator, and then exposed to hypoxia/reoxygenation. We observed a significant reduction of ROS production, resulting in an improvement in cell viability, in iron starved cells exposed to hypoxia/reoxygenation conditions. Thus, we demonstrated that an important part of ROS, produced during ischemic/reperfusion conditions is iron-dependent and that therefore this metal is directly involved in the development and in the progress of ischemic injury.

In addition, my study was focused on the so-called “pleiotropic” effects of statins, in particular on the anti-inflammatory and antioxidant activities of these drugs, that could ameliorate the reperfusion injury, as suggested by their promotion of endothelial NO synthesis (*Vaughan et al., 1996*). Therefore, we tested this hypothesis in our *in vitro* model of myocardial ischemia/reperfusion. We investigated the cytoprotective effects of Simvastatin on H9c2 cells exposed to 6 hours of hypoxia and subsequent reoxygenation. The obtained results demonstrated that Simvastatin improved cell viability by distinct mechanisms:

- Simvastatin reduced the expression of iNOS, strongly induced during ischemia, and the levels of peroxynitrite, one of the key mediators of cell damage;
- Simvastatin decreased the production of ROS, strongly implicated in the ischemic injury;
- Simvastatin reduced LIP extension, leading to a reduced availability of iron to participate in the ROS production;
- Simvastatin induced an increase of ferritin expression, in particular during hypoxic conditions, in agreement with the reduced LIP extension and ROS production, thus explaining the improvement of cell viability, observed after treatment with this drug.

In conclusion these results not only clarify the role that iron plays in the progression of ischemic injury, but also highlight how proteins that regulate the homeostasis of this metal, such as ferritin, may be targets of drugs such as Simvastatin, which could be used in the prevention of oxidative damage induced by ischemic conditions.

Should this be the case, a new horizon as an antioxidant opens for Simvastatin.

6 REFERENCES

- Acehan D., Jiang X., Morgan D.G., Heuser J.E., Wang X., Akey C.W. Three-dimensional structure of the apoptosome: implications for assembly, procaspase-9 binding, and activation. *Mol. Cell* (2002); **9**: 423–32
- Abboud S., Haile D.J. A novel mammalian iron-regulated protein involved in intracellular iron metabolism. *J. Biol. Chem.* (2000); **275**: 19906–19912
- Abd T.T., Eapen D.J., Bajpai A., Goyal A., Dollar A., Sperling L. The Role of C-Reactive Protein as a Risk Predictor of Coronary Atherosclerosis: Implications from the JUPITER Trial. *Curr. Atheroscler. Rep.* (2011); **13**: 154–161
- Adam O., Laufs U. Antioxidative effects of statins. *Arch. Toxicol.* (2008); **82**: 885-892
- Aisen P. Transferrin receptor 1. *Int. J. Biochem. Cell Biol.* (2004); **36**: 2137-43
- Andriopoulos Jr B., Corradini E., Xia Y., Faasse S.A., Chen S., Grgurevic L., Knutson M.D., Pietrangelo A., Vukicevic S., Lin H.Y., Babitt, J.L. BMP6 is a key endogenous regulator of hepcidin expression and iron metabolism. *Nat. Genet.* (2009); **41**: 482–487
- Arndt S., Maegdefrau U., Dorn C., Schardt K., Hellerbrand C., Bosserhoff A.K. Iron-induced expression of bone morphogenic protein 6 in intestinal cells is the main regulator of hepatic hepcidin expression in vivo. *Gastroenterology* (2010); **138**: 372–382
- Arosio P., Ingrassia R., Cavadini P. Ferritins: a family of molecules for iron storage, antioxidation and more. *Biochim. Biophys. Acta* (2009); **1790**: 589–599
- Asghar O., Al-Sunni A., Khavandi K., Khavandi A., Withers S., Greenstein A., Heagerty A.M., Malik R.A. Diabetic cardiomyopathy. *Clin Sci (Lond)* (2009); **116**: 741-760
- Bhalli M.A., Kayani A.M., Samore N.A. Frequency of risk factors in male patients with acute coronary syndrome. *J. Coll. Physicians Surg. Pak.* (2011); **21**: 271-5
- Biederbick A., Stehling O., Rösler R., Niggemeyer B., Nakai Y., Elsässer H.P., Lill R. Role of human mitochondrial Nfs1 in cytosolic iron-sulfur protein biogenesis and iron regulation. *Mol. Cell. Biol.* (2006); **26**: 5675–5687
- Bordoni A., Angeloni C., Leoncini E., Danesi F., Maranesi M., Biagi P.L., Hrelia S. Hypoxia/reoxygenation alters essential fatty acids metabolism in cultured rat cardiomyocytes: protection by antioxidants. *Nutrition, Metabolism & Cardiovascular Diseases* (2005); **15**: 166-173

- Breuer W., Shvartsman M., Cabantchik Z.I. Intracellular labile iron. *Int. J. Biochem. Cell Biol.* (2008); **40**: 350-354
- Budas G.R., Churchill E.N., Mochly-Rosen D. Cardioprotective mechanisms of PKC isozyme-selective activators and inhibitors in the treatment of ischemia-reperfusion injury. *Pharmacological Research* (2007); **55**: 523–536
- Casey T.M., Pakay J.L., Guppy M., Arthur P.G. Hypoxia causes downregulation of protein and RNA synthesis in non contracting mammalian cardiomyocytes. *Circ. Res.* (2002); **90**: 777–783
- Cazzola M., Invernizzi R., Bergamaschi G., Levi S., Corsi B., Travaglini E., Rolandi V., Biasiotto G., Drysdale J., Arosio P. Mitochondrial ferritin expression in erythroid cells from patients with sideroblastic anemia. *Blood* (2003); **101**: 1996–2000
- Ceconi C., Bernocchi P., Borsano A., Cagnoni A., Pepi P., Curello S., Ferrari R. New insights on myocardial pyridine nucleotides and thiol redox state in ischemia and reperfusion damage. *Cardiovasc. Res.* (2000); **47**: 586–594
- Chi N.C., Karliner J.S. Molecular determinants of responses to myocardial ischemia/reperfusion injury: focus on hypoxia-inducible and heat shock factors. *Cardiovascular Research* (2004); **61**: 437– 447
- Cho H.H., Cahill C.M., Vanderburg C.R., Scherzer C.R., Wang B., Huang X., Rogers J.T. Selective translational control of the Alzheimer amyloid precursor protein transcript by iron regulatory protein-1. *J. Biol. Chem.* (2010); **285**: 31217–31232
- Clarke S.L., Vasanthakumar A., Anderson S.A., Pondarre C., Koh C.M., Deck K.M., Pitula J.S., Epstein C.J., Fleming M.D., Eisenstein R.S. Iron-responsive degradation of iron-regulatory protein 1 does not require the Fe–S cluster. *EMBO J.* (2006); **25**: 544–553
- Cmejla R., Petrak J., Cmejlova J. A novel iron responsive element in the 3'-UTR of human MRCK α . *Biochem. Biophys. Res. Commun.* (2006); **341**: 158–166
- Cohen L.A., Gutierrez L., Weiss A., Leichtmann-Bardoogo Y., Zhang D.L., Crooks D.R., Sougrat R., Morgenstern A., Galy B., Hentze M.W. et al. (2010) Serum ferritin is derived primarily from macrophages through a nonclassical secretory pathway. *Blood* (2010); **116**: 1574–1584
- Courselaud B., Pigeon C., Inoue Y., Inoue J., Gonzalez F.J., Leroyer P., Gilot D., Boudjema K., Guguen-Guillouzo C., Brissot P., et al. C/EBP α regulates hepatic transcription of hepcidin, an antimicrobial peptide and regulator of iron metabolism. Cross-talk between C/EBP pathway and iron metabolism. *J. Biol. Chem.* (2002); **277**: 41163–41170
- Crow M.T., Mani K., Nam Y.J., Kitsis R.N. The mitochondrial death pathway and cardiac myocyte apoptosis. *Circ. Res.* (2004); **95**: 957–70

Damy T., Ratajczak P., Robidel E., Bendall J.K., Oliviero P., Boczkowski J., Ebrahimian T., Marotte F., Samuel J.L., Heymes, C. Up-regulation of cardiac nitric oxide synthase 1-derived nitric oxide after myocardial infarction in senescent rats. *FASEB J.* (2003); **13**: 1934–1936

Darshan D., Vanoaica L., Richman L., Beermann F., Kuhn L.C. Conditional deletion of ferritin H in mice induces loss of iron storage and liver damage. *Hepatology* (2009); **50**: 852–860

Deck K.M., Vasanthakumar A., Anderson S.A., Goforth J.B., Kennedy M.C., Antholine W.E., Eisenstein R.S. Evidence that phosphorylation of iron regulatory protein 1 at serine 138 destabilizes the [4Fe–4S] cluster in cytosolic aconitase by enhancing 4Fe–3Fe cycling. *J. Biol. Chem.* (2009); **284**: 12701–12709

De Domenico I., McVey Ward D., Kaplan J. Regulation of iron acquisition and storage: consequences for iron-linked disorders. *Nat. Rev. Mol. Cell Biol.* (2008); **9**: 72–81

De Domenico I., Vaughn M.B., Li L., Bagley D., Musci G., Ward D.M., Kaplan J. Ferroportin-mediated mobilization of ferritin iron precedes ferritin degradation by the proteasome. *EMBO J.* (2006); **25**: 5396–5404

De Domenico I., Ward D.M., Kaplan, J. Specific iron chelators determine the route of ferritin degradation. *Blood* (2009); **114**: 4546–4551

Desagher S., Martinou J.C. Mitochondria as the central control point of apoptosis. *Trends Cell Biol.* (2000); **10**: 369–77.

Di Napoli P., Taccardi A.A., Grilli A., Spina R., Felaco M., Barsottia A., De Caterina R. Simvastatin reduces reperfusion injury by modulating nitric oxide synthase expression: an ex vivo study in isolated working rat hearts. *Cardiovascular Research* (2001); **51**: 283–293

Dupuy J., Volbeda A., Carpentier P., Darnault C., Moulis J.M., Fontecilla-Camps J.C. Crystal structure of human iron regulatory protein 1 as cytosolic aconitase. *Structure* (2006); **14**: 129–139

Dycke C., Bougault C., Gaillard J., Andrieu J.P., Pantopoulos K., Moulis J.M. Human iron regulatory protein 2 is easily cleaved in its specific domain: consequences for the heme binding properties of the protein. *Biochem. J.* (2007); **408**: 429–439

Fleming R.E. Iron and inflammation: cross-talk between pathways regulating hepcidin. *J. Mol. Med.* (2008); **86**: 491–494

Friedlich A.L., Tanzi R.E., Rogers J.T. The 5'-untranslated region of Parkinson's disease α -synuclein messenger RNA contains a predicted iron responsive element. *Mol. Psychiatry* (2007); **12**: 222–223

Gao J., Chen J., Kramer M., Tsukamoto H., Zhang A.S., Enns C.A. Interaction of the hereditary hemochromatosis protein HFE with transferrin receptor 2 is required for transferrin-induced hepcidin expression. *Cell Metab.* (2009); **9**: 217–227

Gao L., Laude K., Cai H. Mitochondrial pathophysiology, reactive oxygen species, and cardiovascular diseases. *Vet. Clin. North. Am. Small. Anim. Pract.* (2008); **38**: 137-55.

Giordano F.J. Oxygen, oxidative stress, hypoxia, and heart failure. *J. Clin. Invest.* (2005); **115**: 500-508

Goforth J.B., Anderson S.A., Nizzi C.P., Eisenstein R.S. Multiple determinants within iron-responsive elements dictate iron regulatory protein binding and regulatory hierarchy. *RNA* (2010); **16**: 154-169

Guerra M.S., Roncon-Albuquerque R. Jr, Lourenço A.P., et al. Remote myocardium gene expression after 30 and 120 min of ischemia in the rat. *Exp. Physiol.* (2006); **91**: 473–480

Hamacher-Brady A., Brady N.R., Gottlieb R.A. The interplay between pro-death and pro-survival signaling pathways in myocardial Ischemia/Reperfusion Injury: apoptosis meets autophagy. *Cardiovasc. Drugs Ther.* (2006) **20**: 445–462

Hentze M.W., Muckenthaler M.U., Galy B. Camaschella C. Two to tango: regulation of mammalian iron metabolism. *Cell* (2010); **142**: 24–38

Hölschermann H., Schuster D., Parviz B., Haberbosch W., Tillmanns H., Muth H. Statins prevent NF-kappaB transactivation independently of the IKK-pathway in human endothelial cells. *Atherosclerosis* (2006); **185**: 240-5

Hubert N., Hentze M.W. Previously uncharacterized isoforms of divalent metal transporter (DMT)-1: implications for regulation and cellular function. *Proc. Natl. Acad. Sci. U.S.A.* (2002); **99**: 12345–12350

Irace C., Esposito G., Maffettone C., Rossi A., Festa M., Iuvone T., Santamaria R., Sautebin L., Carnuccio R., Colonna A. Oxalomalate affects the inducible nitric oxide synthase expression and activity. *Life Sciences* (2007); **80**: 1282–1291

Irace C., Scorziello A., Maffettone C., Pignataro G., Matrone C., Adornetto A., Santamaria R., Annunziato L., Colonna A. Divergent modulation of iron regulatory proteins and ferritin biosynthesis by hypoxia/reoxygenation in neurons and glial cells. *Journal of Neurochemistry* (2005); **95**: 1321–1331

Kautz L., Meynard D., Monnier A., Darnaud V., Bouvet R., Wang R.H., Deng C., Vaultont S., Mosser J., Coppin H., Roth M.P. Iron regulates phosphorylation of Smad1/5/8 and gene expression of Bmp6, Smad7, Id1, and Atoh8 in the mouse liver. *Blood* (2008); **112**: 1503–1509

Kakhlon O, Cabantchik Z.I. The labile iron pool: characterization, measurement, and participation in cellular processes. *Free Radic. Biol. Med.* (2002); **33**: 1037-46

Keel S.B., Doty R.T., Yang Z., Quigley J.G., Chen J., Knoblauch S., Kingsley P.D., De Domenico I., Vaughn M.B., Kaplan, J. A heme export protein is required for red blood cell differentiation and iron homeostasis. *Science* (2008); **319**: 825–828

Kirmizis D., Chatzidimitriou D. Pleiotropic vasoprotective effects of statins: the chicken or the egg? *Drug Des. Devel. Ther.* (2009); **3**: 191-204

Kumar, Abbas, Fausto: *Robbins and Cotran Pathologic Basis of Disease*, 7th Edition
Lee P.L., Beutler E. Regulation of hepcidin and iron-overload disease. *Annu. Rev. Pathol.* (2009); **4**: 489–515

Levi S., Arosio P. Mitochondrial ferritin. *Int. J. Biochem. Cell Biol.* (2004); **36**: 1887–1889

Ludwiczek S., Aigner E., Theurl I., Weiss G. Cytokine-mediated regulation of iron transport in human monocytic cells. *Blood* (2003); **101**: 4148–4154

Madonna R., Di Napoli P., Massaro M., Grilli A., Felaco M., De Caterina A., Tang D., De Caterina R., Geng Y.J. Simvastatin attenuates expression of cytokine-inducible nitric-oxide synthase in embryonic cardiac myoblasts. *J. Biol. Chem.* (2005); **280**: 13503-11

Martini F.H., Timmons M.J., Tallitsch R.B. *Human Anatomy*, 6th edition

Matak P., Chaston T.B., Chung B., Srai S.K., McKie A.T., Sharp P.A. Activated macrophages induce hepcidin expression in HuH7 hepatoma cells. *Haematologica* (2009); **94**: 773–780

Mathur N., Ramasubbu K., Mann D.L. Spectrum of pleiotropic effects of statins in heart failure *Heart Fail. Clin.* (2008); **4**: 153-161

Mattace Raso G., Irace C., Esposito E., Maffettone C., Iacono A., Di Pascale A., Santamaria R., Colonna A., Meli R. Ovariectomy and estrogen treatment modulate iron metabolism in rat adipose tissue. *Biochem. Pharmacol.* (2009); **78**: 1001-7

McKie A.T., Marciani P., Rolfs A., Brennan K., Wehr K., Barrow D., Miret S., Bomford A., Peters T.J., Farzaneh F. et al. A novel duodenal iron-regulated transporter IREG1, implicated in the basolateral transfer of iron to the circulation. *Mol. Cell* (2000); **5**: 299–309

Medina R.J., O'Neill C.L., Devine A.B., Gardiner T.A., Stitt A.W. The pleiotropic effects of simvastatin on retinal microvascular endothelium has important implications for ischaemic retinopathies. *PLoS One* (2008); **3**: e2584

Merle U., Fein E., Gehrke S.G., Stremmel W., Kulaksiz H. The iron regulatory peptide hepcidin is expressed in the heart and regulated by hypoxia and inflammation. *Endocrinology* (2007); **148**: 2663-2668

Meynard D., Kautz L., Darnaud V., Canonne-Hergaux F., Coppin H., Roth M.P. Lack of the bone morphogenetic protein BMP6 induces massive iron overload. *Nat. Genet.* (2009); **41**: 478–481

Misra M.K., Sarwat M., Bhakuni P., Tuteja R., Tuteja N. Oxidative stress and ischemic myocardial syndromes. *Med. Sci. Monit.* (2009); **15**: 209-219

Miura K., Taura K., Kodama Y., Schnabl B., Brenner D.A. Hepatitis C virus-induced oxidative stress suppresses hepcidin expression through increased histone deacetylase activity. *Hepatology* (2008); **48**: 1420–1429

Muckenthaler M.U., Galy B., Hentze M.W. Systemic Iron Homeostasis and the Iron-Responsive Element/Iron-Regulatory Protein (IRE/IRP) Regulatory Network. *Annu. Rev. Nutr.* (2008); **28**: 197–21

Mungrue I.N., Husain M., Stewart D.J. The Role of NOS in Heart Failure: Lessons from Murine Genetic Models. *Heart Failure Reviews* (2002); **7**: 407–422

Nemeth E., Ganz T. The role of hepcidin in iron metabolism. *Acta Haematol.* (2009); **122**: 78–86

Pacher P., Beckman J.S., Liaudet L. Nitric Oxide and Peroxynitrite in Health and Disease. *Physiol. Rev.* (2007); **87**: 315–424

Piccinelli P., Samuelsson T. Evolution of the iron-responsive element. *RNA* (2007); **13**: 952–966

Ping P., Song C., Zhang J., Guo Y., Cao X., Li R.C., Wu W., Vondriska T.M., Pass J.M., Tang X.L., Pierce W.M., Bolli, R. Formation of protein kinase C ϵ -Lck signaling modules confers cardioprotection. *J. Clin. Invest.* (2002); **109**: 499–507

Piper H.M., Abdallah Y., Schaefer C. The first minutes of reperfusion: a window of opportunity for cardioprotection. *Cardiovasc. Res.* (2004); **61**: 365–371

Pitts K.R., Stiko A., Buetow B., et al. Washout of heme-containing proteins dramatically improves tetrazolium-based infarct staining. *J. Pharmacol. Toxicol. Methods* (2007); **55**: 201–208

Pondarre C., Antiochos B.B., Campagna D.R., Clarke S.L., Greer E.L., Deck K.M., McDonald A., Han A.P., Medlock A., Kutok J.L. et al. The mitochondrial ATP-binding cassette transporter Abcb7 is essential in mice and participates in cytosolic iron–sulfur cluster biogenesis. *Hum. Mol. Genet.* (2006); **15**: 953–964

Poulter N. Global risk of cardiovascular disease. *Heart* (2003); **89 (Suppl II)**: ii2–ii5

Ramey G., Deschemin J.C., Vaulont S. Cross-talk between the mitogen activated protein kinase and bone morphogenetic protein/hemojuvelin pathways is required for the induction of hepcidin by holotransferrin in primary mouse hepatocytes. *Haematologica* (2009); **94**: 765–772

Recalcati S., Minotti G., Cairo G. Iron regulatory proteins: from molecular mechanisms to drug development. *Antioxid. Redox Signaling* (2010); **13**: 1593–1616

Rouault T.A. The role of iron regulatory proteins in mammalian iron homeostasis and disease. *Nat. Chem. Biol.* (2006); **2**: 406–414

Sanchez M., Galy B., Dandekar T., Bengert P., Vainshtein Y., Stolte J., Muckenthaler M.U., Hentze M.W. Iron regulation and the cell cycle: identification of an iron-responsive element in the 3'-untranslated region of human cell division cycle 14A mRNA by a refined microarray-based screening strategy. *J. Biol. Chem.* (2006); **281**: 22865–22874

Sanchez M., Galy B., Muckenthaler M.U., Hentze M.W. Iron-regulatory proteins limit hypoxia-inducible factor-2 α expression in iron deficiency. *Nat. Struct. Mol. Biol.* (2007); **14**: 420–426

Sanchez M., Galy B., Schwanhaeusser B., Blake J., Bähr-Ivacevic T., Benes V., Selbach M., Muckenthaler M.U., Hentze M.W. Iron regulatory protein-1 and -2: transcriptome-wide definition of binding mRNAs and shaping of the cellular proteome by IRPs. *Blood* (2011). [Epub. Ahead of print]

Salahudeen A.A., Thompson J.W., Ruiz J.C., Ma H.W., Kinch L.N., Li Q., Grishin N.V., Bruick R.K. An E3 ligase possessing an iron-responsive hemerythrin domain is a regulator of iron homeostasis. *Science* (2009); **326**: 722–726

Santamaria R., Fiorito F., Irace C., De Martino L., Maffettone C., Granato G.E., Di Pascale A., Iovane V., Pagnini U., Colonna A. 2,3,7,8-Tetrachlorodibenzo-p-dioxin impairs iron homeostasis by modulating iron-related proteins expression and increasing the labile iron pool in mammalian cells. *Biochim. Biophys. Acta.* (2011); **1813**: 704–12

Santamaria R., Irace C., Festa M., Maffettone C., Colonna A. Induction of ferritin expression by oxalomalate. *Biochim. Biophys. Acta* (2004); **1691**: 151–159

Schmitz I., Kirchhoff S., Krammer P.H. Regulation of death receptor-mediated apoptosis pathways. *Int. J. Biochem. Cell Biol.* (2000); **32**: 1123–36

Schulz R., Kelm M., Heusch G. Nitric oxide in myocardial ischemia/reperfusion injury. *Cardiovascular Research* (2004); **61**: 402–413

Seznec H., Simon D., Bouton C., Reutenauer L., Hertzog A., Golik P., Procaccio V., Patel M., Drapier J.C., Koenig M., Puccio H. (2005) Friedreich ataxia: the oxidative stress paradox. *Hum. Mol. Genet.* (2005); **14**: 463–474

Sharpe J.C., Arnoult D., Youle R.J. Control of mitochondrial permeability by Bcl-2 family members. *Biochim. Biophys. Acta* (2004); **1644**: 107–13

Shi H., Bencze K.Z., Stemmler T.L., Philpott C.C. A cytosolic iron chaperone that delivers iron to ferritin. *Science* (2008); **320**: 1207–1210

Shi Y. Mechanisms of caspase activation and inhibition during apoptosis. *Mol. Cell* (2002); **9**: 459–470

Shi Y., Ghosh M., Tong W.H., Rouault T.A. (2009) Human ISD11 is essential for both iron–sulfur cluster assembly and maintenance of normal cellular iron homeostasis. *Hum. Mol. Genet.* (2009); **18**: 3014–3025

Shimokawa H., Tsutsui M. Nitric oxide synthases in the pathogenesis of cardiovascular disease. Lessons from genetically modified mice. *Pflugers Arch.: Eur. J. Physiol.* (2010); **459**: 959–967

Simeone L., Mangiapia G., Irace C., Di Pascale A., Colonna A., Ortona O., De Napoli L., Montesarchio D., Paduano L. Nucleolipid nanovectors as molecular carriers for potential applications in drug delivery. *Mol. Biosyst.* (2011); [Epub ahead of print]

Smyth J.W., Hong T.T., Gao D., Vogan J.M., Jensen B.C., Fong T.S., Simpson P.C., Stainier D.Y., Chi N.C., Shaw R.M. Limited forward trafficking of connexin 43 reduces cell-cell coupling in stressed human and mouse myocardium. *J. Clin. Invest.* (2010); **120**: 266–279

Solaini G., Harris D.A. Biochemical dysfunction in heart mitochondria exposed to ischaemia and reperfusion. *Biochem. J.* (2005); **390**: 377–94

Stennicke H.R., Salvesen G.S. Caspases-controlling intracellular signals by protease zymogen activation. *Biochim. Biophys. Acta* (2000); **1477**: 299–306

Taylor A.L., Ziesche S., Yancy C., Carson P., D'Agostino R. Jr, Ferdinand K., Taylor M., Adams K., Sabolinski M., Worcel M., Cohn J.N. African-American Heart Failure Trial Investigators. Combination of isosorbide dinitrate and hydralazine in blacks with heart failure. *N. Engl. J. Med.* (2004); **351**: 2049–57

Third Report of the National Cholesterol Education Program (NCEP). Expert Panel on Detection, Evaluation, and Treatment of High Blood Cholesterol in Adults (Adult Treatment Panel III); Final Report. National Cholesterol Education Program National Heart, Lung, and Blood Institute National Institutes of Health NIH. Publication No. 02-5215, September 2002

Tong W.H., Rouault T.A. Functions of mitochondrial ISCU and cytosolic ISCU in mammalian iron–sulfur cluster biogenesis and iron homeostasis. *Cell Metab.* (2006); **3**: 199–210

Tsutsui M., Shimokawa H., Otsuji Y., Ueta Y., Sasaguri Y., Yanagihara N. Nitric oxide synthases and cardiovascular diseases. Insights from genetically modified mice. *Circ. J.* (2009); **73**: 986–993

Vashisht A.A., Zumbrennen K.B., Huang X., Powers D.N., Durazo A., Sun D., Bhaskaran N., Persson A., Uhlen M., Sangfelt O. et al. Control of iron homeostasis by an iron-regulated ubiquitin ligase. *Science* (2009); **326**: 718–721

- Vaughan C.J., Murphy M.B., Buckley B.M. Statins do more than just lower cholesterol. *Lancet*. (1996); **348**: 1079–1082
- Verhagen A.M., Ekert P.G., Pakusch M., Silke J., Connolly L.M., Reid G.E., et al. Identification of DIABLO, a mammalian protein that promotes apoptosis by binding to and antagonizing IAP proteins. *Cell* (2000); **102**: 43–53
- Vohra H.A., Galinanes M. Effect of the degree of ischaemic injury and reoxygenation time on the type of myocardial cell death in man: role of caspases. *BMC Physiol.* (2005); **19**: 5-14
- Volke M., Gale D.P., Maegdefrau U., Schley G., Klanke B., Bosserhoff A.K., Maxwell P.H., Eckardt K.U., Warnecke C. Evidence for a lack of a direct transcriptional suppression of the iron regulatory peptide hepcidin by hypoxia-inducible factors. *PLoS ONE* (2009); **4**: e7875
- Walden W.E., Selezneva A.I., Dupuy J., Volbeda A., Fontecilla-Camps J.C., Theil E.C., Volz K. (2006) Structure of dual function iron regulatory protein 1 complexed with ferritin IRE-RNA. *Science* (2006); **314**: 1903–1908
- Wallander M.L., Leibold E.A., Eisenstein R.S. Molecular control of vertebrate iron homeostasis by iron regulatory proteins. *Biochim. Biophys. Acta* (2006); **1763**: 668-689
- Wang C.-Y., Liu P.-Y., Liao J.K. Pleiotropic effects of statin therapy: molecular mechanisms and clinical results. *Trends Mol. Med.* (2008); **14**: 37-44
- Wang J., Fillebeen C., Chen G., Biederbick A., Lill R., Pantopoulos K. Iron-dependent degradation of apo-IRP1 by the ubiquitin-proteasome pathway. *Mol. Cell. Biol.* (2007); **27**: 2423–2430
- Wang J., Pantopoulos K. Regulation of cellular iron metabolism. *Biochem. J.* (2011); **434**: 365–381
- Ward D.T., Hamilton K., Burnand R., Smith C.P., Tomlinson D.R., Riccardi D. Altered expression of iron transport proteins in streptozotocin-induced diabetic rat kidney. *Biochim Biophys Acta* (2005); **1740**: 79-84
- Weiss G., Goodnough L.T. Anemia of chronic disease. *N. Engl. J. Med.* (2005); **352**: 1011–1023
- Wood R.J. The iron-heart disease connection: is it dead or just hiding? *Ageing Research Reviews* (2004); **3**: 355-367
- Ye H., Jeong S.Y., Ghosh M.C., Kovtunovych G., Silvestri L., Ortillo D., Uchida N., Tisdale J., Camaschella C., Rouault T.A. Glutaredoxin 5 deficiency causes sideroblastic anemia by specifically impairing heme biosynthesis and depleting cytosolic iron in human erythroblasts. *J. Clin. Invest.* (2010); **120**: 1749–1761

Yeh K.Y., Yeh M., Mims L. Glass J. Iron feeding induces ferroportin 1 and hephaestin migration and interaction in rat duodenal epithelium. *Am. J. Physiol. Gastrointest. Liver Physiol.* (2009); **296**: G55–G65

You S., Wang Q. Ferritin in atherosclerosis. *Clin. Chim. Acta* (2005); **357**: 1-16

Zhang D.L., Hughes R.M., Ollivierre-Wilson H., Ghosh M.C., Rouault T.A. A ferroportin transcript that lacks an iron-responsive element enables duodenal and erythroid precursor cells to evade translational repression. *Cell Metab.* (2009); **9**: 461–473

Zhang Y., Mikhael M., Xu D., Li Y., Soe-Lin S., Ning B., Li W., Nie G., Zhao Y., Ponka P. Lysosomal proteolysis is the primary degradation pathway for cytosolic ferritin and cytosolic ferritin degradation is necessary for iron exit. *Antioxid. Redox Signaling* (2010); **13**: 999–1009

Zimmer M., Ebert B.L., Neil C., Brenner K., Papaioannou I., Melas A., Tolliday N., Lamb J., Pantopoulos K., Golub T., Iliopoulos O. Small-molecule inhibitors of HIF-2 α translation link its 5'-UTR iron-responsive element to oxygen sensing. *Mol. Cell* (2008); **32**: 838–848

Zumbrennen K.B., Wallander M.L., Romney S.J., Leibold E.A. Cysteine oxidation regulates the RNA-binding activity of iron regulatory protein 2. *Mol. Cell. Biol.* (2009); **29**: 2219–2229